MODIFICATION OF ZEOLITES BY CHEMICAL VAPOUR DEPOSITION AND SOME APPLICATIONS OF THE MODIFIED ZEOLITES

HOSNE ARA BEGUM

A dissertation submitted to the University of Dhaka in fulfillment of the requirements for the degree of Doctor of Philosophy

Department of Chemistry
University of Dhaka
Bangladesh

January, 2003

DEDICATED
TO MY
BELOVED
MOTHER-IN-LAW
FATHER-IN-LAW
AND
MY SWEET DAUGHTER MAEESHA

Declaration Certificate

Certified that the work in this thesis entitled **"MODIFICATION OF ZEOLITES BY CHEMICAL VAPOUR DEPOSITION AND SOME APPLICATIONS OF THE MODIFIED ZEOLITES"** submitted by **Hosne Ara Begum** contains experiments and other related research work exclusively carried out by the candidate herself under our supervision. The experimental work has been done mostly in the Laboratories of Precision Synthetic Chemistry, Department of Materials Science, Tottori University, Japan and partly in the Laboratories of Physical Chemistry, Department of Chemistry, University of Dhaka, Bangladesh. The candidate has fulfilled all the terms and conditions for the Ph.D. thesis and presented her work in seminars in the Department of Chemistry and in international conferences. She has already published a paper on the topic as an author and another paper has been submitted as a coauthor. The published paper has been appended at the end of the thesis.

Prof. A. J. Mahmood
Department of Chemistry
University of Dhaka
Dhaka, Bangladesh

ACKNOWLEDGEMENT

It is a great pleasure to express my sincere gratitude to my supervisor Professor Abu Jafar Mahmood, Department of Chemistry, University of Dhaka, Bangladesh for sharing his wisdom, kind advice, encouragement throughout the course of this work and helpful instruction in writing this thesis.

Special thanks and gratitude are extended towards my co-supervisor Professor Tajmeri S. A. Islam, Department of Chemistry, University of Dhaka, Bangladesh for her profound interest in this work and inspiration for all time.

I would like to make a grateful acknowledgement to my co-supervisor Professor Miki Niwa, Department of Materials Science, Tottori University, Japan for his kind and fruitful suggestions and giving me an opportunity to carry out my research work in his laboratory.

I am grateful to Dr. Naonobu Katada, Associate Professor, Department of Materials Science, Tottori University, Japan for his support and helpful instruction during this research. I am also thankful to Dr. Kazu Okumura, Mr. Kageyama, Mr. Matsura, Ms. Tokuko Doi and other members in the laboratories of Professor Niwa for their hearty cooperation with me.

I am specially thanked to Prof. M. M. Rahman, Prof. R. J. Mannan, Dr. Quamrul Ehsan and Dr. Omar Ahmed for their help and constant encouragement. Also I offer my heartfelt thanks to other colleagues in the Department of Chemistry, University of Dhaka, Bangladesh.

I am thankful to the University of Dhaka for granting me study leave for my research work in Japan.

Finally, I am deeply grateful to my mother-in-law Mrs. Nazma Ara Begum and father-in-law Dr. Muslemuddin for their continuous support and encouragement during my study in home and aboard. I also thanked to my parents, brothers, sisters, sister-in-law and brother-in-law for their constant inspiration and encouragement.

I would like to thank to my little daughter Maeesha for her sacrifice and patience.

I am especially grateful to my husband Dr. Tanvir Muslim who inspired me to carry out the research work and endured all the troubles in course of this research.

A also acknowledge the encouragement which I received from my friends and well-wishers.

Hosne Ara Begum

(HOSNE ARA BEGUM)

Contents

List of figures

Chapter One

Chapter Two

Chapter Three

List of tables

Appendix

SUMMARY

Zeolites are porous crystalline aluminosilicate. Due to the microporous character with uniform pore dimensions, zeolites have created significant interest in the study of adsorption, separation and catalysis. Attempts have been made to improve the properties of zeolites for various applications such as separation of hydrocarbons and in the catalytic reactions of organic molecules. To control the solid acidity and shape selectivity, post-synthesis modification of zeolites have been carried out by various ways.

Chemical vapour deposition (CVD) is an important method to modify the external surface and pore-opening size to improve the molecular sieving property and catalytic activity of zeolites. Mainly silicon based compounds have been used to cover the external surface of zeolites with silica. These silicon based compounds are so chosen that they do not enter into the channels of the zeolite. Typically, silicon alkoxide in the vapour phase has been used to interact with zeolite surface hydroxyl groups. A thin layer of silica consisting of siloxane bonds is formed over external surface of zeolite initially by gradual deposition of silicon alkoxide and subsequently by its reaction with water.

Silicalite is the aluminium free form of ZSM-5, having an MFI (Mobil-five) structure. It has elliptical pore opening of 0.51 × 0.57 nm^2 interconnected by zigzag channels with a nearly circular cross section of about 0.54 nm in diameter. It has hydrophobic and organophilic nature compared to other zeolites. Owing to this characteristic, silicalite can be used for environmental applications to selectively adsorb nonpolar hydrocarbon molecules. Recently research interest is aimed at the separation of branched-chain and straight-chain hydrocarbons by the use of silicalite. Since silicalite is suitable for hydrocarbon adsorption, due to its non-acidic property, the control of pore-opening size by chemical vapour

deposition of silica is likely to make it an interesting new material for shape selective separation of hydrocarbons. However, very few reports are available at the moment on the chemical vapour deposition of silica on silicalite. Therefore, an investigation on the simple thermal chemical vapour deposition of silica on silicalite is necessary to prove that selective adsorbents for hydrocarbon are possible to develop.

Zeolite Y has the faujasite (FAU) structure with typical Si/Al ratio between 1.5 and 3.0. It has a pore dimension of 0.74 nm. It is used mainly as catalyst in fluid catalytic cracking (FCC) process and hydrocracking process. It is generally accepted that the cracking activity can be attributed to the Brønsted acidity of the zeolite. The ultrastable Y (USY) zeolite can be prepared by steam dealumination of zeolite Y. It possesses high thermal stability and structural stability in atmosphere. It is highly active hydrocarbon cracking catalyst and it is one of the main components of fluid catalytic cracking processes. Some attempts have been made to modify HY and Hβ zeolites by chemical vapour deposition of silicon alkoxide to control the pore-opening size. The investigation on the preparation of silica deposited USY zeolite for controlling the pore opening size has not yet progressed much.

The presentation in the thesis is divided into two parts. In the first part, results of the synthesis of silicalite, modification of silicalites by chemical vapour deposition of tetramethoxysilane, characterization and some applications are presented, as described in chapter two. In the second part of this thesis, modification of USY zeolite by chemical vapour deposition of tetramethoxysilane has been studied to improve the catalytic activity, as described in chapter three.

Part I:

Silicalite has been synthesized according to the method of Argauer and Landolt. From the XRD measurements, the prepared silicalite crystal has been found to possess MFI type structure. The shapes and the sizes of the crystals were measured by SEM. The shape of silicalite has been found to be hexagonal flat plate with an average crystal size $5.3 \times 3.1 \times 1.5\ (\mu m)^3$. From the TEM measurement it was observed that most of the crystals are large $[(5.1 - 6.8) \times (2.5 - 4.0) \times (0.6 - 2.0)\ (\mu m)^3]$. The distance between two neighbouring micropores is about 1 nm. A band for Si-OH has been found at 3740 cm^{-1} with weak intensity in the IR spectrum of silicalite. The nitrogen adsorption isotherm is IV type (stepped) for silicalite.

The silicalite crystal surface has been modified by chemical vapour deposition of tetramethoxysilane to form a thin layer of silica. A conventional vacuum system equipped with a quartz spring microbalance is used as the laboratory apparatus for the CVD. The CVD-silicalite samples have been prepared by deposition of $Si(OCH_3)_4$ vapour on silicalite crystals at different temperatures ranging from 513 K to 773 K at different contact time. The amount of deposited silica has been determined from the weight gain after calcination in oxygen at 673 K. The rate of deposition of silica on silicalite is very high at the initial stage even at low temperature (513 K). The rate of deposition gradually decreases, particularly at lower temperatures, due to the lack of acid site on silicalite. At 773 K, the deposition rate is high enough to prepare various types of silica deposited silicalite in a reasonable time. No significant change has been observed in the SEM images of CVD-silicalites. From the TEM measurement, it has been found that the deposited layers of silica cover the whole surface of the silicalite crystals and the thickness of the deposited layer is found to be 5–8 nm for 1.9 wt % CVD-silicalite. Silicalite and

CVD-silicalites do not show any difference in the nitrogen adsorption isotherms.

Adsorption of linear and branched chain hydrocarbon (hexane, 2-methylpentane, butane and 2-methylpropane) on silicalite and CVD-silicalites, measured gravimetrically by the McBain method and chromatographically at about 298 K. The adsorption behaviour is almost unchanged for hexane and butane. On the other hand the adsorption of 2-methylpentane and 2-methylpropane is suppressed with the increase of the deposited silica on silicalite. Although the deposited silica on the silicalite is the same, the rate of adsorption of 2-methylpentane was suppressed more than that of 2-methylpropane. The extent of suppression depends on the kinetic diameter, chain length of paraffins and on the amount of deposited silica on silicalite.

Part II:

Low silica content USY (LS-USY) zeolite and high silica content USY (HS-USY) zeolite have been selected for the chemical modification. Silica deposited HS-USY and LS-USY zeolites have been prepared by CVD technique similar to that of CVD-silicalite. The modified zeolites have been characterized by XRD, temperature programmed desorption of ammonia (NH_3-TPD) and IR studies. XRD results show that the deposition of amorphous silica on HS-USY zeolite causes slight decrease of crystallinity (at 331 plane). This decrease in the crystallinity is much more prominent for the silica deposited LS-USY zeolite. NH_3-TPD experiments show that the acid amount decreases with the increase of deposited silica on LS-USY zeolite. In the case of HS-USY zeolite, the amount of acid is not affected much by the CVD. The -OH bands at 3630 and 3560 cm^{-1} disappear in the case of LS-USY zeolite for any deposition due to the interaction of tetramethoxysilane with internal hydroxyl group. In the case

of HS-USY zeolite, the peak intensities of the -OH band at 3633 and 3560 cm^{-1} are slightly decrease without changing the peak positions due to silica deposition on the external surface of USY zeolite. The extent of control of the pore-opening size of HS-USY and LS-USY zeolites have been investigated by the adsorption of a large molecule, namely 1,3,5-TIPB. It is observed that adsorption of 1,3,5-TIPB decreases gradually with the increase of deposited silica on HS-USY zeolite. This indicates the influence of the deposition on the extent of the pore-opening size. In the case of LS-USY zeolite, the adsorption of 1,3,5-TIPB does not change that much with the amount of deposited silica. Some tetramethoxysilane molecules are likely to react with the hydroxyl groups inside the pore of LS-USY zeolite. LS-USY zeolite has higher amount of extra-framework aluminium. The silane compound reacts preferentially with acid sites, originated from aluminium, inside the pore than with the silanol groups on the external surface. Thus, the aluminium concentration particularly the concentration of the extra-framework aluminium, plays an important role in determining the efficiency of CVD on the USY eolith.

Catalytic cracking of 1,3,5-triisiptopylbenzene (1,3,5-TIPB) and 1,3,5-trimethylbenzene (1,3,5-TMB) on USY and silica deposited USY zeolites has been also performed to study their pore-opening size and solid acidity of these zeolites. The pulse technique has been used for this purpose. The deposited silica narrows the pore-opening size and inertise the external surface of USY zeolites.

Chapter One

General Introduction

1.1. Zeolites

Zeolites are porous crystalline aluminosilicates. The zeolite framework consists of an assemblage of SiO_4 and AlO_4 tetrahedra, joined together in various regular arrangements through shared oxygen atoms. As a result an open crystal lattice containing pores of molecular dimensions are formed. Guest molecules can penetrate into these spaces. Since the micropore structure is determined by the crystal lattice it is precisely uniform with no distribution of pore size. Each AlO_4 tetrahedron in the framework bears a net negative charge, which is balanced by an exchangeable cation. The exchangeable cations are located at preferential sites within the framework and play a very important role in determining the adsorptive properties [1]. The exchange of a cation by a suitable ion provides a useful and widely exploited means of modifying the adsorptive and catalytic properties of the material. The structural formula of a zeolite is based on its crystallographic unit cell, the smallest unit of the structure, represented by:

$$M_{x/n}[(AlO_2)_x(SiO_2)_y]\cdot wH_2O$$

Here n is the valence of the cation M, w is the number of water molecules per unit cell, x and y are the numbers of the respective tetrahedra per unit cell. y/x usually has values of 1-5. In the case of high silica zeolites y/x is 10 to 100 [2].

The arrangement of the tetrahedral units in the macroscopic crystal results in the formation of open channels and cavities in the zeolite structure. Different arrangements yield various types of zeolite. It is the intercrystalline porosity, which confers on zeolites their characteristic properties.

In addition to the cations needed to neutralize the framework charge, there is room for salts and water molecules in the channels and cavities of the zeolite. The open frameworks of zeolites also provide an environment in

which cations and water molecules have a high degree of mobility, resulting in good ion-exchange properties and capacity for reversible hydration, respectively.

Uniform pore dimensions, ion-exchange properties, ability to possess acidity and high thermal stability make zeolites suitable for a wide range of industrial applications. Four main areas of applications of zeolites are as follows:

(a) ***As adsorbents/desiccants/separation devices***

Zeolites are widely used as selective molecular sieve adsorbents and drying agents in different chemical process industries. These are also used in large or small scale separation and gas purification processes, which utilize their shape selective properties such as *n*-paraffins from branched paraffins, *p*-xylene from its isomers etc.

(b) ***As catalyst***

The main industrial catalytic applications are in three areas such as petroleum refining, synfuel production and petrochemical production.

(c) ***As detergents***

The use of zeolites as builders in detergent formulations is a large market with even larger potential. Zeolite A is almost exclusively used as a sequestering agent to substitute phosphate.

(d) ***Miscellaneous***

Zeolites, natural or synthetic, have other uses in wastewater treatment, nuclear effluent treatment, animal feed supplements and soil improvement.

The estimated zeolite usage in North America, Western, Europe and Japan in 1988 was a total of approximately 550,000 metric tons [3]. The breakdown is given in Fig. 1.1.

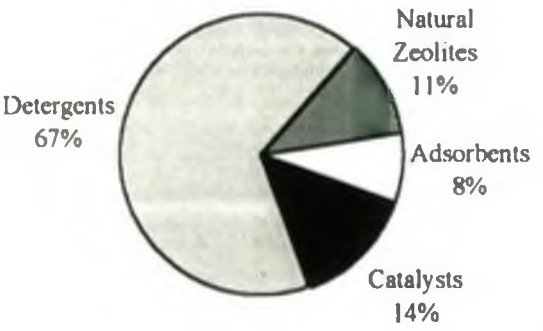

Fig. 1.1. Estimated zeolite consumption in 1988.

1.2. The structure of zeolites

1.2.1. *The primary building unit*

The primary building units of zeolites are the tetrahedral TO_4 frameworks, where T may be Si, Al, P, Ga, Be, etc, as shown in Fig. 1.2.

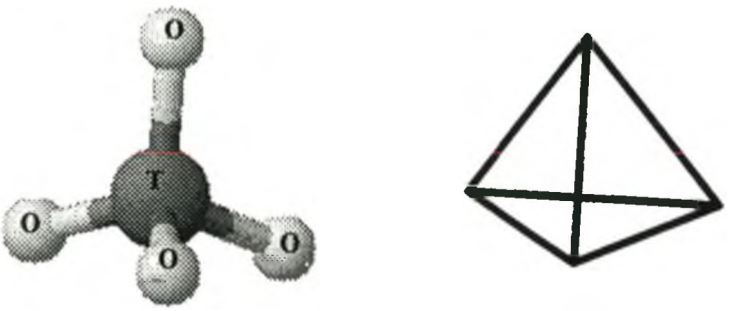

Fig. 1.2. TO_4 tetrahedral framework.

1.2.2. *The secondary building units*

To facilitate the description and to systematize the vast diversity of zeolite topologies, use of 8 secondary structural units based on simple groupings of linked tetrahedra has been suggested [4]. The number of these so-called secondary building units (SBU's) is later increased to 16 (Fig. 1.3) [5]. Thus the structures of zeolites can be reduced to combinations of secondary building units.

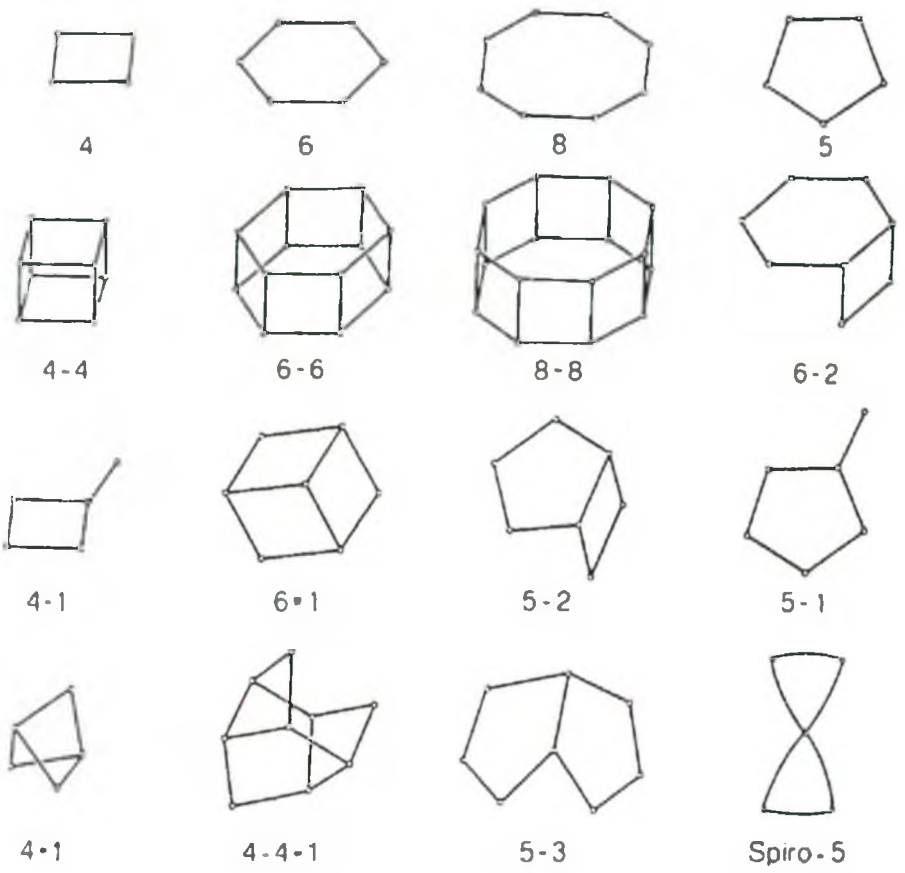

Fig. 1.3. The secondary building units.

The atoms represented by T in Fig. 1.3 are assigned positions at the corners or apices. The O atoms are not shown, but would lie approximately at the midpoints of the lines joining the T atoms.

1.2.3. *Building blocks*

The SBU's may be combined to form building blocks. An example of such a building block is the sodalite unit, depicted in Fig. 1.4a, which is found in faujasite zeolites, X and Y. The sodalite unit is a truncated cubo-octahedron composed of 24 silicon and aluminium ions in tetrahedral coordination with oxygen atoms. These sodalite units are linked together via their hexagonal faces by so-called hexagonal prisms yielding the faujasite structure shown in Fig. 1.4b.

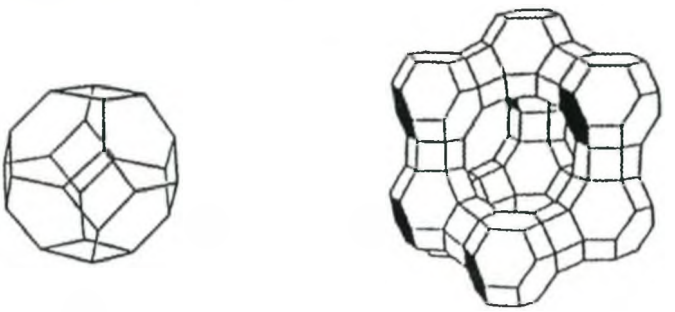

a b

Fig. 1.4. Structure of (a) sodalite unit and (b) faujasite.

The arrangement of sodalite units and hexagonal prism results in the formation of large, almost spherical cavities interconnected by distorted 12 side windows. This cavity is referred to as the supercage. In this manner a

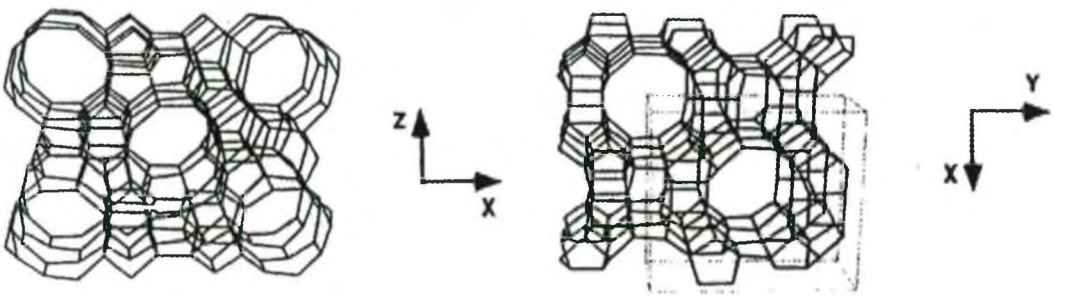

a b

Fig. 1.5. Stereoscopic representations of zeolite topologies.
(a) ZSM-5 and (b) Mordenite.

network of channels and cages is formed. Such networks also exits in other zeolites, but not all of them will have cages. The channel networks may consist of straight parallel channels as in Mordenite, or intersecting network as in ZSM-5. Fig. 1.5 shows the topology of two well-known zeolites, ZSM-5 and Mordenite.

1.2.4. *Zeolite pores*

Depending on the largest channel, zeolites are characterized as small, medium or large pore zeolites if they contain apertures made by rings of 8, 10 or 12 linked tetrahedra respectively [6]. Typical zeolite pore sizes, based on oxygen-packing models, are shown in Fig. 1.6 and some details are given in Table 1.1. Small pore zeolites with 8-ring pores, with free diameter of 0.30-0.45 nm, include zeolite A, carbazite and erinite. They adsorb only straight chain molecules such as *n*-paraffins and *n*-olefins. Medium pore zeolites are formed by a 10-ring, with 0.45-0.60 nm in free diameter, include ZSM-5, ZSM-11, ZSM-22 and ZSM-23. These zeolites are of most interest for the design of shape-selective catalysts. The large pore zeolites with 12-ring pores, diameter 0.60-0.80 nm, are zeolites X and Y and Mordenite.

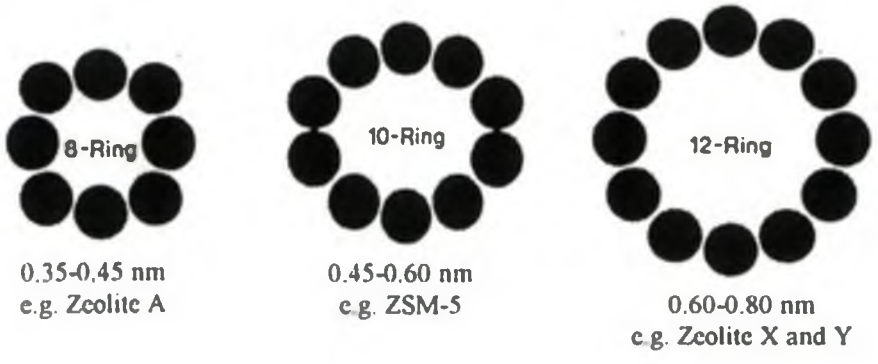

Fig. 1.6. Typical zeolite pore sizes. (illustrated with oxygen packing model).

Table 1.1. Channel systems of some representative zeolites

Type	Name	Ring size of channels	Largest channel diameter (nm)
Small pore	Linde A type	8-8-8	0.41
	Carbazite	8-8-8	0.36 × 0.37
	Erionite	8-8	0.36 × 0.52
Medium pore	ZSM-22	10	0.45 × 0.55
	ZSM-23	10	0.45 × 0.56
	ZSM-48	10	0.53 × 0.56
	Ferrierite	10-8	0.43 × 0.55
	ZSM-5	10-10	0.54 × 0.56
	ZSM-11	10-10	0.51 × 0.55
Large pore	ZSM-12	12	0.57 × 0.61
	Linde L type	12	0.71
	Mazzite	12	0.74
	Mordenite	12-8	0.67 × 0.70
	Beta	12-12	0.64 × 0.76
	Offretite	12-8-8	0.64
	Faujasite	12-12-12	0.74

The channel system may be one-dimensional (e.g. ZSM-22 and ZSM-48), two-dimensional (ferrierite) or three-dimensional (ZSM-5). Multidimensional channels often intersect one another, but this is not always the case. The interconnecting channels may be straight (ZSM-11) or tortuous (ZSM-5). The connectivity of the channel system has major consequence for diffusion and aging characteristics.

The structural characteristics of zeolite ZSM-5, Mordenite and Y are briefly described in Section 1.2.4.1 – 1.2.4.3.

1.2.4.1. ZSM-5

ZMS-5 synthesis was first reported by researches at Mobil [7]. It is a medium pore zeolite belonging to the pentasil group. The unit cell formula of the sodium form of ZSM-5 is shown below, with n typically having a value of 3 or less (but not greater than 27) [8].

$$Na_nAl_nSi_{96-n}O_{192}\cdot 16H_2O \qquad n < 27$$

X-ray diffraction studies have shown that as-synthesized ZSM-5 crystallizes with orthorhombic symmetry and has lattice constants a = 2.01, b = 1.99 and c = 1.34 nm [9]. However, monoclinic symmetry has also been observed [10].

The framework of ZSM-5 consists of linked tetrahedra, which may be considered to join to form eight 5-membered rings (SBU = 5-1). The units are connected through edges to form chains as shown in Fig. 1.7. These chains are further connected to form sheets and the linking of sheet leads to a three dimensional framework structure. The sheets parallel to the (010) and (100) planes are shown in Fig. 1.8.

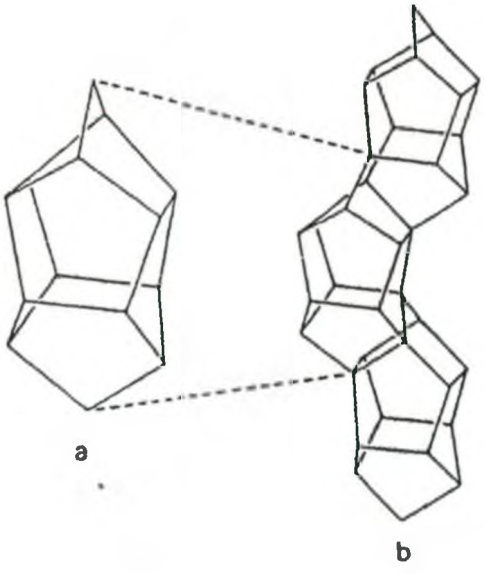

Fig. 1.7. The building blocks of ZSM-5.

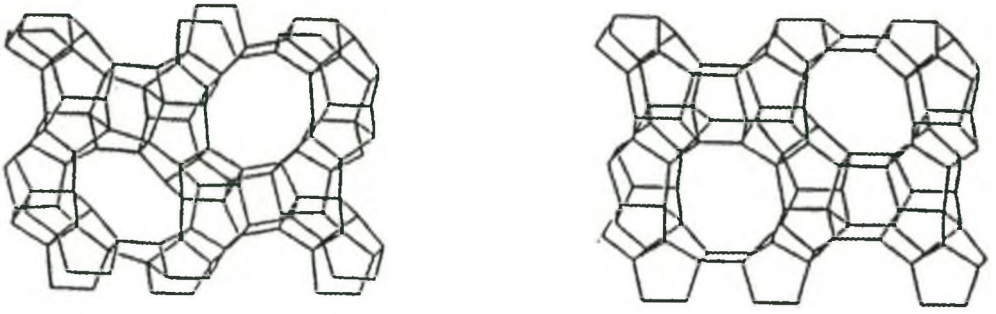

a b

Fig. 1.8. The skeletal diagrams of ZSM-5 unit cell. (a) (010) plane, showing the opening of the straight channel and (b) (100) plane, showing the opening of the sinusoidal channel.

The ZMS-5 framework contains two intersecting channel systems, one sinusoidal running parallel to the (010) plane and the other straight and parallel to the (100) plane, as shown in Fig. 1.9. In the elliptical 10-membered ring (10 Al or Si atoms) openings that control the channels are seen in Fig. 1.8. The sinusoidal channels have a diameter of 0.51 × 0.55 nm, whereas the straight channels have a diameter of 0.53 × 0.56 nm [9].

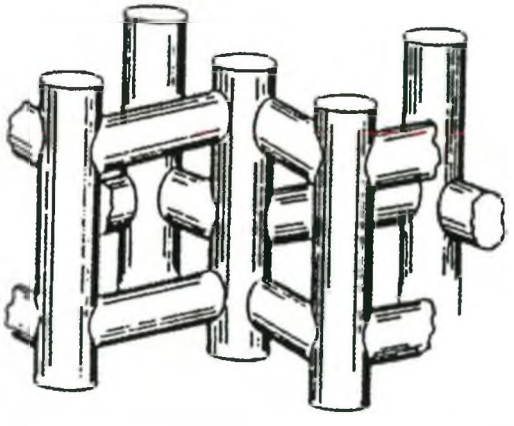

Fig. 1.9. The channel structure of ZSM-5.

1.2.4.2. Mordenite

Synthesis of Mordenite was reported by Barrer in 1948. Mordenite is a large pore zeolite, and crystallizes with orthorhombic symmetry. The lattice constants are a = 1.81 nm, b = 0.75 nm [9]. The unit cell formula is

$$Na_nAl_nSi_{48-n}O_{96}\cdot 24H_2O \qquad n \approx 8$$

The building units of Mordenite consist of 4- and 5-membered rings crosslinked by the sharing of neighbouring oxygens to form chains [11]. Mordenite contains a two-dimensional channel system for diffusion. For practical applications it is considered to be a uni-dimensional large pore molecular sieve with side pockets that arise due to constraint on the 8-member ring. The large channels have a diameter of 0.65 × 0.70 nm, whereas the small channels have a diameter of 0.26 × 0.57 nm [9]. Fig. 1.10 shows the framework topology of Mordenite.

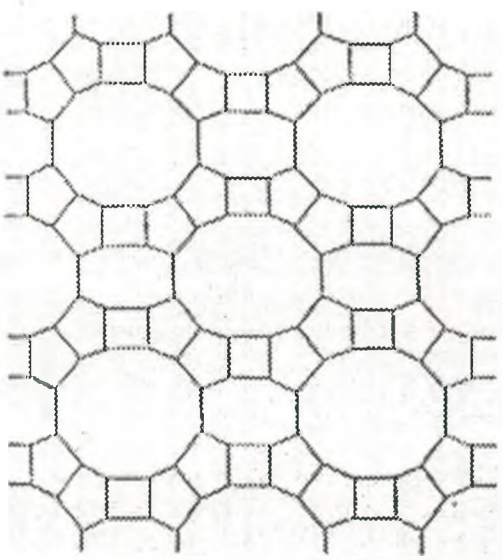

Fig. 1.10. Framework topology of Mordenite.

1.2.4.3. Zeolite Y

The synthetic zeolite Y has a faujasite (FAU) framework structure shown in Fig. 1.4. The crystallographic unit cell consists of an array of 8 supercages and 8 sodalite cages containing a total of 192 AlO_2 and SiO_2 tetrahedral units [12]. A typical unit cell contents are shown as:

$Na_{56}[(AlO_2)_{56}(SiO_2)_{136}]\cdot 250\ H_2O$ (Si/Al = 1.5 to about 3.0)

The structure of Y zeolites consists of three-dimensional framework of SiO_4 and AlO_4 tetrahedra, joined to form an array called sodalite cages or β-cages (14-hedron). The sodalite cages joined through hexagonal prisms containing a center of symmetry. Through the condensation pattern of 14-hedron, void spaces are generated. The largest void spaces in the structure are called "supercages" or α-cages. Supercages have a free diameter of 1.3 nm and are made of four 12-membered oxygen rings having a free dimension of 0.74 nm, [13-15]. Quite large molecules such as neopentane and tertiary butyl amine can penetrate into these pores.

The ultrastable Y (USY) zeolite is prepared by steam dealumination of zeolite Y. It is highly active hydrocarbon cracking catalyst and one of the main components of fluid catalytic cracking processes [16, 17]. Bronsted acid sites are generated in USY zeolite by thermal decomposition of ammonium ions, which have been previously introduced into its exchangeable sites by steam dealumination [18].

1.3. The acidity of zeolites

It has been mentioned in Section 1.2.2 that zeolites contain tetrahedrally bound silicon and aluminum with oxygen bridge in between. Each tetrahedrally coordinated aluminum atom induces a negative framework charge. This charge is neutralized by the presence of exchangeable cations. It is this charge balancing phenomenon that is responsible for the acidity and activity of zeolites.

Zeolites are commonly synthesized in the sodium form, that is, one Na^+ occupies an exchangeable cation site. The sodium cations are exchanged by ammonium cations. On heating ammonium-exchanged zeolites release ammonia, thereby yielding the active proton form as shown in the following reaction [19, 20].

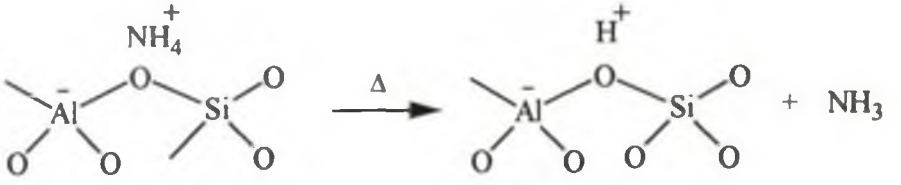

Different hydroxyl groups are found in zeolite structures. Fig. 1.11 shows a schematic view of a microcrystallite of a zeolite catalyst showing (non-acidic) terminal hydroxyls on the outer surface and (acidic) bridged hydroxyls on the walls of the micropores. More hydroxyl groups may exist on extraframework aluminum species or they may remain connected with open Si-O-Si links [21].

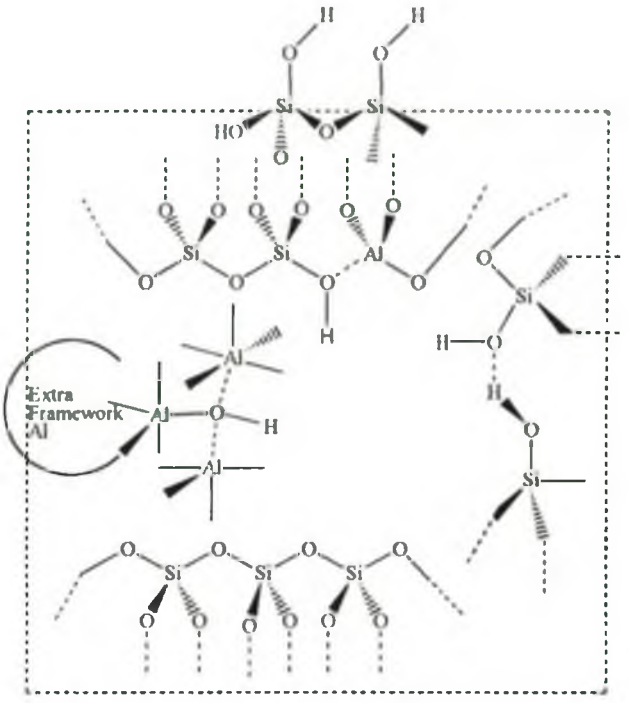

Fig. 1.11. Schematic presentation of hydroxyl groups in zeolite.

Ward has investigated the nature of the active sites on H^+ form zeolite Y, and observed three hydroxyl stretching bands at 3742, 3643 and 3540 cm^{-1} in its infrared spectrum [22]. These observations are in agreement with those of Uytterhoeven *et al.* [19]. The 3742 cm^{-1} band probably represents Si-OH terminal groups (similar to those on silica) or they may be associated with amorphous impurities in the structure [22]. The bands at 3643 and 3540 cm^{-1} represent hydroxyl groups at different crystallographic locations.

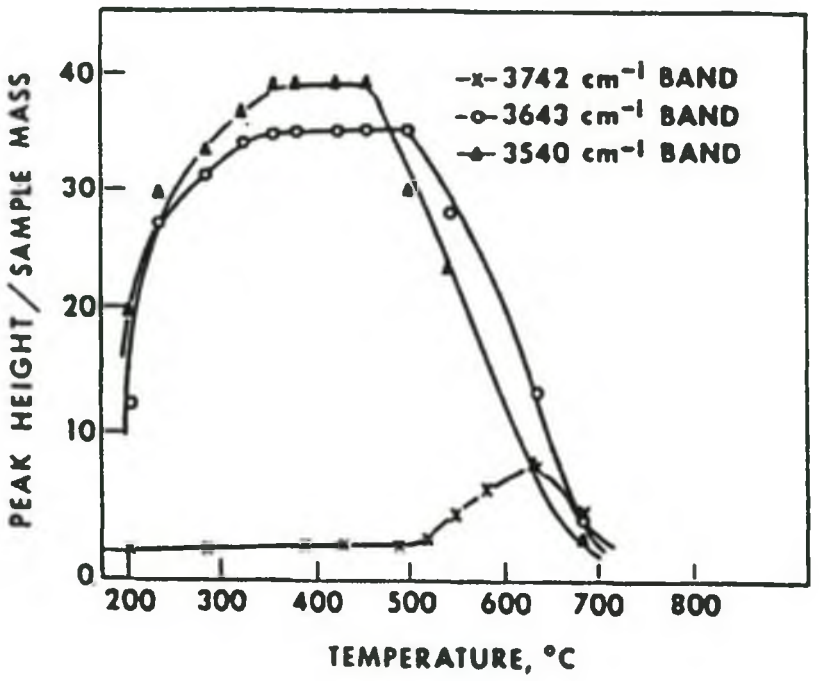

Fig. 1.12. Intensity of the hydroxyl group stretching frequencies of zeolite Y at different calcination temperatures.

Ward has noted that the maximum intensity of the hydroxyl bands of zeolite Y has reached at calcination temperatures of 350°C. Fig. 1.12 shows that the intensities remain constant between 350-500°C, and then they decrease [22]. The 3742 cm^{-1} band intensity increases to a maximum at a calcination temperature of 640°C before decreasing. From these, Ward has concluded that the hydroxyl groups, functioning as Brønsted acid sites, are largely responsible for catalytic activity [22].

The O-H bond of the attached -OH group is covalent [23, 24] and the acid strength for the different types of hydroxyl groups in zeolites differs [21]. It has been widely accepted that the number of Brønsted sites is determined by the number of aluminum atoms in the framework [25]. An important factor, which controls the acid strength of the Brønsted sites, is the lattice composition. As the aluminium content changes, the deprotonation energy, and thus the strength of the Brønsted sites, varies.

Kazansky has found that the covalent hydroxyl interaction energy varies little with acidity and concluded that the factor contributing most to strong acidity is the stabilization of the negative charge left on the framework after deprotonation [26]. The existence of other negative centres (*i.e.* other aluminium atoms in the lattice) in close proximity would hinder this stabilization. Aluminium atoms in the second coordination sphere (*i.e.* the 12 T-atoms which are linked to the acid site by an -O-Si-O- group) lead to a decrease in acid strength [20].

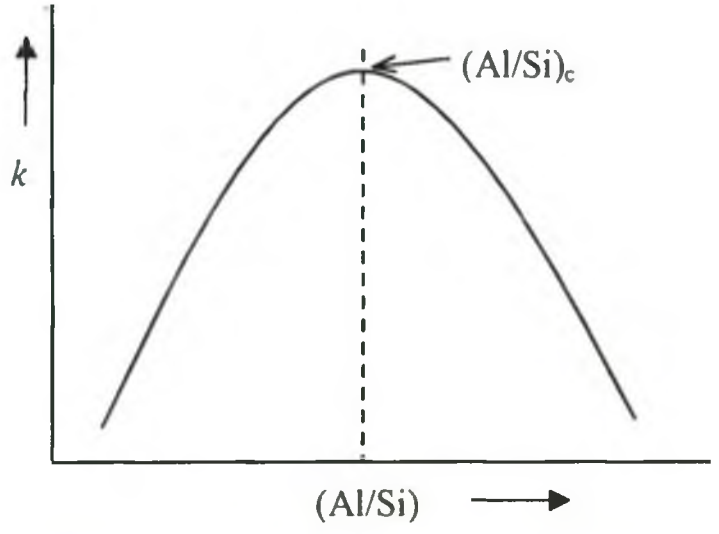

Fig. 1.13. Dependence of acid-catalyzed reaction on zeolite Al/Si ratio. $(Al/Si)_c$ is critical value and k is the rate of reaction.

Brønsted acid-catalyzed reactions will be proportional to the content of a zeolite as long as the intrinsic acidity of a proton remains unchanged, since the proton concentration is proportional to the Al/Si ratio. Once the Al/Si ratio exceeds a critical value $(Al/Si)_c$, the intrinsic acidity of a zeolite proton starts decreasing (Fig. 1.13), resulting in an overall decrease in the rate of reaction [20].

While Brønsted acidity decreases rapidly above calcination temperatures of 500°C, the concentration of Lewis acid sites is small below 475°C, but increases rapidly at higher temperatures (Fig. 1.14).

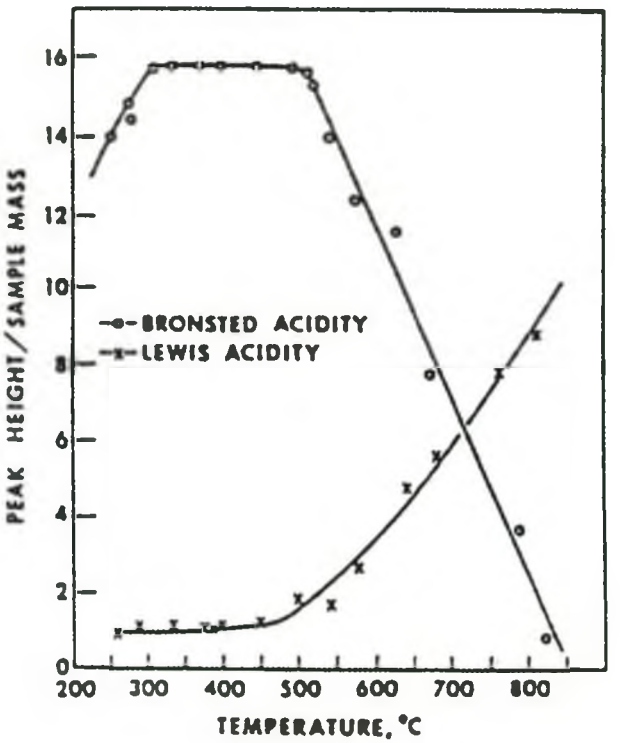

Fig. 1.14. Acid site populations on zeolite Y as a function of calcination temperature.

Uytterhoeven [19] and Ward [22] have suggested that if the Brönsted acid sites are due to hydroxyl groups, then conversion to Lewis acid sites should occur with increasing temperature, according to the following scheme.

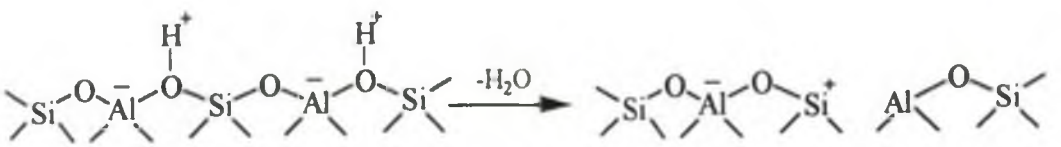

This leaves 3-coordinated silicon and aluminium.

However, Kühl has proposed that 3-coordinated aluminium is removed from the crystal structure by the formation of oxyaluminium species [27, 28]. These AlO^+ or $Al_xO_y^{n+}$ clusters are termed the "true" Lewis sites, and are frequently formed when zeolites are dealuminated by acid or steam treatment [29-32].

1.4. Zeolite synthesis

Zeolites, with the possible exception of silicalites, are synthesized using a system containing H_2O-SiO_2-Al_2O_3-(alkali, alkaline earth, organic cation) at temperatures below 200°C and at autothermal pressures [33]. The chemical sources, which are needed in principle for zeolite synthesis, are given in Table 1.2.

Table 1.2. Chemical sources and their function in zeolite synthesis

Source	Function(s)
SiO_2	Primary building unit of framework
AlO_2^-	Provides framework charge
OH^-	Mineralizer, acts as a host for a guest molecule
Alkali cation, template	Counters framework charge, acts as a guest molecule
H_2O	Acts as solvent and guest molecule

The silicon sources, such as colloidal silica, waterglass or fumed silica, might be different in terms of the degree of polymerization of the Si species. Zeolites are typically synthesized at a pH ranging from 8-12 [34]. In these alkaline solutions, the most abundant forms of Si are monomeric and oligomeric Si species [34], while the most abundant form of Al is monomeric $Al(OH)_4^-$ [35, 36]. The mono- and oligomeric Si and

monomeric Al species react to produce gel containing aluminosilicate structures [37]. Aging of the gel or raising the temperature of the gel increases the depolymerization or dissolution of the Si species. This dissolution will increase the concentration of dissolved silica [37].

The increase in concentration of solute will transform a stable solution into a metastable solution, and finally into a labile one, as shown by Fig. 1.15 [38]. In the labile region nucleation as well as crystal growth are possible, in the metastable region only crystal growth is possible, whereas no nucleation or crystal growth can occur in the stable region. Hence the achievement of supersaturation by depolymerization of Si species is a requirement for nucleation in the labile region.

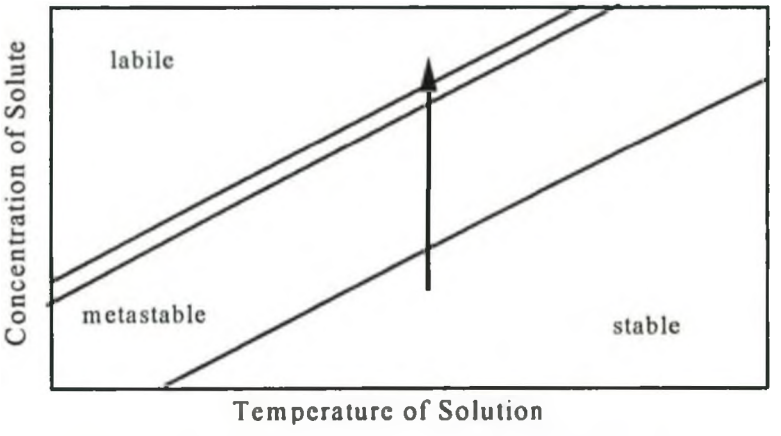

Fig. 1.15. The solubility-supersolubility diagram.

Primary nucleation from a supersaturated solution can be divided into homogeneous nucleation (spontaneous nucleation from clear solutions) and heterogeneous nucleation (induced by impurities, gel phase). Secondary nucleation is induced by the presence of seed crystals [37, 38]. Heterogeneous nucleation occurs at the liquid-gel interface, and crystallization proceeds into the gel, whereas the driving force for crystallization is equal in all directions in homogeneous nucleation [39].

Nuclei will grow by addition or condensation of precursor species towards full-grown crystals. There is general agreement that crystal growth occurs in solution, specifically at the crystal plane-solution interface, probably by condensation of dissolved species onto the growing crystal surface [37]. Hence, as reacting species are being depleted, the system changes from a labile to a metastable and finally to a stable region. There are at least three types of crystal building units involved in crystal growth that have been proposed, *viz.* the primary building unit (the tetrahedral monomeric species), the secondary building units (resembling the SBU's of Meier and Olson), and the cation templating [34].

The chemical composition of a synthesized hydrogel influences the nucleation and crystal growth, nature of the crystalline material, the lattice aluminium content and distribution, the crystal size and morphology.

1.4.1. *Temperature and Time*

An increase in temperature will increase both nucleation and the crystal growth rate [37]. However, H_2O molecules are required to fill the pores and thereby stabilize the porous structure. As a liquid phase is required for this, an upper temperature limit for zeolite formation is to be expected [40]. Crystallinity normally increases with time, and according to Ostwald's rule of successive phase transformations the thermodynamically most stable phase is time dependent [40, 41].

1.4.2. *Alkalinity*

The pH of synthesis solutions is usually between 8 and 12. The role of the OH^- anions in the alkaline conditions is that of mineralizing or mobilizing agents. Mineralizing agents brings the Si and Al species into solution at an adequate rate to create a supersaturated solution, so that nucleation and

crystal growth can occur. In general, increasing the pH shortens the time required for formation of nuclei, and accelerates crystal growth. The Si/Al ratio tends to decrease with increasing pH, as Al incorporation is greater at higher pH [35].

1.4.3. *Templates (structure directing species)*

In aqueous solutions cations are known to influence the ordering of H_2O molecules. *Structure-making* cations such as Na^+ or Li^+ interact strongly with the H_2O molecules because of their high charge density, and the H_2O molecules are (re-)organised around the cations [42]. Cations such as NH_4^+, K^+ and Rb^+ are *structure-breaking* because their interaction with the H_2O molecules is not strong enough to form organised H_2O clusters, thereby "breaking" the H_2O structure [42]. The hydrophobic character of the alkyl chains of organic cations such as tetraalkylammonium ions may be responsible for the H_2O organizing effect near the alkyl chains, thereby stabilizing the H_2O network near the alkyl-chain containing cation. These organised H_2O molecules can be replaced by silicate and aluninate tetrahedra and in this way leads to the formation of zeolite crystal structures [37].

The H_2O molecule is an important templating species. It is affected by interaction with cations, H_2O molecules have the solvating and hydrolyzing ability, and they enhance the formation of a zeolite structure during crystal growth by filling the pore system. This stabilizes the porous lattices [40].

A schematic version of the crystallization of an amorphous alumino-silicate gel to a zeolite is given in Fig. 1.16 [43, 44].

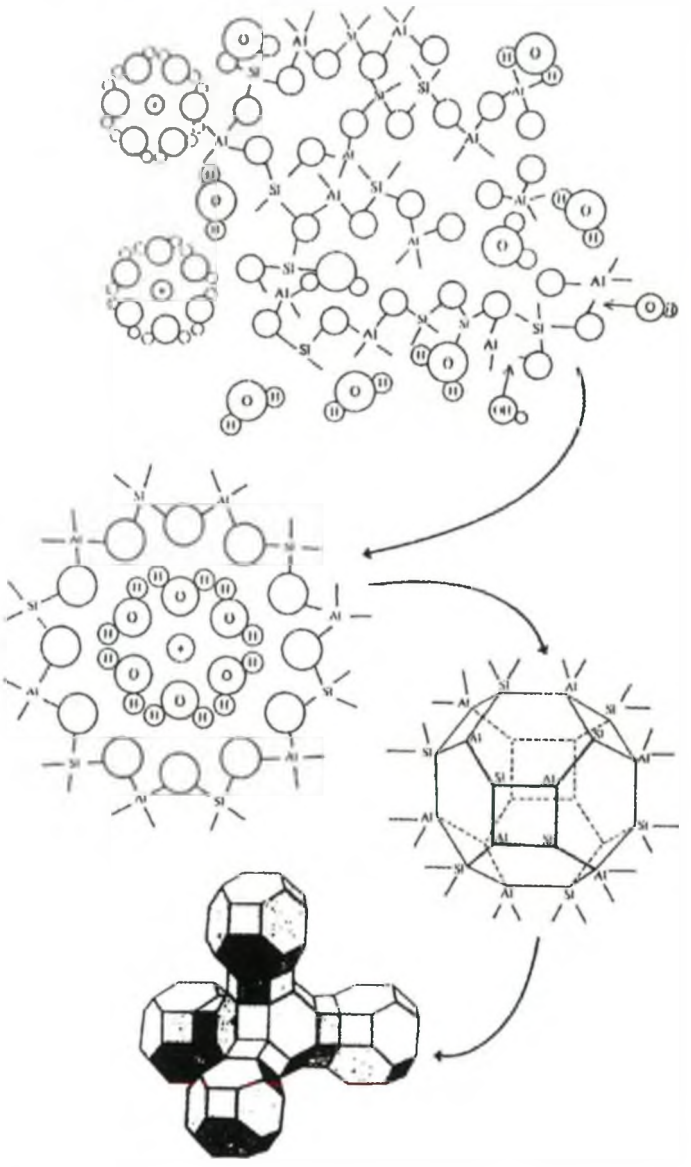

Fig. 1.16. Schematic representation of the formation of zeolite crystal nuclei in a hydrous gel. The gel structure, (centre), is depolymerized by OH^- ions. Tetrahedra regroup about hydrated sodium ions to form the basic polyhedral units.

1.4.4. *Synthesis of ZSM-5*

ZSM-5 can be synthesized with a wide Si/Al ratio. The siliceous analogue of ZSM-5 is Silicalite-1 [45, 46]. ZSM-5 is usually synthesized using the tetrapropylammonium ion (TPA^+) as an organic template. However, the synthesis of ZSM-5 in the presence of other amines, alcohols or without organic template has also been reported [42, 47]. Nagy *et al.* [48] has reported that the number of TPA^+ ions in ZSM-5 corresponds with number of channel intersections, suggesting that the TPA^+ ions act as structure directing templates located at the channel intersections.

Nucleation of ZSM-5 is found to be more rapid with structure-making alkali cations (Li^+, Na^+) than with structure-breaking alkali cations (K^+, Rb^+, Cs^+) [49] and at higher pH values [50, 51]. High nucleation rate produces large number of smaller crystals, whereas smaller numbers of larger crystals are formed at low nucleation rates.

It has been observed that during ZSM-5 synthesis the crystallization rate and crystallite size decreases when the Al content increases [52]. The incorporation of Al into the structure is disruptive, and leads to the growth of smaller crystals. In ZSM-5, aluminium zoning may occur in the crystals [53-57].

1.5. Modification of zeolites

Due to the microporous character with uniform pore dimensions, zeolites have created significant interest in adsorption and separation technology, and in catalysis. To control the solid acidity and shape selectivity, post-synthesis modification of a zeolite is carried out by different ways [58]:

a) *Structural modification:* The framework SiO_2/Al_2O_3 ratio is changed resulting in a change in acid activity. The techniques involved:

(i) dealumination of zeolites

- by hydrothermal treatment (steam dealumination) [59-62]
- by reaction with chelating agent [e.g. ethylenediamine tetraacetic acid (EDTA), acetylacetone (ACAC)] [60, 63,64]
- by reaction with $SiCl_4$ (or other halide) vapour [65, 66]
- by hydrothermal chemical treatment with acids (e.g. HNO_3), bases (e.g. NaOH) and salts (e.g. KF) [67] and

(ii) stoichiometric exchange of Al^{3+} by Ga^{3+}, B^{3+}, Fe^{3+} ions [68, 69].

b) *External surface modification:* Selected size of pore opening is achieved by the addition of large organometallic species on the surface of the zeolite crystal, which is not adsorbed into the pore system. Chemical vapour deposition (CVD) methods have been developed for modification of surface for its coating applications in the semiconductor industry and catalysis. CVD technique is the deposition of a coating from the vapour phase onto the surface of zeolite. This technique only considers the modification of the surface of pores and not the modification of the structure itself. An exception is the solid/vapour reaction of the zeolite with $SiCl_4$ that modifies the structure as well as the surface of the crystal. Such a modification will depend on the zeolite [70]. On the other hand, $Si(OMe)_4$, or $Ge(OMe)_4$, reacts only with the surface of a crystal [71-74].

c) *Internal pore modification:* This is done by blocking or altering the structural acid sites and /or by restricting the internal pore diameter. Adsorption and subsequent decomposition of small inorganic molecules, silane and diborane, can give these kinds of modification in the zeolite structure [75].

The shape selectivity of a zeolite can be improved by controlling the factors: like crystal size, pore size, strength of acidity and external surface.

1.6. Characterization of zeolites and modified zeolites

Before a zeolite can be used for a certain application it is necessary to characterize this zeolite, to see if it has the desired properties for that application. Zeolite syntheses, modification, characterization and application are strongly interrelated (Fig. 1.17).

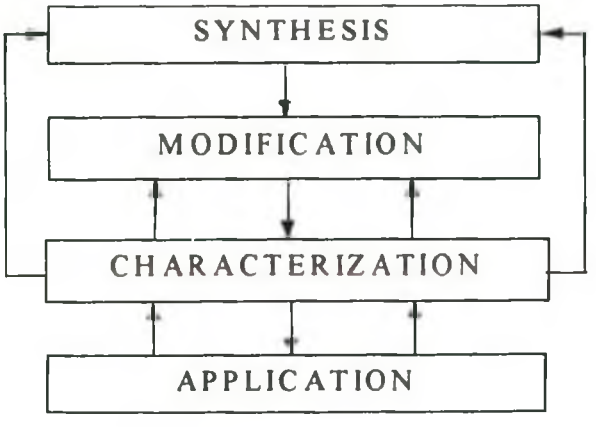

Fig. 1.17. Schematic representation of interrelation of zeolite characterization.

Zeolites and modified zeolites can be characterized in terms of their structures and structural defects, pore structures and their acidity.

1.6.1. *Zeolite structure and structural defects*

The best way to check zeolite structure is by X-ray diffraction (XRD). This method is based on the fact that every crystalline material has its own characteristic X-ray diffraction pattern. Normally the first check is the comparison of the observed X-ray diffraction pattern with the simulated pattern.

The intensity of the diffraction peaks can be used to determine the crystallinity of the samples. For that purpose the intensity of one particular peak (or a number of peaks) is compared with the intensity of the same peak (or peaks) of a standard sample.

The X-ray crystallinity then can be calculated from the following equation: [76]

$$\text{X-ray crystallinity} = \frac{\text{Intensity of peak hkl of sample}}{\text{Intensity of peak hkl of standard}} \times 100\% \quad \ldots\ldots 1.1$$

Furthermore, the width of the diffraction peaks gives information about the average crystallite size of the investigated zeolite sample.

According to Scherrer [77], the relation between linewidth (B) and crystallite size (t) is given by the following formula.

$$t\,(\text{nm}) = \frac{0.9\,\lambda\,(\text{nm})}{B\cos\theta} \quad \ldots\ldots 1.2$$

X-ray diffraction thus can give information about crystal structure, degree of crystallinity and crystallite size. It is, however, impossible to obtain information about the presence of structural defects by this method. The presence of fault planes and/or stacking faults in the structure can be observed by high-resolution electron microscopy (HREM) such as

scanning electron microscopy (SEM), transmission electron microscopy (TEM), etc.

1.6.2. *Pore structure of zeolites*

For use as molecular sieve or as shape selective catalyst it is essential to characterize the zeolite system. Adsorption measurements with molecules of different sizes give direct information about the dimensions of the pore system.

Generally, the adsorption isotherm (the amount of gas adsorbed as function of the partial pressure of the gas at constant temperature) gives information about the pore structure. This is the method often applied for characterizing materials having meso (2-50 nm) and macropores (>50 nm). Problems arise, however, in the characterization of micropores (<2 nm) the dimensions of which are close to those of the adsorbing molecules. In this case the adsorption process is a filling of the micropores instead of multilayer adsorption on which the interpretation of adsorption isotherms is generally based.

This, together with the requirement to measure the adsorption isotherms at very low pressures, make it very difficult to obtain detailed information on the pore structure of zeolites by this method.

At the moment there are two comparable methods that are reported in literature and by which it is possible to determine the micropore volume of zeolites from the N_2 adsorption isotherm. These are:

(i) t-plot method: The volume of the adsorbed N_2 is plotted against the statistical thickness (t) of the adsorbed layer [78]. This results in a straight line and extrapolation to t = 0 gives the micropore volume.

(ii) α_s method: The volume of the adsorbed N_2 is plotted against the reduced standard adsorption (α_s) [79]. Extrapolation to $\alpha_s = 0$ gives, again, the micropore volume.

1.6.3. *Determination of zeolite acidity*

The acidity of zeolites is mainly caused by the presence of Brønsted acid sites but high temperature treatments may also generate Lewis acid sites, described in Section 1.3.

For complete characterization of zeolite acidity it is therefore, necessary to determine number and strength of both types of acid sites. Of the several methods that have been develop for this purpose the most important are:

- titration methods
- adsorption of bases
- desorption of bases
- IR spectroscopy
- NMR spectroscopy

1.6.3.1. Titration methods

The acid-strength of a Brønsted acid depends on its proton donating ability. To determine such acidity of solid acids a number of aniline bases are used as indicators. Acids of different strength give different colour changes in the presence of these indicators [80]. However, it is not possible to distinguish between Brønsted and Lewis acidity by the indicator method. Moreover, the indicator molecules cannot enter the zeolite pores, and thus can react only with the acid sites at the outer surface of the zeolite.

1.6.3.2. Adsorption of bases: Calorimetric measurements

When an acid is neutralized by a reaction with a base the enthalpy change takes place. The enthalpy of neutralization is larger for the stronger acids and it can be used to characterize the acid-strength. Auroux *et al.* [81] have used this method for several zeolites, such as H-ZSM-5 and Na-ZSM-5. The drawbacks of this method are the accessibility of the acid sites and the long time is needed to reach equilibrium.

1.6.3.3. Desorption of bases: Temperature programmed desorption (TPD)

When bases come in contact with acid sites of zeolites, they are adsorbed there. Higher temperatures are needed to desorb bases from strong acidic sites than that required for weaker acidic sites. This temperature difference can be used to characterize the acid sites present in a zeolite sample. Temperature programmed desorption (TPD) of ammonia is one of the important method to measure the interaction between solid acid and the simple base molecule. It is convenient for quick determination of the number of acid sites on zeolites [82-86]. First, the zeolite is brought in contact with base (NH_3) to neutralize the acid sites present. Then the temperature is raised at a constant rate and the amount of desorbed base is recorded [either by mass spectrometer (GC-MS) or by a thermal conductivity detector (TCD)]. In this way a desorption spectra is obtained (Fig. 1.18).

Usually, two desorption peaks are observed in the TPD spectra, as shown in Fig. 1.18. These are named *l*- and *h*-peaks due to the low and high temperatures of desorption, respectively. The *h*-peak is the desorption peak of ammonia which is adsorbed on the acid sites, whereas the *l*-peak is assigned to ammonia weakly held or physically adsorbed on the zeolite.

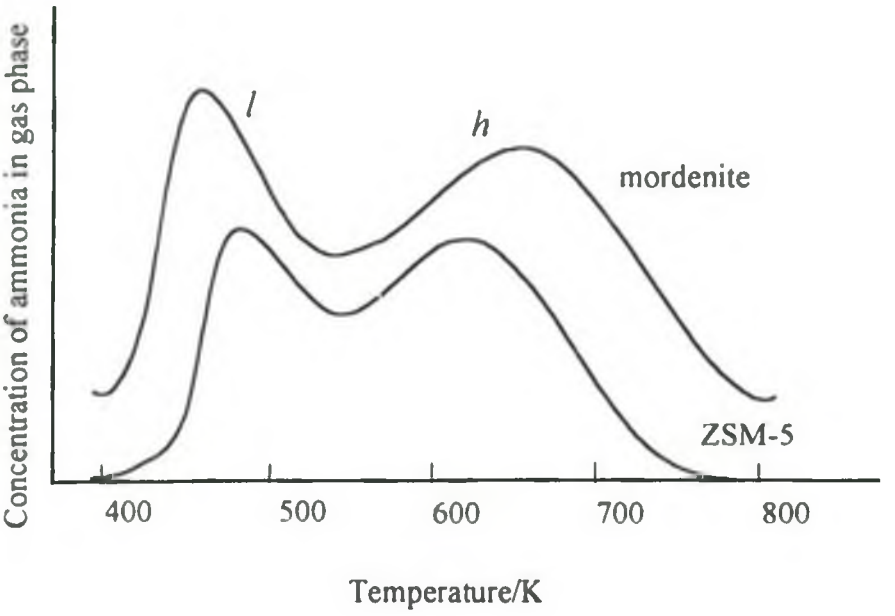

Fig. 1.18. TPD spectra on H-mordenite (SiO_2/Al_2O_3 = 15.0) and H-ZSM-5 (SiO_2/Al_2O_3 = 23.8).

The *l*-peak is identified by the desorption experiment. The *l*-peak is removed by evacuation after ammonia is adsorbed. It is found that prolonged evacuation at 373 K for 16 h removes the *l*-peak completely, but it does not affect the *h*-peak at all [87]. On the Na-type zeolites, only the *l*-peak is observed because the Na-type zeolite does not have any acidity.

Addition of water vapour to the carrier gas deleted the *l*-peak completely, while it does not affect the *h*-peak at all. When water is adsorbed, the H_2O molecules replace ammonia molecules of the *l*-peak. This interesting experiment is an evidence in the identification of the *l*-peak [88].

In the quantitative measurement of the acid sites, only the *h*-peak is important. The intensity of the *l*-peak or the total intensity of *l*- and *h*-peaks has no physical meaning, although these have been measured and discussed frequently in the literature. The intensity of the *l*-peak is neither

correlated with the number of weak acid sites, nor with any activity of catalytic active sites.

The TPD spectrum is analyzed by the curve fitting method. The measurement of the acid strength and the distribution of the acid sites based on the assumption that equilibrium exists between the gaseous and adsorbed ammonia, and the readsorption of ammonia freely occurs [89]. The experimental TPD spectrum is simulated by a theoretical spectrum. The concentration of ammonia at different temperatures can be calculated from the following equations

$$C_g = -\frac{\beta A_0 W}{F}\frac{d\theta}{dt} = \frac{\theta}{1-\theta}\frac{P^0}{RT}exp\left(-\frac{\Delta H}{RT}\right)exp\left(\frac{\Delta S}{R}\right) \quad \text{.....1.3}$$

Here C_g is the concentration of ammonia in gas phase (mol m^{-3}), β is the heating rate (K s^{-1}), A_0 is the amount of desorbed ammonia (mol kg^{-1}), W is the sample amount (kg), F is the flow rate of the carrier gas (m^3 s^{-1}), θ is the surface coverage, P^0 is the pressure under standard conditions (1.013×10^5 Pa), R is the gas constant (8.314 J K^{-1} mol^{-1}), T is the temperature (K), ΔH is the enthalpy change (adsorption enthalpy of ammonia, J mol^{-1}), and ΔS (JK^{-1} mol^{-1}) is the standard entropy change of 95 J K^{-1} mol^{-1}. The parameters ΔH_{avg}, the averaged value of ΔH, σ, distribution (standard deviation) of ΔH, are adjusted to fit the simulated curve with the observed one. Thus the set of data which give the best fitted curve is selected, and this show the acidic property of the zeolite sample.

1.6.3.4. IR spectroscopy

A more direct study of the Brønsted-acidic -OH groups in zeolites is possible by IR-spectroscopy [90], is based on the dependence of the O-H stretching frequency on the acidity.

The weaker the O-H bond, the lower the stretching frequency and the higher the acid-strength. Fig. 1.19 shows a typical IR spectrum of a thin wafer of HNaY after dehydration.

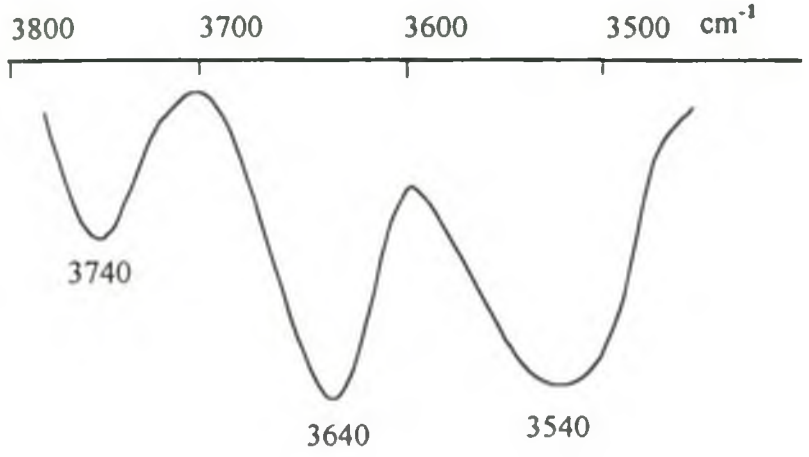

Fig. 1.19. IR spectrum of HNaY.

The spectrum shows three peaks in the O-H stretching region. The peak at 3740 cm^{-1} is assigned to the non-acidic silanol group that are present at the outer surface of the zeolite crystals and at structural defects.

The peaks at 3640 cm^{-1} and 3540 cm^{-1} correspond to -OH groups having lower O-H bond strength. One of these bands, at 3640 cm^{-1}, disappears after adsorption of pyridine. Accordingly, this band is assigned to the accessible acidic -OH group.

1.6.3.5. ^{29}Si and ^{27}Al MAS-NMR

Since the introduction of the magic angle spinning (MAS) technique to NMR spectroscopy it is possible to obtain high resolution spectra from solid samples. Lippmaa *et al.* [91], has the first who applied this method in 1981 to record the ^{29}Si-spectra of zeolites. Since then the technique has

been developed rapidly and at the moment it is widely applied in zeolite research.

Application of the ^{29}Si MAS-NMR technique to zeolites helps in finding a number of separate Si peaks in spectra. For the faujasite structure, in which all T-atoms (Si and Al) are crystallographically equivalent, it is possible to distinguish up to five different peaks that can be attributed to Si connected to 0, 1, 2, 3 and 4 Al atoms, respectively through oxygen (Fig. 1.20).

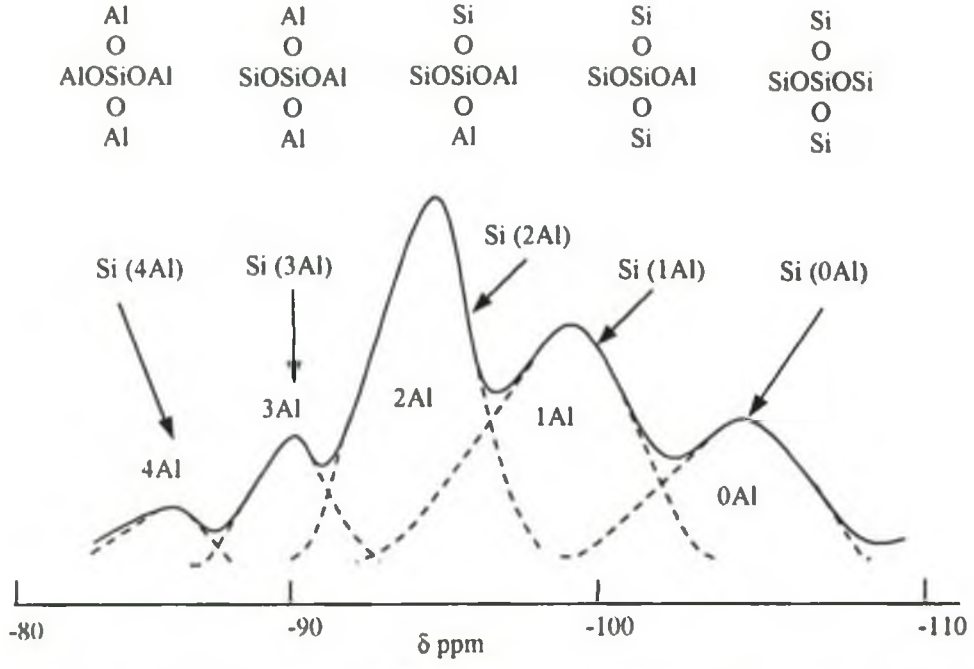

Fig. 1.20. ^{29}Si MAS-NMR spectrum of NaY zeolite with Si/Al = 2.5.

As the intensity of a peak is proportional to the number of the Si atoms concerned, it is possible to calculate the total number of Si atoms (N_{Si}) by summation of the peak intensities where C is the proportionality constant [92].

$$N_{Si} = C.\sum_{n=0}^{4} I(Si - nAl) \qquad \ldots\ldots\ldots\ldots\ldots\ldots 1.4$$

If the Löwenstein rule is obeyed, every framework Al atom is surrounded by 4 Si atoms. So, the total number of framework Al atoms can be calculated from:

$$N_{Al} = C \sum_{n=0}^{4} \frac{n}{4} I(Si - nAl) \qquad \text{..... 1.5}$$

The framework Si/Al ratio can then simply be calculated from:

$$Si/Al = \frac{N_{Si}}{N_{Al}} = \frac{\sum_{n=0}^{4} I(Si - nAl)}{\sum_{n=0}^{4} \frac{n}{4} I(Si - nAl)} \qquad \text{..... 1.6}$$

In principle, it is possible to determine Al directly by ^{27}Al MAS NMR. In practice, however, several problems can arise that hamper the interpretation of the results. The main reason for these problems is the fact that the Al nucleus possesses a quadrupole moment that may give rise to strong line broadening especially in the case that the Al is present in a low symmetry environment.

1.7. Shape selective catalysis and adsorption

If the majority of the catalytic sites are confined in the channel structure and if the channels are small, the fate of the reactant molecules and the probability of forming product molecules are determined mostly by molecular dimension and configuration. Molecules with dimensions less than a critical size only can enter the channels, to have access to internal catalytic sites, and react there. Furthermore, only unretained molecules can appear in the final product. Catalysts displaying such selectivity are said to be shape selective.

Csicsery [93] has distinguished between three types of shape selectivity. In *reactant shape selectivity* some of the molecules in a reactant mixture are too large to diffuse through the catalyst channels to reach active sites. In *product shape selectivity* only product molecules with sufficiently small dimensions can diffuse out of the channels and appear as products. In *restricted transition state shape selectivity* certain reactions are prevented because the corresponding transition state requires more space than is available in the cavities or channels of the catalyst (Fig. 1.21) [94]. Reactant and product selectivities are mass transfer limited and are therefore affected by crystallite size, whereas transition state selectivity is not.

An additional concept of secondary shape selectivity has been introduced by Santilli and Zones [95]. When, as in the above cases, shape selectivity is a result of direct interactions between molecules and a channel system, the term *primary shape selectivity* is applied. In zeolite catalysis, *secondary shape selectivity* occurs when one molecule interferes with the reactivity of another because of steric constraints imposed by the channels. Secondary shape selectivity is a phenomenon, which does not happen, in an unhindered environment.

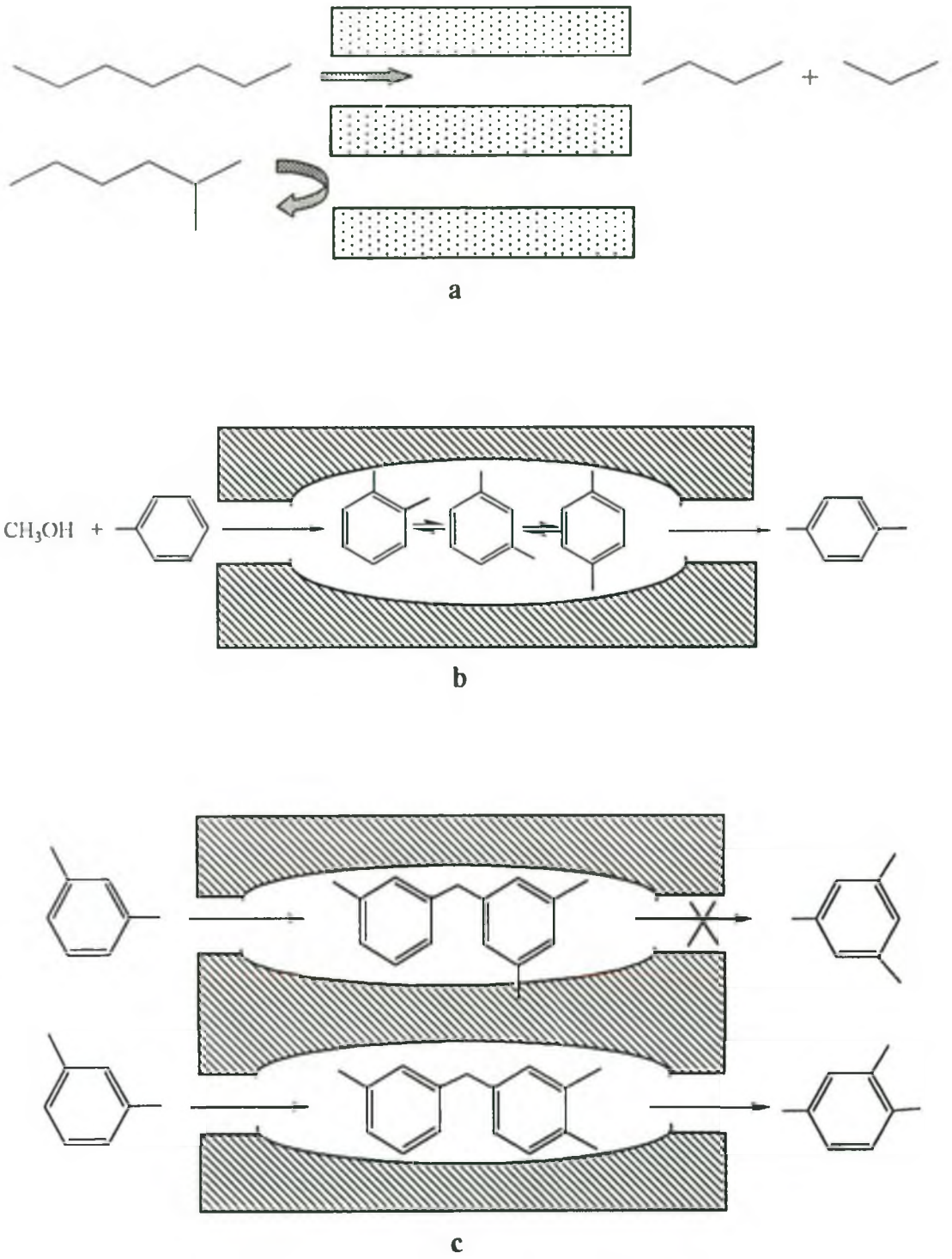

Fig. 1.21. Different types of shape selectivities. (a) Reactant selectivity, (b) product selectivity, (c) restricted transition-state selectivity.

An extension of this type of shape selectivity is *inverse shape selectivity* [96]. This type of shape selectivity is the result of the repulsive forces between the zeolite and the reactants. In this case transition states or products tend to favour the reaction, production or diffusion of sterically smaller molecules. Inverse shape selectivity occurs when attractive forces alter the catalytic and adsorptive selectivities of molecules. Hence sterically larger molecules may be adsorbed or converted preferentially because of greater attractive forces between the channel walls and the larger molecules.

Denounce [97] has suggested that molecular shape selective effects are not necessarily restricted to the intracrystalline volume of the zeolites, although this would clearly favour their occurrence. He has suggested that molecular shape selectivity should occur whenever a catalyst selects or prefers specific reactants or products on the basis of their size and shape in order to match its own active site steric requirements. The external surface of zeolites offers channel openings and cut channels (half cavities) due to their framework structure.

Zeolites are used as an adsorbent to separate mixtures in the gas or liquid phase. The principle of separation using zeolite is based on the difference in the equilibrium constant of adsorption or its molecular sieving effect. The molecular sieving by dehydrated zeolites is caused by the difference between their sizes and adsorbate molecules and/or differences between the pore opening dimensions [98].

Molecules with kinetic diameters smaller than the pore openings can be adsorbed, but not the larger molecules. In boundary cases a minimum temperature of adsorption may be required. The molecular sieve effect is illustrated in Fig. 1.22 for calcium A zeolite with an 8-ring pore of oxygen.

n-Octane (Fig. 1.22a) readily accesses the internal void through the pore whereas *iso*-octane (Fig. 1.22b) is larger than the pore and is excluded [99].

a b

Fig. 1.22. Molecular sieve effect of CaA zeolite, (aperture 0.50 nm), (a) *n*-octane (kinetic diameter σ = 0.43 nm) penetrates through eight ring aperture and (b) *iso*-octane (kinetic diameter σ = 0.50 nm) cannot penetrate.

1.8. Chemical vapour deposition (CVD) -A survey of relevant work

The review is about the modification of zeolites by the chemical vapour deposition (CVD). This only includes the methods of CVD, deposition mechanism, conservation of the internal zeolite structure, control of pore-opening, factors affecting the deposition, shape selective adsorption and associated reactions.

Chemical vapour deposition (CVD) is an important method to modify the external surface and pore-opening size to improve the molecular sieving property and catalytic activity of zeolites. Mainly silicon based compounds have been used to cover the external surface of zeolites with silica [100]. These silicon based compounds are so chosen that they do not enter into the channels of the zeolite. The externally deposited silicon compounds are decomposed to form a silica layer inertising the external surface of the zeolite.

The silicon based compounds that have been used including $Si(OCH_3)_4$ [101], $Si(OC_2H_5)_4$ [102, 103], $Si(OC_4H_9)_4$ [102], $Si(OCH_3)(CH_3)_3$, $Si(OCH_3)_2(CH_3)_2$, $Si(OCH_3)_3(CH_3)$ and $Si(OCH_3)(C_3H_7)_3$ [100], $Si(CH_3)_4$ [104]. Tetramethoxysilane ($Si(OCH_3)_4$, TMOS) and tetraethoxysilane ($Si(OC_2H_5)_4$, TEOS) are mostly used silane compounds for CVD. The molecular diameters of TOMS and TEOS are 0.89 ± 0.02 nm [101] and 0.96 ± 0.02 nm [105] respectively.

Chemical vapour deposition methods have been used to deposit silicon compounds on the external surfaces of zeolites such as Mordenite [71, 101, 106], HZSM-5 [102, 107, 108], Beta zeolite [109], zeolite A [73, 110], zeolite Y [105], Offretite [111], zeolite ZK-5 [112, 113] and zeolite Rho [112]. Moreover, chemical vapour deposition has been used to create

Brønsted acidity by depositing silica on, alumina [114, 115] or titania and zirconia [116].

Richter *et al.* have reported to use 12-tungstosilicic acids for modification of zeolite surface [117]. The Keggin unit, $(SiW_{12}O_{40})^{4-}$, does not appear to penetrate the ZSM-5 channel system but becomes deposite on the external surface. On thermal decomposition, WO_3 is highly loaded and the acid sites in the channel system are lost. This is not exclusively caused by further dealumination but it is partially attributed to site blocking by WO_3. Obviously, the decomposition of the acid involves mobile species of smaller sizes which are able to migrate into the interior of the zeolite.

1.8.1. *Methods of deposition*

Three methods of depositing silicon compounds have been employed, *viz.* (i) a static vacuum system [71, 74], (ii) a vapour phase flow system [102, 118], and (iii) liquid phase deposition [106, 112, 119]. The conditions used for the deposition vary considerably.

In chemical liquid deposition, silicon alkoxide is typically deposited at ambient temperature in the presence of a diluent such as toluene or *n*-hexane. In vapour phase flow system, silicon alkoxide in a mixed vapour of toluene, methanol or water is typically passed over the desired zeolite at elevated temperature. Usually, silicon alkoxide is pure when a static vacuum technique is used. However, the sample has been exposed to moisture can also be used. Deposition temperatures range from ambient to high temperature.

1.8.2. *Deposition mechanism of silicon alkoxides*

Niwa and co-workers have analyzed the deposition of silicon alkoxides on Mordenite [71, 104] and HZSM-5 [74]. Static vacuum technique has been used, at various temperatures. The amount of deposition has been controlled by varying the zeolite mass, partial pressure of silicon alkoxide and by repeating the deposition procedure. The weight gain is measured by a microbalance.

Niwa *et al.* have further reported that during deposition of TMOS at ambient temperatures, decomposition products (methanol, dimethyl ether) are adsorbed by Mordenite [104]. These are subsequently desorbed by raising temperature. When TMOS has been deposited at 220°C on Mordenite, methanol and dimethyl ether are detected by gas chromatography. At higher deposition temperatures, *viz.* 320°C, lower hydrocarbons such as ethylene and propane are detected. Possibly these products are due to methanol conversion on Mordenite surface. However, hydrocarbons with more than 4 carbon atoms have not been found.

The layer deposited on Mordenite has been studied by IR spectroscopy [71]. Deposition of TMOS at 200°C revealed the C-H stretching at 2900 cm^{-1} as well as at 1600, 1480 and 1370 cm^{-1}. The band corresponding to -OH group of Mordenite at *ca.* 3600 cm^{-1} becomes broad upon deposition. The sample is then evacuated successively at 265, 315, 370 and 400°C. Evacuation at 265°C does not change the IR spectrum. At 315°C the C-H stretching at 2900 cm^{-1} is missing, the 1480 cm^{-1} band is diminished in intensively and the O-H band at 3600 cm^{-1} is reappeared. After exposure to oxygen at 400°C, the original IR spectrum of the Mordenite sample is restored. It is to be noted that calcination removes the IR bands at 1600 and 1370 cm^{-1}. Hence adsorbed residue during the deposition of TMOS is desorbed above 300°C, and irreversibly deposited carbonaceous material is

removed only by calcination. Further, Brønsted acid sites are not altered by the deposition of TMOS, although they are affected by the adsorbed organic molecules at relatively low temperatures.

When TOMS deposits on SiO_2, the intensity of absorbance of the isolated Si-OH group decreases, whereas a band at 1460 cm^{-1} strongly indicates the presence of a methoxy group in the sample. A broad band at 3400 cm^{-1} indicates the presence of adsorbed methanol [104]. Only by evacuation the methoxy bands do not completely disappear. However, all the methoxy bands are disappeared upon reaction with water at 320°C.

Niwa *et al.* [104] have selected silanes compounds like $Si(OCH_3)_4$, $Si(OCH_3)(CH_3)_3$ and $Si(CH_3)_4$ for vapour deposition. $Si(CH_3)_4$ has been found to be most reactive. This is because $Si(CH_3)_4$ is physically adsorbed and does not deposite on Mordenite. This observation led to conclusion that the methoxy group has to be present for successful deposition of the silane. It is also found that $Si(OCH_3)_4$ is more reactive than $Si(OC_2H_5)_4$ [120]. Kim *et al.* [100] have investigated the use of $Si(OCH_3)(CH_3)_3$, $Si(OCH_3)_2(CH_3)_2$, $Si(OCH_3)_3(CH_3)$, $Si(OCH_3)_4$ and $Si(OCH_3)_3(C_3H_7)_3$. It has been concluded that $Si(OCH_3)(CH_3)_3$, $Si(OCH_3)_2(CH_3)_2$ and $Si(OCH_3)_3(CH_3)$ can enter the channels of HZSM-5 and inertise the internal acid sites, whereas $Si(OCH_3)_4$ and $Si(OCH_3)$ $(C_3H_7)_3$ cannot. As $Si(OCH_3)(C_3H_7)_3$ has only one methoxy group, Kim *et al.* [100] have proposed that, it stabilizes on the surface as an isolated species. $Si(OCH_3)_4$ has four functional methoxide groups, and can be polymerized into a siloxane network structure (...Si-O-Si-...), which can ultimately lead to effective control of the pore-opening size.

Based on the above considerations, a scheme of reaction mechanism for the deposition of TMOS on zeolites is proposed by Niwa *et al.* [104], shown in Fig. 1.23. First, the alkoxide attracts to hydroxyl oxygen on the

external surface, subsequently anchors onto as trimethoxide and yield trace methanol. The trimethoxide is then hydrolyzed, either by exposing the sample to water or by water remained in the zeolite system, leading to the formation of new hydroxyl groups. The newly formed hydroxyl groups react further with the gaseous alkoxide or the vicinal trimethoxy group. Subsequently polymeric silica layer consisting of siloxane bonds (...-Si-O-Si...) is obtained. The carbonaceous residue can be removed by calcination.

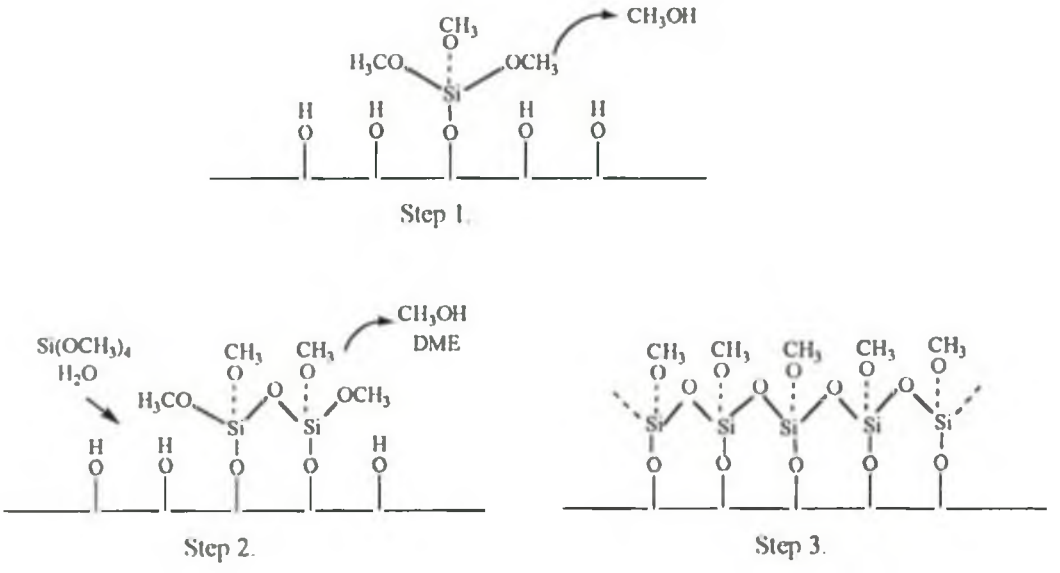

Fig. 1.23. Reaction scheme for the chemical vapour deposited TMOS.

1.8.3. *Conservation of the internal zeolite structure and acidity*

Temperature programmed desorption of ammonia (NH_3-TPD) studies of H-Mordenite [71] and HZSM-5 [74] indicate that neither the peak temperature nor the desorbed amount of NH_3 changes the samples which are modified by TMOS deposition in a static vacuum system. Bhat *et al.* [121] have reported that there is no change in the NH_3-TPD spectrum or the amount of NH_3 desorbed from HZSM-5 when TEOS is deposited on the catalyst by vapour phase flow system.

Both the H_2O (kinetic diameter, σ = 0.265 nm) and N_2 (σ = 0.364 nm) adsorption capacities and adsorption rates on the TMOS modified Mordenite and the HZSM-5 samples remain unchanged [71, 74, 107]. However, for larger molecules such as *p*-xylene (σ = 0.585 nm) and *o*-xylene (σ = 0.68 nm) the adsorption rates decrease significantly with increasing amounts of deposited TMOS. Niwa *et al.* [101] have also reported on the rates of hexane, 2-methyl pentane and 2,2-dimethyl butane sorption on modified Mordenite. The suppression of rate is more effective especially for the branched molecules by increasing amount of TOMS deposition on modified Mordenite.

The NH_3-TPD and adsorption capacity studies shown that the internal zeolite structure and acidity are conserved (*i.e.* TOMS and TEOS deposition do not affect the internal volume and acid sites of the zeolites). However, it has been shown that [110] lower olefins (C_2H_4, C_3H_6, and 1-C_4H_8) can be separated by controlling the pore-opening size of TMOS modified zeolite A. Oxygen and nitrogen can also be separated by controlling the pore-opening size of TMOS modified zeolite A [73].

X-Ray photoelectron spectroscopy (XPS) has also showed an increase in the silicon content on the surface of Mordenite samples modified with TMOS in a static vacuum system [71], and of HZSM-5 samples modified with TEOS in liquid phase [119]. This confirms that the silicon alkoxides are not deposited uniformly in the zeolite bulk, but that the external surface is enriched in silicon.

1.8.4. *Control of the pore-opening size*

Niwa *et al.* [74, 101] have calculated the number of layers of silica that are formed on the external surface from the weight gain, assuming that the deposited silica forms a layer structure. The number of layers required to

obtain shape-selectively improved HZSM-5 is about four to six layers [74], but only one to three layers are required for Mordenite [74, 101]. Furthermore, Hibino *et al.* [122] have shown that the acidity diminishes as the number of layers increases. Approximately four silica layers are required to eliminate the conversion of 1,3,5-triisopropylbenzene over both Mordenite and HZSM-5.

In order to obtain a better understanding of the deposited layer and its control over pore-opening size, germanium alkoxides have been used. GeO_2 layer on the external surface of Mordenite is formed and it is possible to distinguish between the deposited GeO_2 layer and the zeolite [72, 123]. Spectroscopic techniques such as EXAFS, SPS and TEM can be used to analyze the structure of the deposited GeO_2 layer. The uniformity of the pore-opening size depends on sorption profiles of molecules like water, *n*-hexane and *p*-xylene. When the CVD-Mordenite is stored under humidity of 100 % followed by heating it at 500°C, the deposited GeO_2 is found to be transformed from an ultra-thin layer into bulky particles on the external surface. The shape-selectivity is gradually deteriorated with the increase of particle size. This does not occur for samples stored under dry conditions.

1.8.5. *Factors affecting the deposition*

To obtain different amounts of silica on the external surfaces, various parameters have been altered for the different methods of deposition. While a static vacuum system has been used, the deposited amount is measured *in situ* in a microbalance by changing the sample size or the partial pressure of the silicon alkoxide [71, 74]. To obtain highly deposited samples, the deposition has been repeated up to 7 times after the evacuation [74]. The deposition temperature or the time period, during which the silicon alkoxide mixture is exposed to the catalyst in a vapour

phase flow system, varies to change the amount of deposition on the sample [109, 121]. In liquid phase deposition, the concentration of the silicon alkoxide mixture has been varied [112, 119].

To obtain 50 % TEOS deposition over HZSM-5, SiO_2-Al_2O_3, γ-Al_2O_3 and kieselguhr by varying temperature in a vapour phase flow system. From this, Wang *et al.* [102] has concluded that the rate of TEOS decomposition strongly depends on the strength of the acid sites. Hibino *et al.* have reported that Mordenite samples with Si/Al ratios of 9.9, 19.9 and 36.8 requires similar amount of TMOS deposition to reduce the conversion of 1,2,5-triisopropylbenzene, which is used as a measure of the external surface acidity, by the same degree [122]. IR-studies show that the alkoxide reacts with the terminal silanol (Si-OH) groups (Section 1.6.3.4). The external surface acidic hydroxyl (Al-OH) groups are inertises by the conversion of 1,3,5-triisopropylbenzene. From this it has been concluded [122] that the alkoxide also reacts with the external surface acidic hydroxyl groups. Because the Si/Al ratio has no effect on the degree of inertisation of the Mordenite samples, it has been [122] proposed that the alkoxide reacts equivalently with both terminal silanol and acidic hydroxyl groups. This is contrary of the conclusions of Wang *et al.* [102]. However, the pore-opening size depends on the Si/Al ratio [122]. The pore opening of highly siliceous Mordenite is not readily narrowed. The silica layer consists of Si-O-Si bonds, whereas the zeolite contains both Si-O-Si and Si-O-Al bonds, resulting in different bond lengths or bond angles between the silica layer and the zeolite. This difference becomes larger as the aluminium content of the zeolite increases. The Si-O-Si bond of the silica layer protruded into the pore, and narrow the pore-opening size to a greater extent for zeolites with a low Si/Al ratio than that of siliceous zeolites [122]. This may explain why the shape-selectivity of a relatively aluminium-rich Mordenite improves with the deposition of one to three layers of silica, whereas four to six layers are required for a relatively

siliceous HZSM-5 [74].

Comparing HZSM-5 samples with varying morphologies and crystal sizes, the crystallites with greater specific external surfaces (e.g. small or rough crystals) require greater amounts of silica deposition than crystallites with relatively smaller specific external surfaces (e.g. large or regular crystals) [102, 108]. In addition, it has been reported that when extra-framework aluminium species existed on the external surface of HZSM-5, the amount of silica deposition required to inertise the external surface increased [107, 108, 122]. Hibino *et al.* have reported that the degree of inertisation of the external surface of Mordenite does not depend on the cation, like Na^+ or H^+.

1.8.6. *Shape selective adsorption*

Chemical vapour deposited Na-zeolite A can separate oxygen and nitrogen on the basis of the difference of their molecular sizes [73]. The deposited silicon alkoxide that created silica overlayers control the pore-opening size so precisely, that it effectively suppresses the rate of adsorption of oxygen and nitrogen. It is known that the diffusion rates of *o*- and *p*-xylene on CVD-Mordenite [101], HZSM-5 [107], octane and 3-methylheptane on HZSM-5 can be precisely controlled. Previously Niwa and Murakami [120] have studied the rate sorption of water, hexane and *o*- and *p*-xylene on silica deposited H-Mordenite and H-Mordenite. The rate of sorption of *o*- and *p*-xylene on silica deposited H-Mordenite is suppressed completely while that of water remains unaltered. Separation of lower olefins by CVD zeolite A has also been shown [110]. The rate of adsorption of lower olefin is generally suppressed by modification of zeolite A. However, the extent of suppression appears to depend upon the chain length of the olefins and on the amount of deposited silica.

1.8.7. *Reaction studies*

It is to be noted that deposited silica effectively intrudes the zeolite surface and controls the extent of pore-mouth opening. Both of these phenomena may lead to better selectivity, either by preventing non-shape selective reactions on the external surface or by controlling the reactant or product shape selectivity of the zeolite.

1.8.7.1. Inertisation of the external surface

To determine the activity of the external surface of HZSM-5 and Mordenite, cracking of 1,3,5-triisopropylbenzene (TIPB) has been carried out at 300°C [107, 122]. TIPB (σ = 0.85 nm) is much larger than the pore size of HZSM-5 (σ = 0.54-0.56 nm). The cracking of this molecule takes place only on the external surface [70]. TIPB is also not able to enter the channels of CVD-Mordenite (σ = 0.67-0.70 nm) [122]. Depending on the amount of deposited silica the conversion of TIPB decreases 14 % for HZSM-5 and 18 % for Mordenite to about zero on the respective silica modified materials [107, 122]. It is noted that [124] TIPB conversion of 84% on the parent HZSM-5 decreases to 2 % for TEOS modified ZSM-5. In order to completely inertise the external surface of ZSM-5 by the amount of deposited silica for the conversion of TIPB is dependent on the type of silicon alkoxide, the better being TEOS [100].

Therefore the TIPB probe reaction has confirmed that the external surface is inertised by chemical deposition methods. The results of cracking of C_8-paraffins on modified Mordenite shows the cracking of octane is unaffected, whereas 2,2,4-trimethylpentane is unreactive on modified zeolite samples [101]. Hence the inertisation of the external surface acid sites by the silica deposition does not affect the internal acid sites.

1.8.7.2. Activity and selectivity of the modified zeolites

Chemical vapour deposition method has frequently been used to modify zeolites as catalysts for improving *p*-selectivity of several reactions. These reactions are isomerization of *o*-xylene [107], the disproportionation of toluene [107], the alkylation of toluene and ethylbenzene with methanol or ethylene on ZSM-5 [102, 103, 107, 118, 121, 124-126], as well as toluene isopropylation [127] and cumene disproportionation [109] over zeolite Beta.

The fraction of the *p*-isomer in the xylene fractions for toluene disproportionation, alkylation of toluene with methanol and *o*-xylene isomerization, all reaches 98 % using ZSM-5 samples with 13.3 wt % silica deposition [107]. It is further reported that [102, 103, 125] *p*-selectivity is greater than 98 % for the ethylation of toluene and ethylbenzene on silica modified ZSM-5. However, the modification may result in decreased conversions when modified samples are compared to the parent sample [102, 103, 107]. It is reported that the increase in *p*-selectivity is caused mainly by the narrowing of the pore-opening rather than by the inertisation of the acid sites on the external surface [100, 107].

The selective synthesis of dimethylamine (DMA) over silica modified zeolites ZK-5 [112, 113], Rho [112] and Mordenite [106] is not significant, whereas the activity of ZK-5 is greatly reduced [112]. From this it has been concluded that the increase in selectivity towards the smaller mono- and dimethylamine on silica modified Mordenite is the result of pore mouth narrowing, which reduces the diffusion rate of the larger trimethylamine [106].

Methanol conversion on silica modified HZSM-5 [74] and silica modified Mordenite [128] shows that the amount of large (aromatic) molecule

decreases and that of small (olefin) molecules increases. Details of the aromatic product distribution revealed a remarkable change towards the smaller isomers with increasing deposition. This indicates greatly enhanced shape selectivity due mainly to pore narrowing and to inertisation of the external surface. The lifetime of silica modified ZSM-5 is not significantly altered by the deposition [74] although the silica deposition causes a rapid loss of activity in dealuminated Mordenite [128].

1.8.7.3. The adsorbed species during reaction

The adsorbed species during reaction on silica-modified zeolites have been analyzed using IR techniques. Mirth *et al.* [126] have reported that the narrowing of the pore-opening results in decrease diffusion rates of larger molecules. Hence in the alkylation of toluene with methanol or ethylene, it has been found that the concentration of the adsorbed reaction products, such as *o*- and *m*-isomers or trimethylbenzenes, increases for modified samples. This is because these bulky molecules become trapped in the channels [124, 126]. Furthermore, isomerization of the trapped *o*-and *m*-isomers to the *p*-isomer results in a high *p*-selectivity. However, it is noted that the molecules trapped in the channels due to their low diffusion rates blocks the acid sites, resulting in decrease in activity of the material. Similar results have obtained by Gründling *et al.* for the selective synthesis of dimethylamine over Mordenite [106].

1.9. Plan of study

Zeolites are widely used in the separation of hydrocarbons and in the catalytic reactions of organic molecules. Considerable amount of work has been done to improve the properties of zeolites for various applications. The chemically modified zeolites have created a great interest among the researchers to find out their new applications. The present study also aims at modifying the zeolites to improve their adsorbent and catalytic properties.

Recently, the research interest is aimed at the separation of branched-chain and straight-chain hydrocarbons by the use of silicalite. Since silicalites are non-acidic in nature and is suitable for hydrocarbon adsorption, the control of pore-opening size by chemical vapour deposition (CVD) of silica is likely to make them an interesting new materials for shape selective separation of hydrocarbons. However, very few reports are available at the moment on the chemical vapour deposition of silica on silicalite. Silicalite membranes have been modified by ozone and alkoxide counter-diffusion CVD-technique and the deposition conditions are optimized to deposit the silica on the non-acidic material without decomposing the membrane structure [129]. However, studies on CVD of silica on silicalite crystal surface by simple thermal system and its application have not progressed yet.

A part of the present study is devoted to modify the silicalite crystal surface by deposition of silica on it. This part of study is planned to develop technique to control the pore-opening size of silicalite by simple thermal chemical vapour deposition of silica (static system). Then the investigation will be done to prove that CVD-silicalites are selective adsorbents for hydrocarbons. With this end in view the following will be studied –

(i) Preparation of silicalite crystals.

(ii) Modification of silicalite crystals by CVD technique.

(iii) Characterization of the silicalites and modified silicalites by XRD, SEM, TEM, IR and N_2-adsorption.

(iv) Examination of the morphology and determination of the thickness of the deposited silica layer on the silicalite crystals.

(v) Investigation of the shape selective separation of linear and branch chained hydrocarbons using CVD-silicalites

a) gravimetrically

b) chromatographically

Some attempts have already been made to modify HY and Hβ zeolites by chemical vapour deposition using silicon alkoxide to control the opening size [16, 130, 131]. Kim *et al.* [16] has studied the changes in the pore-opening size and pore volume of HY zeolites after silica deposition by $Si(OCH_3)_4$ or $Si(OCH_3)_2(CH_3)_2$. The pore opening of HY zeolites with high aluminium concentration cannot be controlled by the deposition of silica. However, the pore opening size of HY zeolites with a low aluminium concentration can be controlled. The reasons for this are not yet known. Until now, no report on the preparation of silica deposited USY zeolite for controlling the pore opening is found. It may be mentioned that structural stability and high reactivity make USY zeolite useful for catalytic cracking process. Accordingly, ultrastable Y (USY) zeolite has also been included in the present study.

We invent to modify the USY zeolite to improve its shape selective property. This part of the study will mainly focus on the control of pore-opening size and solid acidity of high siliceous and low siliceous USY zeolites for selective catalytic cracking. At the same time, we shall also investigate the reason behind the failure of low siliceous HY zeolite in the

controlling of pore size. The study is designed in following manner-

(i) Preparation of silica deposited USY zeolites by CVD technique. Two types of USY zeolite have been selected.
   a. High siliceous USY zeolite, HS-USY (SiO_2 /Al_2O_3 = 29.0)
   b. Low siliceous USY zeolite, LS-USY (SiO_2 /Al_2O_3 = 7.51)

(ii) Characterization of the unmodified and modified USY zeolites by various methods, such as, XRD, NH_3-TPD and IR-studies.

(iii) Adsorption of 1,3,5-triisiptopylbenzene on USY and silica-deposited USY zeolites to know their pore-opening sizes.

(iv) Catalytic cracking of 1,3,5-trimethylbenzene (1,3,5-TMB) and 1,3,5-triisiptopylbenzene (1,3,5-TIPB) on USY and silica-deposited USY zeolites.

1.10. References

[1] Mortier, W., in "Compilation of Extra Framework Sites in Zeolites", Butterworths, Guildford, England (1982).

[2] Flanigen, E. M. and Jansen, J. C., in "Introduction of Zeolite Science and Practice", edited by H. van Bekkum, Elsevier, New York, Vol. **58**, p. 18 (1991).

[3] Moscou, L., *Stud. Surf. Sci. Catal.*, **58**, 1 (1991).

[4] Meier, W. M., in "Molecular Sieves", Society for Chemical Industry, London, p. 12 (1968).

[5] Meier, W. M. and Olson, D. H., in "Atlas of Zeolite Structure Types", Structure Commission of IZA, 3rd Revised Edition, Butterworth-Heinemann (1992).

[6] Haag, W. O. and Chen, N. Y., in 'Catalyst Design Progress and Perspectives", edited by L. L. Hegedus, John Wiley and Sons, p. 165 (1987).

[7] Argauer, R. J. and Landolt, G. R., U.S. Patent 3, 702, 886 (1972).

[8] Kokotailo, G. T., Lawton, S. L., Olson, D. H. and Meier, W. M., *Nature*, **272**, 437 (1978).

[9] Meier, W. M., Olson, D. H. and Baerlocher, C., in 'Atlas of Zeolite Structure Types", Structure Commission of IZA, 4th Revised Edition, Butterworth-Heinemann (1996).

[10] De Vos Burchart, E., Van Bekkum, H. and Van de Graaf, B., *Zeolites*, **13**, 212 (1993).

[11] Szostak, R., in "Handbook of Molecular Sieves", Van Nøstrand Reinhold, New York (1992).

[12] Martens, J. A., Xiong, Y. L., Feijen, E. J. P., Grobet, P. J. and Jacobs, P. A., *J. Phys. Chem.*, **97**, 5132 (1993).

[13] Breck, D. W. and Flanigen, E. M., in "Molecular Sieves", Society of Chemical Industry, London, p. 47 (1968).

[14] Rabo, J. A., Angell, C. L., Kasai, P. H. and Schomaker, V., *Faraday Disc. Chem. Soc.*, **41**, 328 (1966).

[15] Gallezot, P., Ben Taarit, Y. and Imelik, B., *J. Catal.*, **26**, 481 (1972).

[16] Kim, J. -H., Ikoma, Y. and Niwa, M., *Micropor. Mesopor. Mater.*, **32**, 37 (1999).

[17] Corma, A., Miguel, P. J., Orchilles A. V. and Koermer, G. S., *J. Catal.*, **135**, 45 (1992).

[18] Kuehne, M. A., Kung H. H. and Miller J. T., *J. Catal.*, **171**, 293 (1997).

[19] Uytterhoeven, J. B., Christner, L. G. and Hall, W. K., *J. Phys. Chem.*, **69**, 2117 (1965).

[20] Niewenhuys, B. E., Ponec, V., Van Koten, G., Van Leeuwen, P. W. N. M. and Van Santen, R. A., *Stud. Surf. Sci. Catal.*, **79**, 89 (1993).

[21] Sauer, J., *J. Molec. Catal.*, **54**, 312 (1989).

[22] Ward, J. W., *J. Catal.*, **9**, 225 (1967).

[23] Kazansky, V. B., *Stud. Surf. Sci. Catal.*, **85**, 251 (1994).

[24] Van Santen, R. A., *Stud. Surf. Sci. Catal.*, **85**, 273 (1994).

[25] Stach, H., Jänchen, J., Jerschkewitz, H. -G., Lohse, U., Parlitz., B. and Hunger, M., *J. Phys. Chem.*, **96**, 8473 (1992).

[26] Kazansky, V. B., *Acc. Chem. Res.*, **24**, 379 (1991).

[27] Kühl, G. H., in "Proceeding 3rd International Conference on Molecular Sieves, Recent Progress Reports", edited by J. B. Uytterhoeven, Univ. Leuven Press, Vol. **127**, p. 227 (1973).

[28] Kühl, G. H., *J. Phys. Chem. Solids*, **38**, 1259 (1977).

[29] Scherzer, J., *ACS Symp. Ser.*, **248**, 157 (1984).

[30] Karge, H. G. and Dondur, V., *J. Phys. Chem.*, **94**, 765 (1990).

[31] Karge, H. G., Dondur, V. and Weitkamp, J., *J. Phys. Chem.*, **95**, 283 (1991).

[32] O'Donovan, A. W., O'Connor, C. T. and Koch, K. R., *Micropor. Mater.*, **5**, 185 (1995).

[33] Sand, L. B., *Pure Appl. Chem.*, **52**, 2105 (1980).

[34] Jansen, J. C., *Stud. Surf. Sci. Catal.*, **58**, 77 (1991).

[35] Barrer, R. M., *Zeolites*, **1**, 130 (1981).

[36] Barrer, R. M., in "Zeolite Synthesis", *ACS Symp. Ser.*, Vol. **398**, edited by M. L. Occelli and H. E. Robson, ACS, Washington DC, p. 11 (1989).

[37] Feijen, E. J. P., Martens, J. A. and Jacobs, P. A., *Stud. Surf. Sci. Catal.*, **84**, 3 (1994).

[38] Jacobs, P. A., in " Zeolite Microporous Solids: Synthesis, Structure, and Reactivity", *NATO ASI Ser.*, Vol. **352**, edited by E.G., Derouane, F., Lemos, C. Naccache, and F. R. Ribeiro, Kluwer Academic Publishers, Dordrecht, p. 3 (1992).

[39] Jansen, J. C., Engelen, C. W. R. and Van Bekkum, H., in " Zeolite Synthsis," *ACS Symp. Ser.*, Vol. **398**, edited by M. L. Occelli and H. E. Robson, ACS, Washington D. C., p. 257 (1989).

[40] Barrer, R. M., in "Hydothermal Chemistry of Zeolites", Academic Press, London (1982).

[41] Katovic, A., Subotic, B., Smith, I., Despotovic, A. and Curic, M., in "Zeolite Synthesis", *ACS Symp. Ser.*, Vol. **398**, edited by M. L. Occelli, and H. E. Robson, ACS, Washington DC, p. 124 (1989).

[42] Gilson, J. -P., in "Zeolite Microporous Solids: Synthesis, Structure, and Reactivity", *NATO ASI Ser.*, Vol. **352**, edited by E. G., Derouane, F., Lemos, C. Naccache, and F. R. Ribeiro, Kluwer Academic Publishers, Dordrecht, p. 19 (1992).

[43] Iler, R. K., "The Colloid Chemistry of Silica and Silicates", Cornell Univ. Press, Ithaca, N. Y., p. 26 (1955).

[44] Breck, D. W., in "Zeolite Molecular Sieves", edited by E. Robert, Krieger Publishing Company, Inc., Malabar, Florida USA, p. 341 (1974).

[45] Flanigen, E. M., Bennett, J. M., Grose, R. W., Cohen, J. P., Patton, R. L. and Kirchner, R. M., *Nature*, **271**, 512 (1978).

[46] Fyfe, C. A., Gobbi, G. C. and Kennedy, E. G., *Appl. Catal.*, **5**, 227 (1983).

[47] Jacobs, P. A. and Martens, J. A., *Stud. Surf. Sci. Catal.*, **33**, 100 (1997).

[48] Nagy, J. B., Gabelica, Z. and Derouane, E. G., *Zeolites*, **3**, 43 (1983).

[49] Gabelica, Z., Blom, N. and Derouane, E. G., *Appl. Catal.*, **5**, 227 (1983).

[50] Derouane, E. G. and Gabelica, Z., *J. Solid State Chem.*, **64**, 296 (1986).

[51] Szostak, R., in "Molecular Seives- Principles of Synthesis and Identification", edited by B. H. Davis, Van Nøstrand Reinhold, New York (1989).

[52] Van der Gaag, F. J., Jansen, J. C. and Van Bekkum, H., *Appl. Catal.*, **17**, 201 (1985).

[53] Suib, S. L., Stucky, G. D. and Blattner, R. J., *J. Catal.*, **65**, 174 (1980).

[54] Denounce, E. G., Gilson, J. P., Gabelica, Z., Mousty-Desbuquoit, C. and Verbist, J., *J. Catal.*, **71**, 447 (1981).

[55] Von Ballmoos, R. and Meier, W. M., *Nature*, **289**, 782 (1981).

[56] Hughes, A. E., Wilshier, K. G., Sexton, B. A. and Smart, P., *J. Catal.*, **80**, 221 (1983).

[57] Chao, K. and Chern, J., *Zeolites*, **8**, 82 (1988).

[58] Szostak, R., in "Introduction of Zeolite Science and Practice", edited by H. van Bekkum, E. M. Flanigen and J. C. Jansen, Elsevier, New York, Vol. **58**, p. 153 (1991).

[59] Scherzer, J., in "Catalytic Materials", American Chemical Society, p. 157 (1984).

[60] Kerr, G. T. and Shipman, G. F., *J. Phys. Chem.*, **72**, 3071 (1968).

[61] Kerr, G. T., *J. Phys. Chem.*, **73**, 2780 (1969).

[62] McDaniel, C.V. and Maher, P. K., in "Zeolite Chemistry and Catalysis", edited by J. A. Rabo, ACS, Washington, D.C., p. 285 (1974).

[63] Beaumont, R. and Barthomeuf, D., *J. Catal.*, **26**, 218 (1972).

[64] Beaumont, R. and Barthomeuf, D., *J. Catal.*, **27**, 45 (1972).

[65] Beyer, H. K. and Belenkaya, I., in "Catalysis by Zeolites", edited by B. Imelik, et.al., Elsevier, Amsterdam, p. 203 (1980).

[66] Beyer, H. K., Belenkaya, I., Hange, F., Tielen, M., Grobet, P. J. and Jacobs, P. A., *J. Chem. Soc. Faraday Trans. 1*, **81**, 2889 (1985).

[67] Barrer, R. M. and Coughlan, B., in "Molecular Sieves Derived from Clinoptilolite by Progressive Removal of Framework Charge: Characterization of sorption of CO_2 and Krypton", Society of Chemical Industry, London, p. 141 (1968).

[68] Miyamoto, T., Katada, N., Kim, J. -H. and Niwa, M., *J. Phys. Chem. B*, **102**, 6738 (1998).

[69] Katada, N., Miyamoto, T., Begum, H. A., Naito, N., Niwa, M., Matsumoto, A. and Tsutsumi, K., *J. Phys. Chem. B*, **104**, 5511 (2000).

[70] Namba, S., Inaka, A. and Yashima, T., *Zeolites*, **6**, 107 (1986).

[71] Niwa, M., Kato, S., Hattori, T. and Murakami, Y., *J. Chem. Soc., Faraday Trans. 1*, **80**, 3135 (1984).

[72] Hibino, T., Niwa, M., Murakami, Y. and Sano, M., *J. Chem. Soc., Faraday Trans. 1*, **85**, 2327 (1989).

[73] Niwa, M., Yamazaki, K. and Murakami, Y., *Ind. Eng. Chem. Res.*, **30**, 38 (1991).

[74] Niwa, M., Kato, M., Hattori, T. and Murakami, Y., *J. Phys. Chem.*, **90**, 6233 (1986).

[75] Vansant, E. F., in "Innovation in Zeolite Material Science", edited by P. J. Grobet, *et. al.*, Elsevier, Amsterdam, p. 143 (1988).

[76] ASTM Standards on Catalysts, D3906-85a (1988).

[77] Scherrer, P., *Göttinger Nachrichten*, **2**, 98 (1918).

[78] Lippens, B.C. and De Boer, J. H., *J. Catal.*, **4**, 319 (1965).

[79] Gregg, S. J. and. Sing, K. S. W., in "Adsorption, Surface Area and Porosity", 2nd Edition, Academic Press (1982).

[80] Moscou, L. and Moné, R., *J. Catal.*, **30**, 417 (1973).

[81] Auroux, A. and Vedrine, J. C., in "Catalysis by Acids and Bases" Elsevier, Vol. **20**, p. 311, (1985).

[82] Barthomeuf, D., *J. Phys. Chem.*, **97**, 10092 (1993).

[83] Jozefowics, L. C., Karge, H. G. and Coker, E. N., *J. Phys. Chem.*, **98**, 8053 (1994).

[84] Shen, J., Cortright, R. D., Chen, Y. and Dumesic, J. A., *J. Phys. Chem.*, **98**, 8067 (1994).

[85] Katada, N., Iijima, S., Igi, H. and Niwa, M., *Stud. Surf. Sci. Catal,*. **105**, 1227 (1997).

[86] Bagnasco, G., *J. Catal.*, **159**, 249 (1996).

[87] Hashiguchi, T. and Sakai, S., in "Preprint of the 11th Meeting on the Reference Catalyst of Japan", The Catalysis Society of Japan, Tokyo, p. 6 (1987).

[88] Chester, A. W., Higgins, J. B., Kuehi, G. H., Schlenker, J. L. and Woolery, G. L., in "Preprint of the 11th Meeting on the Reference Catalyst of Japan", The Catalysis Society of Japan, Tokyo, p. 22 (1987).

[89] Niwa, M. and Katada, N., *Catal. Surveys Jpn.*, **1**, 215 (1997).

[90] Flanigen, E. M., in "ACS Monograph 171", edited by J. A. Rabo, (1976).

[91] Lippmaa, E., Magi, M., Samoson, A., Tarmak, M. and Engelhardt, G., *J. Am. Chem. Soc.*, **103**, 4992 (1981).

[92] Engelhardt, G. and Michel, D., in "High Resolution Solid State NMR of Silicates and Zeolites", John Wiley & Sons (1987).

[93] Csicsery, S. M., in "Zeolite Chemistry and Catalysis, ACS Monograph 171", edited by J. A. Rabo, p. 680 (1979).

[94] Haag. W. O., Lago R. M. and Weisz, P. B., *Faraday Disc. Chem. Soc.*, **72**, 317 (1982).

[95] Santilli, D. S. and Zones, S. I., *Catal. Lett.*, **7**, 383 (1990).

[96] Santilli, D. S., Harris, T. V. and Zones, S. I., *Micropor. Mater.*, **1**, 329 (1993).

[97] Derouane, E. G., *J. Catal.*, **100**, 541 (1986).

[98] Breck, D. W., in "Zeolite Molecular Sieves, Structure, Chemistry and Use", John Wiley & Sons, Inc., New York, p. 593 (1974).

[99] Flanigen, E. M., in "Introduction of Zeolite Science and Practice", edited by H. van Bekkkum, E. M. Flanigen and J. C. Jansen, Elsevier, New York, Vol. **58**, p. 20 (1991).

[100] Kim, J. -H., Ishida, A., Okajima, M. and Niwa, M., *J. Catal.*, **161**, 387 (1996).

[101] Niwa, M., Morimoto, S., Kato, M., Hattori, T. and Murakami, Y., in "Proceedings of 8th International Congress on Catalysis", Vol. **IV**, p. 701 (1984).

[102] Wang, I., Ay, C. -L., Lee, B. -J. and Chen, M. -H, in "Proceedings of 9th International Congress on Catalysis", Calgary, p. 324 (1988).

[103] Das, J., Bhat, Y. S. and Halgeri, A. B., *Catal. Lett.*, **20**, 349 (1993).

[104] Niwa, M., Kawashima, Y., Hibino, T. and Murakami, Y., *J. Chem Soc., Faraday Trans. 1*, **84**, 4327 (1988).

[105] Yue, Y. -H., Tang, Y. and Gao, Z., *Stud. Surf. Sci. Catal.*, **105**, 2059 (1997).

[106] Gründling, C., Eder-Mirth, G. and Lercher, J. A., *J. Catal.*, **160**, 299 (1996).

[107] Hibino, T., Niwa, M. and Murakami, Y., *J. Catal.*, **128**, 551 (1991).

[108] Bhat, Y. S., Das J., Rao, K. V. and Halgeri, A. B., *J. Catal.*, **159**, 368 (1996).

[109] Tsai, T. -C. and Wang, I., *Appl. Catal.*, **77**, 209 (1991).

[110] Niwa, M., Yamazaki, K. and Murakami, Y., *Ind. Eng. Chem. Res.*, **33**, 371 (1994)

[111] Chamoumi, M., Brunel, D., Fajula, F., Geneste, P., Moreau, P. and Solofo, J., *Zeolites*, **14**, 282 (1994).

[112] Bergna, H. E., Keane, M., Ralston, D. H., Sonnichsen, G. C., Abrams, L. and Shannon, R. D., *J. Catal.*, **115**, 148 (1989).

[113] Fetting, F. and Dingerdissen, U., *Chem. Eng. Technol.*, **15**, 202 (1992).

[114] Sato, S., Tokumitsu, M., Sodesawa, T. and Nozaki, F., *Bull. Chem. Soc. Jpn.*, **64**, 1005 (1991).

[115] Sheng, T. -C. and Gay, I. D., *J. Catal.*, **145** , 10 (1994).

[116] Niwa, M., Katada, N. and Murakami, Y., *J. Catal.*, **134**, 340 (1992).

[117] Richter, M., Janchen, J., Jerschkewitz, H. -G., Parlitz, B. and Schreier, E., *J. Chem Soc., Faraday Trans. I*, **87**, 1461 (1991).

[118] Bhat, Y. S., Das, J. and Halgeri, A. B., *Appl. Catal.*, **115**, 257 (1994).

[119] Yue, Y. -H., Tang, Y., Liu, Y. and Gao, Z., *Ind. Eng. Chem. Res.*, **35**, 430 (1996).

[120] Niwa, M. and Murakami, Y., *J. Phys. Chem. Solids*, **50**, 487 (1989).

[121] Bhat, Y. S., Das, J. and Halgeri, A.B., *J. Catal.*, **155**, 154 (1995).

[122] Hibino, T., Niwa, M. and Murakami, Y., *Zeolites*, **13**, 518 (1993).

[123] Niwa, M., Hidalgo, C., Hattori, T. and Murakami, Y., *Stud. Surf. Sci. Catal.*, **28**, 297 (1986).

[124] Cejka, J., Zilkova, N., Wichterlova, B., Eder-Mirth, G. and Lercher, J. A., *Zeolites*, **17**, 265 (1996).

[125] Wang, I., Ay, C. -L., Lee, B. -J. and Chen, M. -H, *Appl. Catal.*, **54**, 257 (1989).

[126] Mirth, G., Cejka, J., Krtil, J. and Lercher, J. A., *Stud. Surf. Sci. Catal.*, **88**, 241 (1994).

[127] Parikh, P. A., Subrahmanyam, N., Bhat, Y. S. and Halgeri, A. B., *Appl. Catal.*, **90**, 1 (1992).

[128] Sawa, M., Kato, K., Hirota, K., Niwa, M. and Murakami, Y., *Appl. Catal.*, **64**, 297 (1990).

[129] Nomura, M., Yamaguchi, T. and Nakao, S., *Ind. Eng. Chem. Res.*, **36,** 4217 (1997).

[130] Ito, H., Okamoto, S. and Furuta, A., *Nippon Kagaki Kaishi,* 420 (1989).

[131] Chun, Y., Chen, X., Yan, A. -Z. and Xu, Q. -H., *Stud. Surf. Sci. Catal.*, **84**, 1035 (1994).

Chapter Two

Modification of Silicalite Crystals by Chemical Vapour Deposition of Tetramethoxysilane

2.1. Previous studies

Silicalite is the aluminium free form of ZSM-5 zeolite, having an MFI (Mobil five) structure. It has elliptical pore opening of 0.51 × 0.57 nm^2 interconnected by zigzag channels with a nearly circular cross section of about 0.54 nm in diameter (Fig. 2.1) [1]. It has hydrophobic and organophilic nature compared to other zeolites. Owing to this characteristic, silicalite can be used for environmental applications to selectively adsorb nonpolar hydrocarbon molecules in water [2]. Another important character of silicalite/ZSM-5 is that its 10-member oxygen ring opening size is similar to that of aromatic molecules, such as benzene and xylene [3]. The structure and the size of the micropore of silicalite make it suitable for application in shape selective adsorption of hydrocarbons and aromatic compounds.

Adsorption equilibria of hydrocarbons on silicalite and ZSM-5 zeolites have been studied by many researchers. Flanigen *et al.* have reported synthesis, crystal structure and properties of silicalite [1]. They have studied the adsorption of different hydrophobic and hydrophilic adsorbate on silicalite. Adsorption isotherms of C_1 to C_4 alkanes and isobutane, CO_2, SF_6 and C_5–C_{10} normal alkanes on silicalite crystals at different temperatures have also been studied [2, 4]. A virial equation has been used to correlate the experimental data and to calculate the isostetic heat of adsorption and the limiting heat of adsorption at zero loading. The adsorption isotherms of isobutane exhibit inflection points at loading of 4-6 molecules/unit cell in a certain temperature range. This unusual adsorption behaviour is attributed to adsorption of isobutene at in different locations of the channel system.

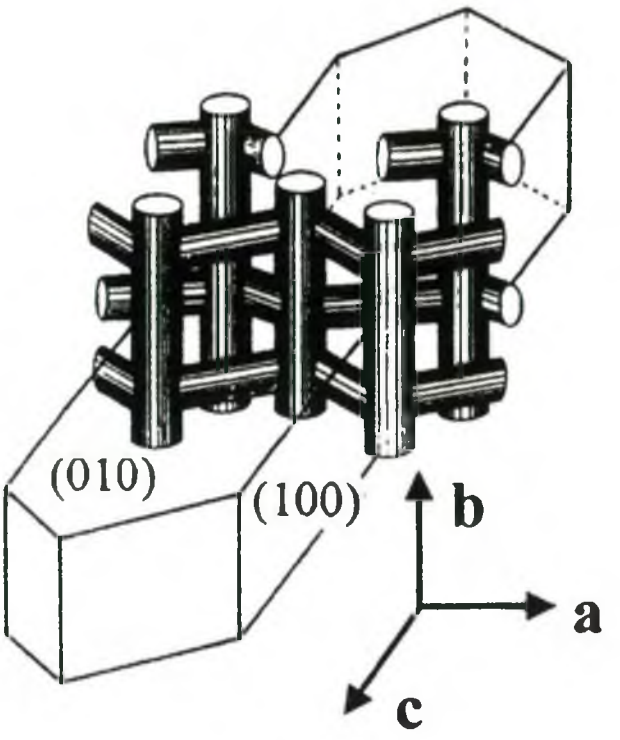

Fig. 2.1. A model of the microporous structure in silicalite.

Abdul-Rehman *et al.* have studied the quaternary, ternary, binary and pure component sorption of C_1–C_4 alkanes on silicalite pellets [5]. The adsorption equilibria of methane to butane have been measured by chromatographic method [6]. Gravimetric equilibrium isotherms for the adsorption of branched and cyclic C_6 paraffins on silicalite have been studied [7]. It is noted that the magnitude of adsorption equilibrium constants follows the trend, double-branched < single-branched < cycloparaffins. The intercrystalline diffusivities in silicalite for several branched and cyclo-C_6 paraffins have also been studied [8]. The following general trend has been observed for the diffusivites: linear > single-branched > double (ternary C)-branched > cycloparaffins > double (quaternary C)-branched. Enthalpy of adsorption for the single-branched paraffins increases slightly with loading, but for the double-branched and cyclic paraffins the variation of heat of adsorption with coverage is more pronounced [8].

Separations of cyclic, branched and linear hydrocarbon (C_5–C_9) mixtures with the help of silicalite membranes have been studied at 360 to 510 K [9]. Mixtures of branched, cyclohexane and *n*-hexane has been separated with high selectivities for *n*-hexane at lower temperatures. The separation behaviour has been attributed to molecular sieving effect not to preferential adsorption of one species. In this respect the permeances of the linear alkanes strongly decrease with increasing chain length [9].

Isotherm for adsorption of H_2, CH_4, N_2, CO, Ar, CO_2, and Kr have been measured at two temperatures (305 K and 342 K) over a pressure range of 0-18.0 atm on silicalite. The isosteric heats of adsorption for these gases at the limit of zero coverage increase as the polarizability of the adsorbate increases [10].

The isomorphous substitution of a quadrivalent silicon atom in the framework by trivalent aluminium is the origin of the acid sites and catalytic functions of zeolite. The modified silicalites have been prepared by incorporating Ga and Fe in place of Si. The acidic property of gallosilicate and ferrisilicate have been studied by temperature programmed desorption of ammonia (NH_3-TPD) [11, 12]. Generation of acid sites by isomorphous substitution of silicon by gallium and iron is presumed to be the origin of the catalytic function.

Fine control of the pore-opening sizes of zeolites by chemical vapour deposition (CVD) of silicon alkoxide has been studied for shape selective catalytic reactions. The pore-opening size of H-mordenite can be effectively reduced by *ca.* 0.1 and 0.2 nm by deposition of 1-2 and 3 molecular layers of silicon oxide on it [13]. The modified mordenite has been used for selective cracking of octane isomers [14]. Selective formation of *p*-xylene form methanol conversion [15] and also from toluene alkylation [16] has been observed for modified HZSM-5. This study has been extended to the deposition using various silicon compounds [17]. The CVD technique has also been applied to the development of selective adsorbates. The separation of oxygen and nitrogen has been studied using chemical vapour deposited zeolite A [18]. Deposited silica control the pore-opening size so precisely that it effectively suppresses the rate of adsorption of nitrogen, with molecular sizes larger than oxygen only by 0.02 nm [18]. Separation of C_2-C_4 olefins has also been studied by using the Si-deposited zeolite A. The chromatographic response and gravimetric measurements show that the rate of adsorption of olefins is suppressed by the deposition of silica on zeolite A. The suppression of the diffusion rate of olefins depends on the chain length of olefins and on the amount of deposited silica [19].

2.2. Experimental

2.2.1. *Materials and reagents*

Ludox HS40 colloidal silica (40 % wt % SiO_2) was procured from Aldrich Chemical Co., USA. Tetra-*n*-propylammonium bromide (TPA-Br), hexane and tetramethoxysilane or tetramethyl orthosilicate (TMOS) were obtained from Tokyo Chemical Industries, Ltd., (TCI), Japan. Butane and 2-methylpentane were obtained from Wako Chemical Co., and Sumitomo-Seika, Japan, respectively. 2-Methylpropane was purchased from Fluka, Switzerland. All other reagents and chemicals were of analytical grade. When necessary chemicals were also purified. Distilled water was used for preparation of solutions. When required deionized water was also used.

2.2.2. *Synthesis of silicalite*

Silicalite was synthesized according to Argauer and Landolt [20]. Table 2.1 shows the proportion of different ingredient for synthesis. Two parts of A (Ludox HS40 colloidal silica in water) and one part of B (solution of tetra-*n*-propylammonium bromide, TPA-Br, H_2SO_4 and water) were added dropwise to aqueous solution of sodium chloride. The pH of the solution was adjusted to 10.3 by adding NaOH solution dropwise. The mixture was kept at 443 K for 24 h at autothermal pressure in a Teflon-lined autoclave and stirred mechanically at 800 rpm. The product was filtered and washed with deionized water for several times to remove the Cl^- ions. Then the silicalite sample was dried for overnight in an oven at 373 K.

To remove the template, TPA-Br, the dried silicalite was placed in a porcelain dish and calcined in air at 803 K for 3 h in a furnace. After detemplation, white crystals of silicalite were repeatedly treated with 400

mL 0.1 M NH_4NO_3 solution at 353 K until all Na^+ ions were replaced by NH_4^+ ions.

Subsequently NH_4^+ ions, were removed by calcining the sample at 803 K for 3 h. These silicalite samples were preserved in a saturator containing saturated aqueous NH_4Cl solution. Any stress on these silicalite samples was avoided, as the crystallites collapsed under stress.

Table 2.1. Synthesis condition for silicalite

Solution A		Solution B		Solution C	
H_2SO_4	4.44 g	LUDOX HS-40	49.6 g	NaCl	25.9 g
TPA-Br	7.78 g	Water	56.2 g	Water	100 g
Water	57.5 g				

2.2.3. *Characterization of silicalite crystals*

2.2.3.1. X-ray diffraction (XRD)

A Rigaku Miniflex Plus diffractometer was used to obtain X-ray diffraction patterns and 0.45 kW CuKα (wavelength = 0.1542 nm) radiation was applied. The samples were analyzed at ambient conditions. The following parameters were used for the diffraction measurements:

- voltage 30 kV
- current 15 mA
- goniometer Miniflex goniometer
- filter Kβ filter
- scanning mode continuous repetition
- scanning range 5.00 ~ 50.00°
- scanning speed 0.5 ° / min
- scanning width 0.01°

- scanning axes	2θ /θ
- sampling interval	1 sec
- θ-offset	0.00

2.2.3.2. Scanning electron microscope (SEM)

Scanning electron microscope (SEM) was used in order to find out the morphology and crystal size of silicalite samples. The samples were loaded on mounted plastic tapes (carbon and glue mixture). Gold vapour was deposited on it in vacuum using a Giko IB-3 Ion-coater for 40 seconds at 5 to 6 mA current. SEM photographs were taken using a JEOL JSM-5800 scanning microscope with the magnification of 6000 to 10000 and accelerating voltage 15 kV.

The external surface area of the silicalite crystallite was calculated by using the following equation:

External surface area (m^2/g) = (m^2)/ weight (g)

$$= (m^2)/\text{volume}(m^3) \times \text{density}(g/m^3) \quad \ldots\ldots 2.1$$

2.2.3.3. Transmission electron microscope (TEM)

Samples for TEM examination were prepared in isopropanal suspension. The suspension was dropped on a carbon-coated microgrid attached to a copper grid. Isopropanal was evaporated and the crystals adhered to the carbon-coated grid. A high-resolution field emission TEM (JEM-2010F, JEOL), operating at 200 keV was used. A TV camera system was used to observe the effect of rapid and weak incident electron beam on the sample. A digital photographic system attached to the JEM-2010F to photograph the events. The system was 10 times more sensitive than the generally used process [21, 22]. This arrangement avoided the damage of crystals caused by normal TEM.

2.2.3.4. Infrared (IR) studies

8 to 10 mg of the silicalite powder was made into pellet to fit into a self-supporting disc in the *in-situ* cell [Fig. 3.3 (b)]. The cell was evacuated at 773 K for 1 h, and then cooled at room temperature (~ 298 K). The IR spectrum was taken by a JASCO FTIR-5300 spectrometer.

2.2.3.5. N_2-adsorption isotherm

For this purpose, the arrangement shown in Fig. 2.2 was used. The following experimental conditions were used:

Sample amount:	200 mg
Pretreatment:	673 K for 1 h, (increment of temperature 5 K min^{-1})
Evacuation:	1.0×10^{-3} Torr
Nitrogen adsorbed at (Torr):	10, 20, 30, 40, 50, 75, 100, 125, 150, 200, 250, 300, 400, 500, 600,700, 780
P/P_0 :	0 to 0.95 where, P= equilibrium pressure and P_0 = saturation vapour pressure of nitrogen

The silicalite sample was taken in the system as "adsorbent" (Fig. 2.2) and degassed until the system pressure was ~10^{-3} Torr. Temperature was than raised to 673 K and the sample was heated for one hour at this temperature. CH.2 was closed and the sample was allowed to cool down. A liquid nitrogen Dewar flask was used to cool the sample at 77 K. Nitrogen was then allowed to come in contact with the sample (adsorbent) at 77 K and the equilibrium pressure (P) of nitrogen was measured.

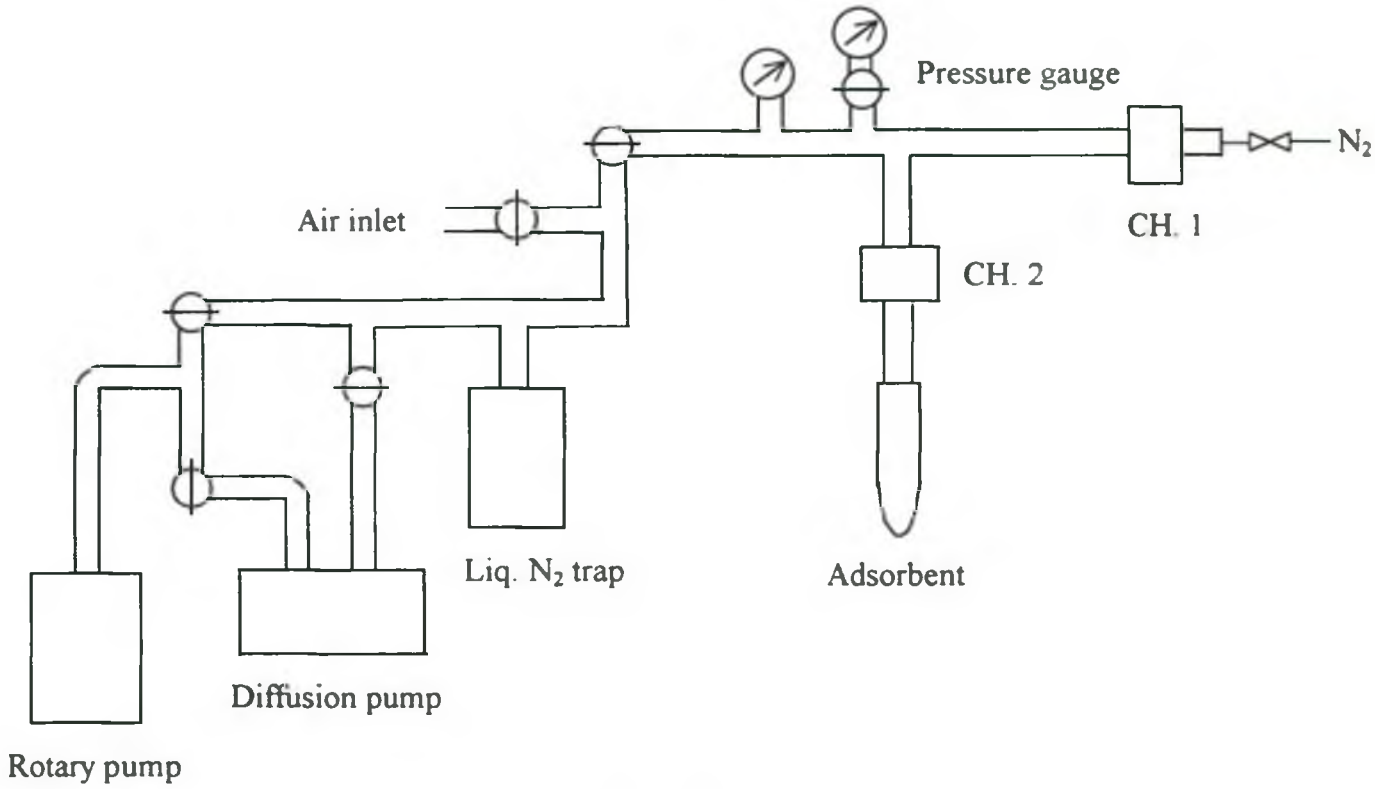

Fig. 2.2. Schematic diagram of N_2 adsorption apparatus.

The system was programmed for different doses of nitrogen gas and the corresponding equilibrium nitrogen pressures were automatically recorded.

The volume of nitrogen adsorbed by the silicalite sample at a definite pressure of nitrogen was calculated. The volume of adsorbed nitrogen amount per gram of silicalite was plotted against different P/P^0 values.

2.2.4. *Modification of silicalite crystals by chemical vapour deposition (CVD) of tetramethoxysilane*

2.2.4.1. Preparation of CVD-silicalites at different temperatures

On the basis of a previously reported work [19], a vacuum system equipped with a quartz spring microbalance was fabricated (Fig. 2.3). This was used as the laboratory apparatus for CVD. The silicalite, as crystals (about 0.3 g), was taken in the quartz basket (*h*) attached to the quartz spring. Tetramethoxysilane was kept in the liquid reservoir (*o*). Before deposition of the tetramethoxysilane (TMOS), the silicalite sample was degassed at *ca.* 10^{-3} Torr at 673 K for 2 h until no weight change was observed for 30 minute. Temperature of reaction was then adjusted. This weight, the initial weight, was programmed as zero. The tetramethoxysilane was chilled in liquid nitrogen and purified by trap-to-trap distillation. The vapour pressure of TMOS in the system was maintained *ca.* 2.5 Torr by controlling the temperature of the reservoir in the ice bath. The TMOS vapour was allowed to come in contact with sample and the weight gain was observed. When the change in weight was very slow, the reservoir stopcock was closed and the system was evacuated. This removed products like methanol that formed when TMOS came in contact with silicalite sample at 673 K. This process was repeated until desired gain in weight was observed. The final increase in weight was recorded. The resultant increase in weight was measured *in situ* by the

quartz microbalance. The materials thus deposited were calcined and oxidized, by oxygen (from *q* at 200 Torr), at 673 K to remove the carbonaceous residues. The system was again evacuated (*ca.* 10^{-3} Torr) at the same temperature at which the constant weight gain was measured. This gain in weight showed the extent of modification by deposition on silicalite.

Above procedure was repeated at 513 K, 593 K and 773 K and the extent of modification were evaluated.

2.2.4.2. Preparation of CVD-silicalites of different amounts of deposit

Four different CVD-silicalites having 0.75 wt %, 1.3 wt %, 1.9 wt %, and 2.7 wt % deposit were prepared at 773 K, by varying contact times of TMOS vapour and duration of the experiment.

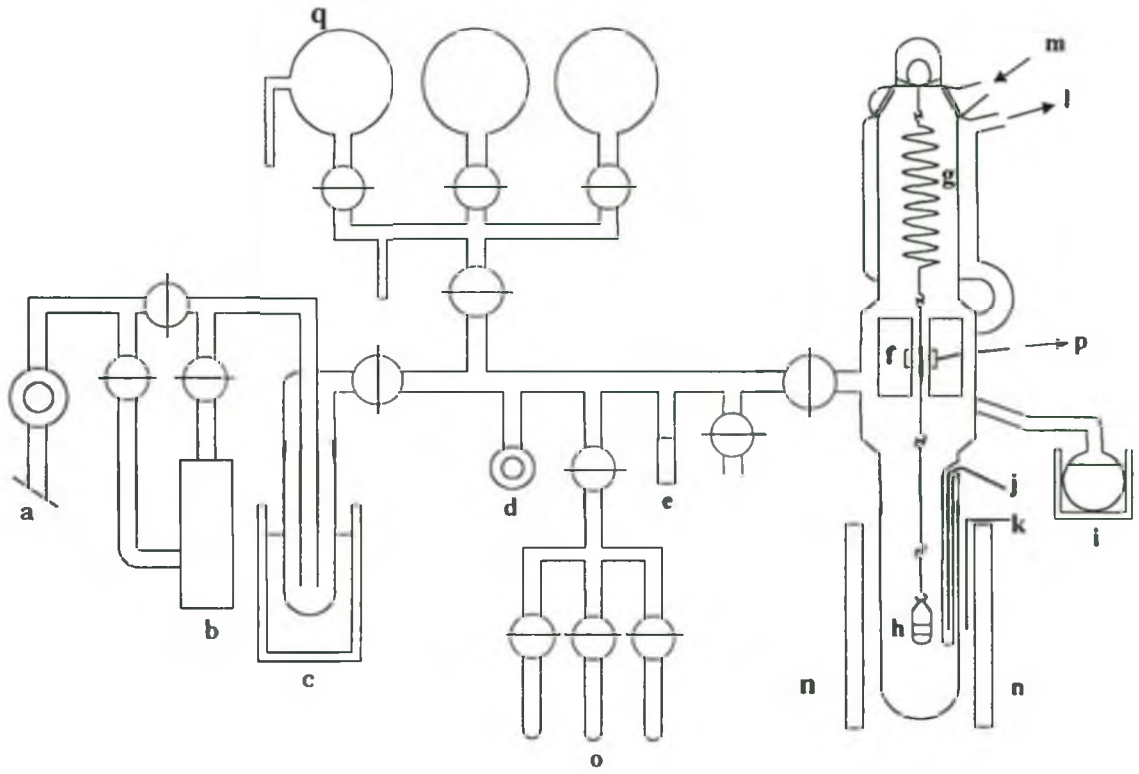

Fig. 2.3. Apparatus of chemical vapour deposition.

(a) Vaccum pump, (b) diffusion pump, (c) liquid nitrogen trap, (d) pirani gauge,
(e) transducer, (f) differential transformer, (g) quartz spring microbalance, (h) quartz basket,
(i) CCl_4 container, (j, k) thermocouple, (l, m) from/to condenser, (n) furnace,
(o) liquid reserviors (alkoxide), (p) interfacing device to computer, (q) gas reservoirs.

2.2.5. *Characterization of prepared CVD-silicalites*

Scanning electron microscope (SEM), transmission electron microscope (TEM) and nitrogen adsorption methods were used to characterize CVD-silicalite samples (Section 2.2.3.2, 2.2.3.3 and 2.2.3.5).

The thickness (D, nm) of the silica layer deposited on the external surface of a silicalite crystal was estimated using the following equation [23]:

$$D = (N/SD) \times L \qquad \text{..... 2.2}$$

where SD is the cation site density of zeolite, (SD = 8.91 atom nm^{-2}) [14], L is the distance between neighbouring silicon atoms in a SiO_2 crystal (L = 0.32 nm), and N is the surface concentration of deposited silica. N is obtained from the following:

$$N \text{ (Si atom nm}^{-2}) = \left[\frac{(W/100) \times A}{M \times ES}\right] \div 10^{18} \qquad \text{..... 2.3}$$

where W (wt %) is the amount of deposited silica, A is the Avogadro Number, M is the weight of SiO_2 (g/mol), and ES is the external surface area of the zeolite.

2.2.6. *Adsorption of linear and branched chain paraffins on silicalite and CVD-silicalites*

2.2.6.1. Gravimetric measurements of rate of adsorption

Adsorption experiments of different adsorbates, hexane, 2-methylpentane, butane and 2-methylpropane, were carried out gravimetrically by the McBain method [19] in the static condition using the system shown in Fig.

2.3. All the adsorbates were purified before use. 0.1 g of silicalite or CVD-silicalite sample was taken for each experiment. The sample was evacuated (~ 10^{-3} Torr) at 673 K for 2 h. The adsorbate was chilled at liquid nitrogen temperature and purified by trap-to-trap distillation. For adsorption measurement the pressures of the purified hexane and 2-methylpentane were kept at their vapour pressure at 273 K. On the other hand the pressures of purified butane and 2-methylpropane were kept at 40 Torr at room temperature. The purified adsorbate was admitted to the sample in basket maintained at 298 K. Adsorption was continued for one hour.

2.2.6.2. Chromatographic response

A chromatographic instrument was fabricated. The idea was borrowed from the work of Furusawa and Lechert [24, 25] to suit the present study. A Hitachi-163 Gas Chromatograph with a Shimadzu C-R64 Chromatopac as integrator and flame ionization detector (FID) was used. The schematic diagram is shown in the Fig. 2.4. 0.05 g silicalite (adsorbent) was taken in a glass column in between two quartz-wool plugs. The adsorbent was pretreated at 673 K for 1 h with a flow of 30 mL min^{-1} of dry helium. 0.1 mL of hexane vapour (adsorbate) with nitrogen equivalent to 0.82 μmol of hexane was injected with a syringe into the adsorbent with a carrier (He) flow rate 30 mL min^{-1} at 298 K. The eluted portion came to the detector through a stainless steel column without packing material. Using the same procedure, adsorption experiment of 2-methylpentane performed by injecting 0.1 mL (1.1 μmol) of 2-methylpentane on silicalite and the chromatogram was recorded. Same adsorption experiments of hexane and 2-methylpentane were also performed by using various CVD-silicalites as adsorbents. The similar method was followed in the adsorption experiments of butane and 2-methylpropane on silicalite and CVD-silicalites. In each case, 0.1 mL (4.1 μmol) of gaseous sample (butane or 2-methylpropane) was injected with a syringe into 0.05 g of the adsorbent.

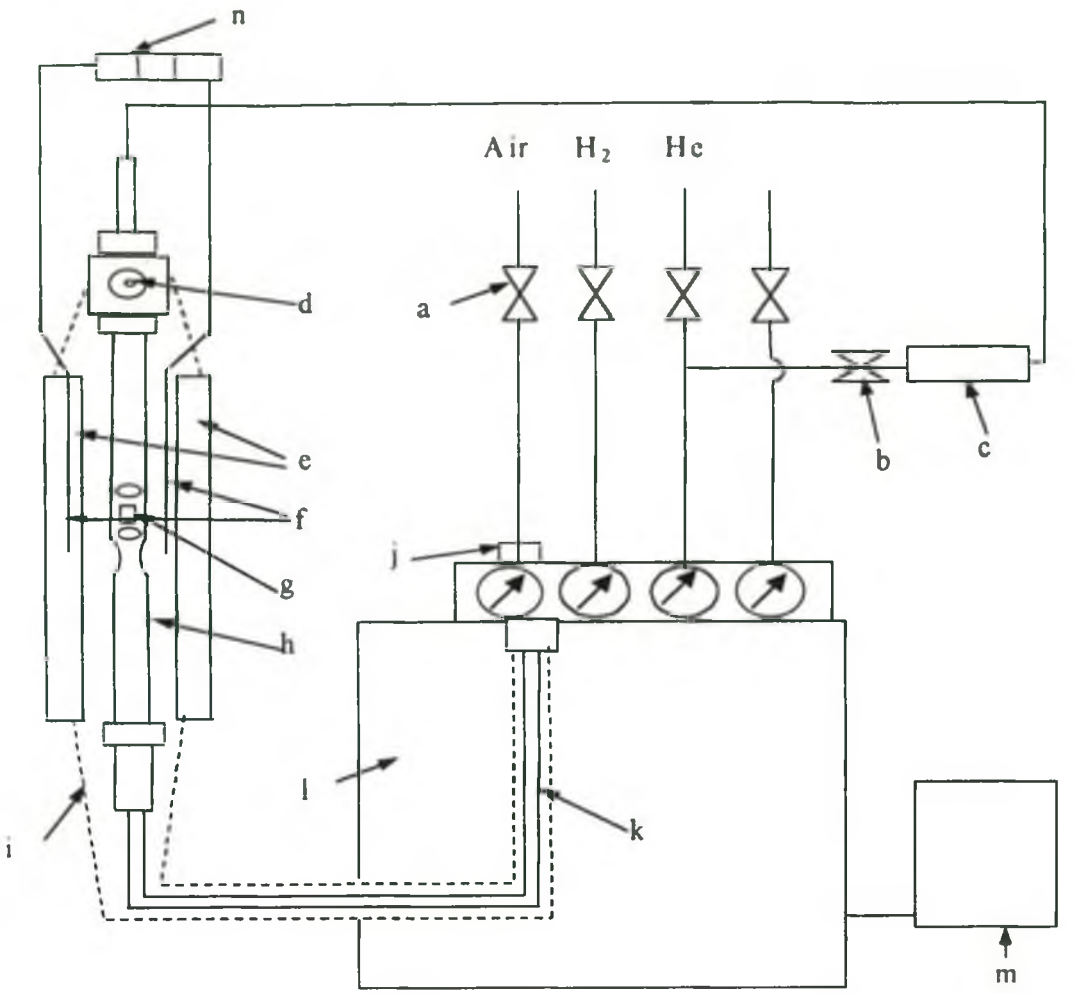

Fig. 2.4. Schematic representation of the chromatographic adsorption.

(a) Stop valve, (b) flow controller valve, (c) drier,
(d) injection port, (e) furnace, (f) thermocouple,
(g) adsorbent, (h) glass column, (i) ribbon heater,
(j) GC injection port, (k) stainless steel column, (l) GC oven,
(m) integrator (n) temperature controller.

2.3. Results

2.3.1. *Characterization of silicalite crystals*

From the XRD measurements (Fig. 2.5), the prepared silicalite crystal has been identified having the MFI type structure. The shape and the size of the crystals have been measured by SEM. The shape of silicalite is hexagonal flat plate with an average crystal size $5.3 \times 3.1 \times 1.5\ (\mu m)^3$, as shown in Fig. 2.6. Based on this SEM photograph, the external geometrical surface area of silicalite has been found as $1.3\ m^2\ g^{-1}$, the density being as usual $1.76\ g\ cm^{-3}$. From the TEM measurement, it has been observed that most of the crystals are large $[(5.1 - 6.8) \times (2.5 - 4.0) \times (0.6 - 2.0)\ (\mu m)^3]$. They are single crystals (from diffraction pattern) and microporous. The distance between two neighbouring micropores is about 1 nm (Fig. 2.7). A band for Si-OH has been found at $3740\ cm^{-1}$ with weak intensity in the IR spectrum of silicalite. The nitrogen adsorption isotherm is IV type (stepped) for silicalite (Fig. 2.8). The results confirm a previous observation [26].

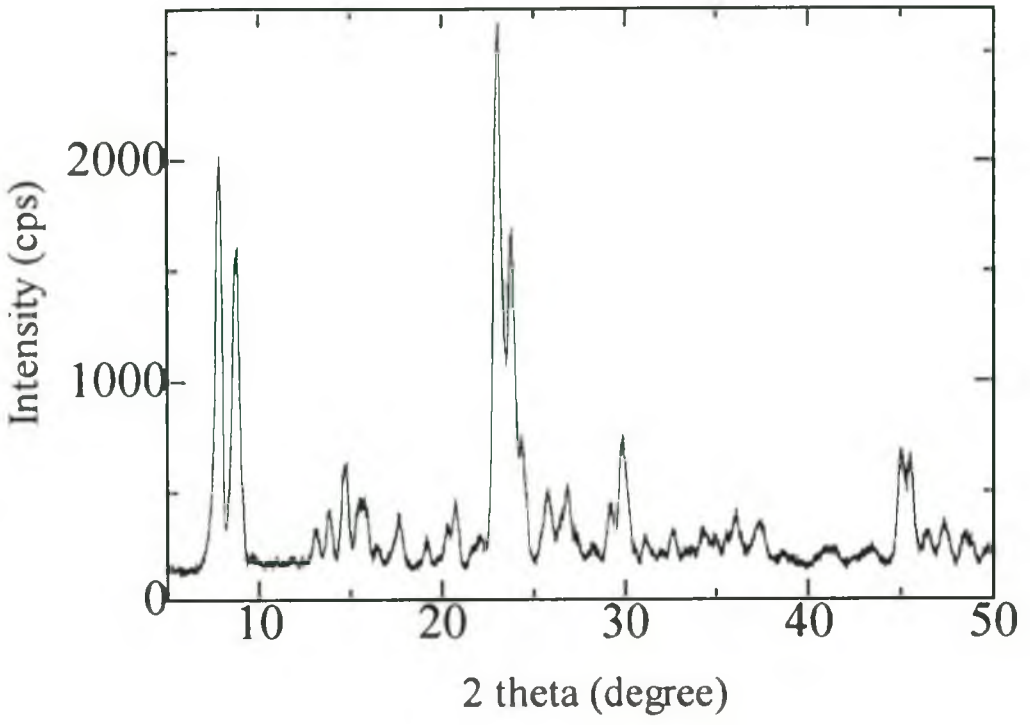

Fig. 2.5. X-ray diffraction pattern of silicalite crystals.

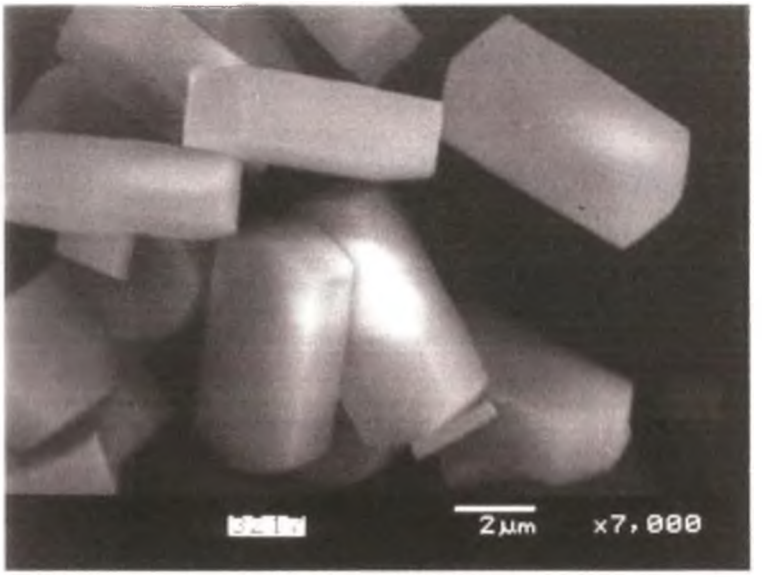

Fig. 2.6. SEM image of silicalite crystals.

Fig. 2.7. TEM image of silicalite crystal

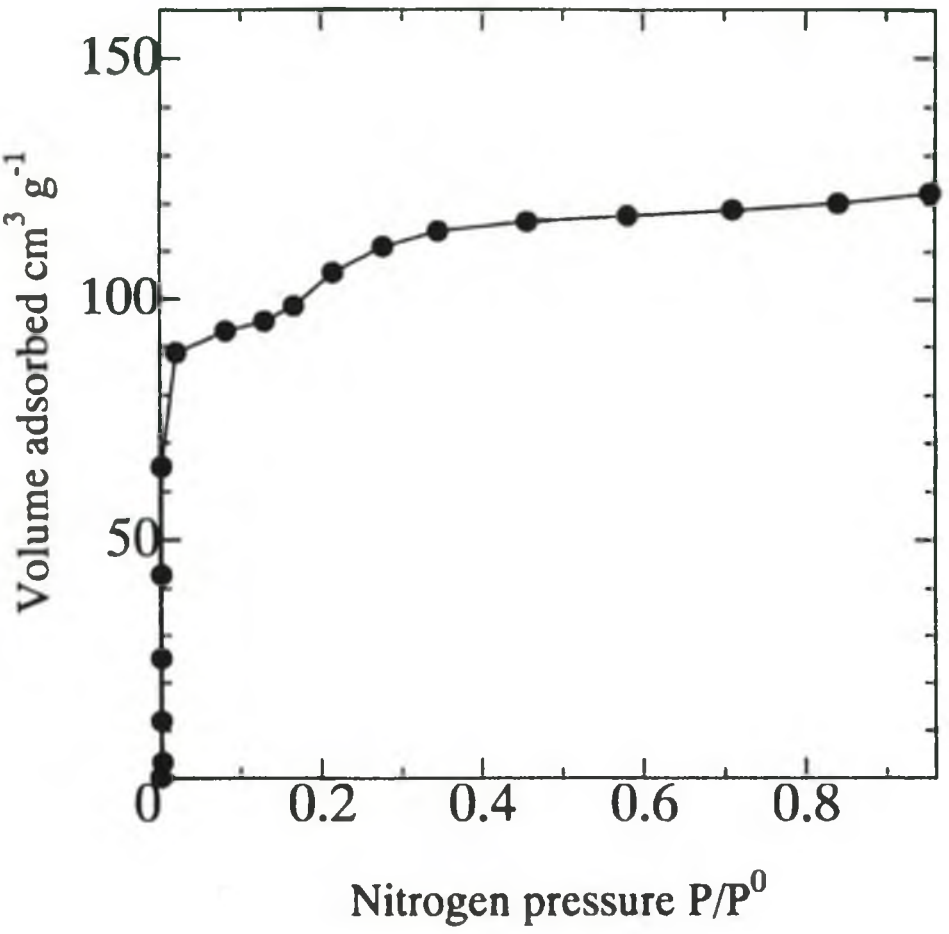

Figure 2.8. Nitrogen adsorption isotherm of silicalite crystals.

2.3.2. *Chemical vapour deposition of silica on silicalite crystals*

The increase of weight during chemical vapour deposition on silicalite at different temperatures is shown in Fig. 2.9 and the results are presented in Table 2.2. Fig. 2.9 shows that the rate of deposition of silica on silicalite is high at the initial stage even at low temperature. The rate of deposition gradually decreases, particularly at lower temperatures (513 K and 593 K) due to the lack of acid sites on silicalite, and high deposition with high rate becomes increasingly difficult. Even at 673 K, the deposition rate is considerably slow to be practical for preparing silicalite with high silica deposition. At 773 K, the deposition rate is high enough to prepare various types of silica deposited silicalite within a reasonable time. For this reason, in the present study, 773 K is chosen as the deposition temperature for preparing various CVD-silicalites. Silicalites with different amounts of deposited silica have been prepared varying the contact time. Four different CVD-silicalites (0.75 wt %, 1.3 wt %, 1.9 wt %, and 2.7 wt %) have been prepared at 773 K (Table 2.3).

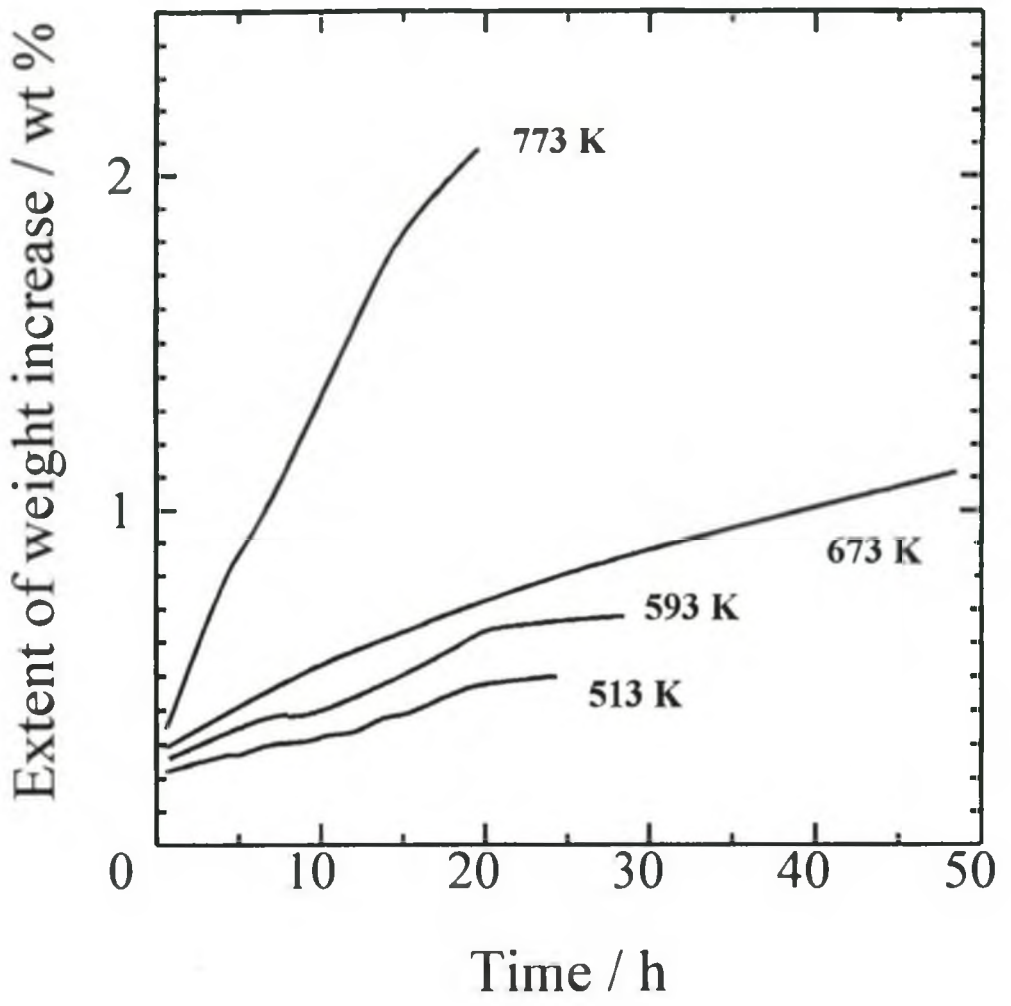

Fig. 2.9. The increase of weight on silicalite by chemical vapour deposition at different temperatures.

Table 2.2. CVD by $Si(OCH_3)_4$ on silicalite at different temperatures.

Deposition temperature (K)	Deposition time (h)	Weight increase upon deposition (wt %)	Weight after oxidation (wt %)	Surface concentration[a] of Si atom (nm^{-2})	Number of deposited silica layer
513	25	0.50	0.2	15	~2
593	29	0.73	0.5	39	4
673	49	1.15	0.8	62	7
773	19	2.1	1.9	147	16

[a] Surface concentration, on the external surface of silicalite.

Table 2.3. Preparation of silica deposited silicalite at different contact times at 773 K.

Run No.	Contact time for deposition (h)	Weight increase after oxidation (wt %)	Surface concentration[a] of Si atom (nm^{-2})	Number of deposited silica layer
1	9	0.75	58	6
2	14	1.3	100	11
3	19	1.9	147	16
4	44	2.7	208	23

[a] Surface concentration, on the external surface of silicalite.

2.3.3. *Characterization of prepared CVD-silicalites*

No significant change of the prepared CVD-silicalites has been observed in the SEM images (Fig. 2.10) although temperature as high as 773 K and about 20 h contact time were used.

From the TEM measurements (Fig. 2.11), it is clear that the deposited layer of silica covered the whole surface of the silicalite crystal (1.9 wt % CVD-silicalite), and the thickness of the deposited layer is found to be 5–8 nm. For 2.7 wt % CVD-silicalite crystals, the thickness of the deposited silica layer is about 7-10 nm. The theoretically calculated thickness of silica layer on the silicalite is 5.1 nm for 1.9 wt % CVD-silicalite sample, and 7.4 nm for 2.7 wt % CVD-silicalite sample, respectively. This shows satisfactory agreement between the experimental measurements and theoretical calculation.

Silicalite and CVD-silicalites do not show any difference in the nitrogen adsorption isotherms (Fig. 2.12).

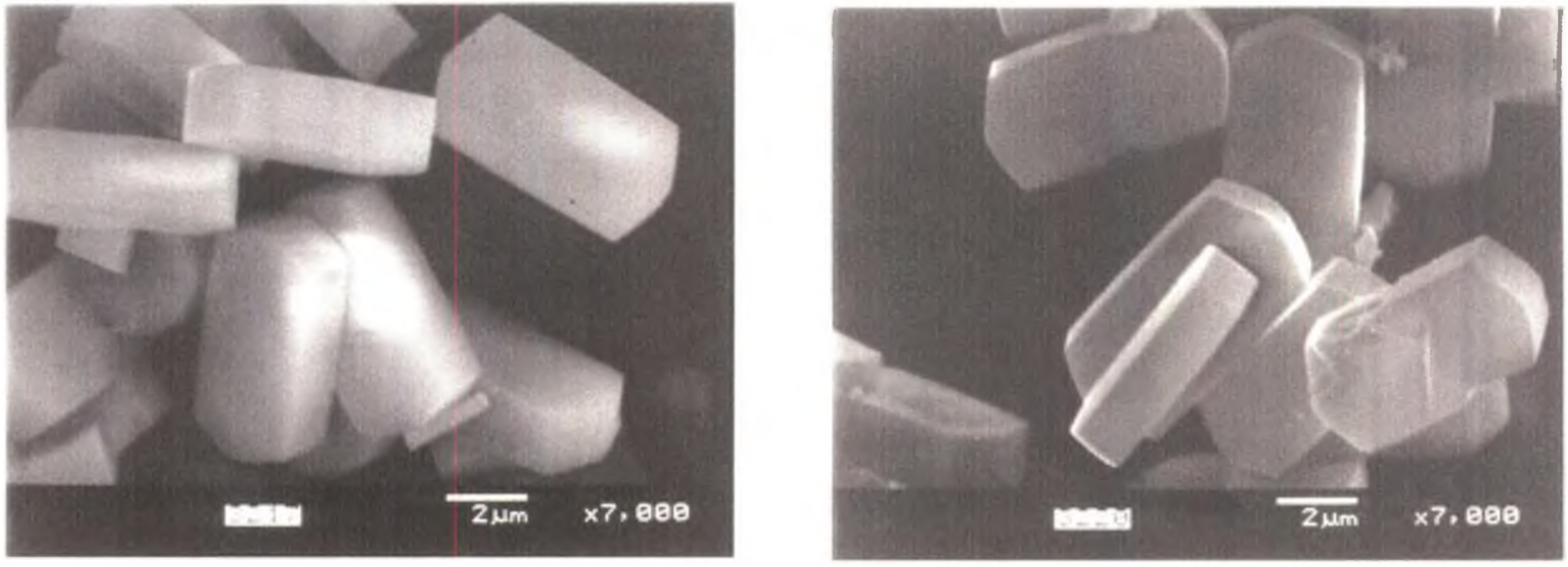

a b

Fig. 2.10. SEM images of (a) silicalite and (b) 1.9 wt % CVD-silicalite.

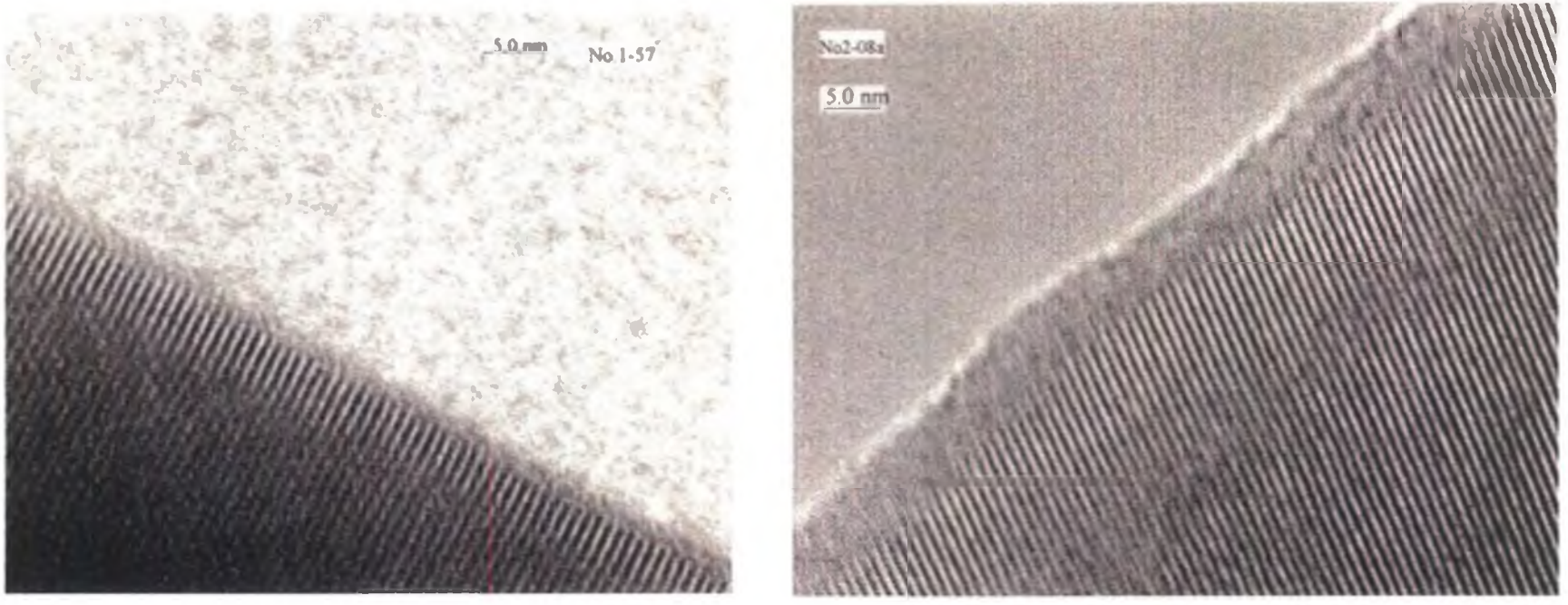

a b

Fig. 2.11. TEM images of (a) silicalite and (b) 1.9 wt % CVD-silicalite.

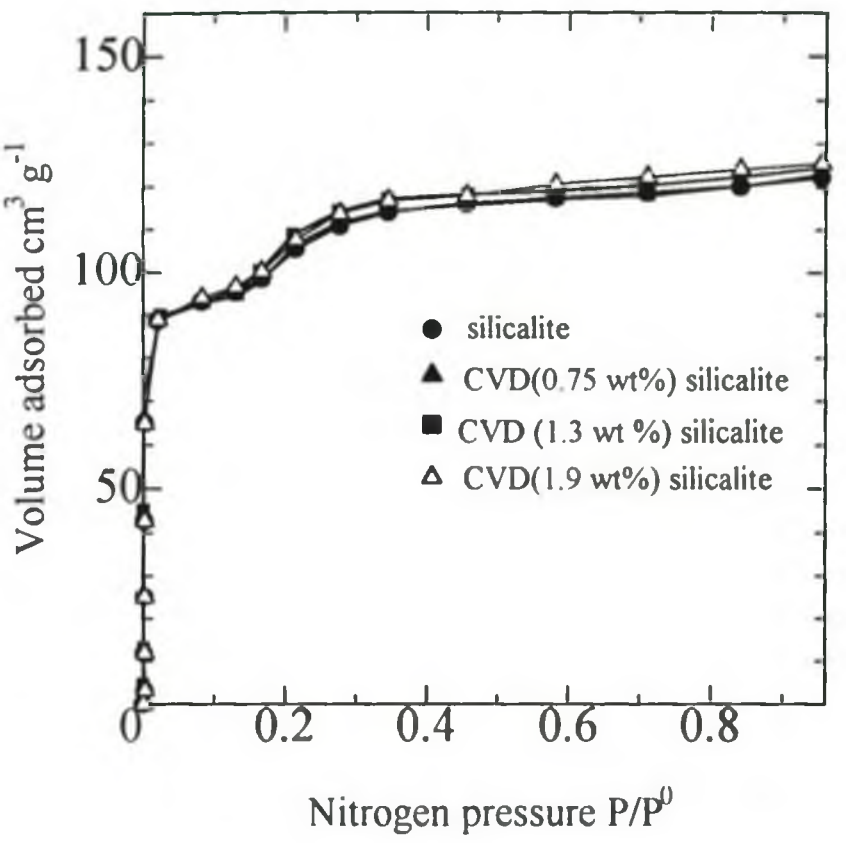

Fig. 2.12. Nitrogen adsorption isotherm of silicalite and CVD-silicalite samples.

2.3.4. *Adsorption characteristics*

2.3.4.1 Adsorption study by gravimetric method

The adsorption of hexane (kinetic diameter σ = 0.43 nm) and 2-methylpentane (σ = 0.50 nm) has been measured gravimetrically on silicalite and CVD-silicalites with different degrees of silica deposition, shown in Fig. 2.13 and Fig. 2.14. The amount of hexane adsorbed at equilibrium seems to be higher than that of 2-methylpentane on unmodified silicalite (Fig. 2.13a and Fig. 2.14a). The adsorption of hexane seems to be slightly suppressed on the CVD-silicalites (Fig. 2.13b–2.13e). The adsorption of 2-methylpentane is distinctly suppressed when 0.75 wt % SiO_2 is deposited on (Fig. 2.14b) and this suppression becomes quite significant when the silica amount on silicalite increases from 1.3 to 2.7 wt % (Fig. 2.14c–2.14e). The adsorption of butane (σ = 0.43 nm) and 2-methylpropane (σ = 0.50 nm) has also been studied gravimetrically. The adsorption of butane (Fig. 2.15) shows similar adsorption pattern as that of hexane (Fig. 2.13). The adsorption of 2-methylpropane is significantly suppressed on 1.3 wt % CVD-silicalite (Fig. 2.16c), and further suppression of adsorption is observed as the amount of deposited silica on silicalite increases (Fig. 2.16d and Fig. 2.16e).

The rate of adsorption has been analyzed using the following equation [27]:

$$\frac{Q_t}{Q_e} = \frac{6}{r}\left(\frac{D}{\pi}\right)^{\frac{1}{2}} t^{\frac{1}{2}} = kt^{\frac{1}{2}} \quad \left[taking \ \frac{6}{r}\left(\frac{D}{\pi}\right)^{\frac{1}{2}} \ as \ k \right] \qquad \ldots\ldots\ldots\ldots\ldots 2.4$$

where Q_t and Q_e are the amount adsorbed at time t and at the equilibrium, respectively. Q_t represents different amounts of adsorption at the initial stage. The adsorption equilibrium for hexane or butane on silicalite/CVD-silicalites is established very quickly but it takes considerably long time to

reach equilibria for 2-methylpentane and 2-methylpropane. For this, the Q_e value for each adsorbate has been taken as the adsorbed amount on silicalite in 1 h. r is the radius of the pore of zeolite crystal, D is the diffusion coefficient, and k is the adsorption rate constant. D has been assumed to remain constant [27]. On the basis of this equation the adsorption rate constants (k) of the adsorbates are obtained from the slopes of Q_t/Q_e vs. $t^{1/2}$ plot and the results are presented in Table 2.4.

The values of k also suggest that the adsorption rates of 2-methylpentane and 2-methylpropane suppressed with increasing of deposited silica on silicalite, while those of hexane and butane only slightly varied with the deposited silica (Table 2.4).

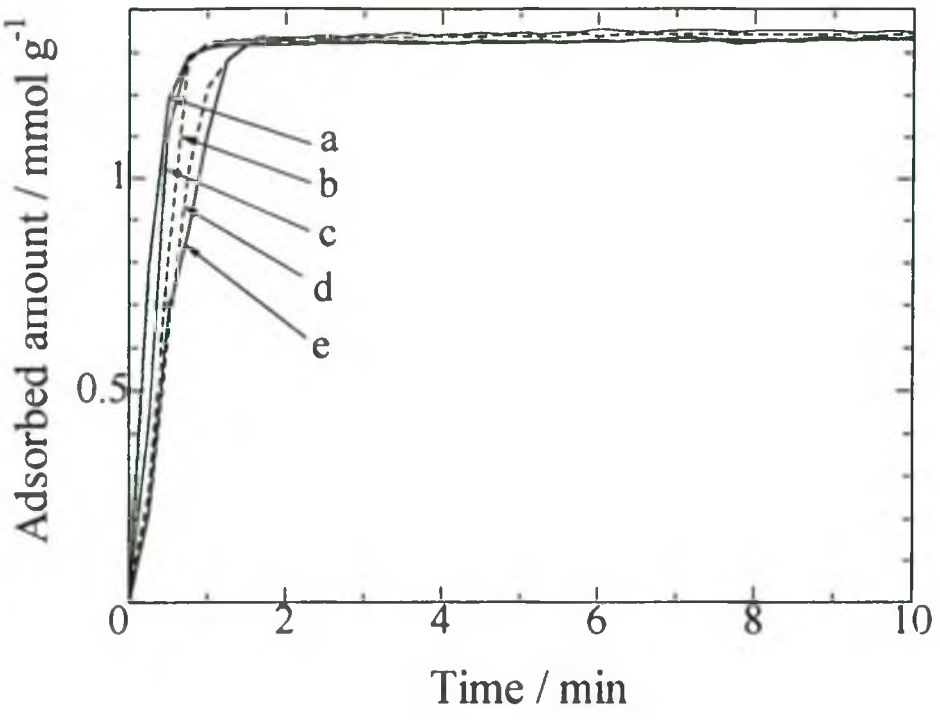

Fig. 2.13. Adsorption of hexane on silicalite and CVD-silicalites.

(a) Silicalite, (b) 0.75 wt %, (c) 1.3 wt %, (d) 1.9 wt % and (e) 2.7 wt % CVD-silicalite.

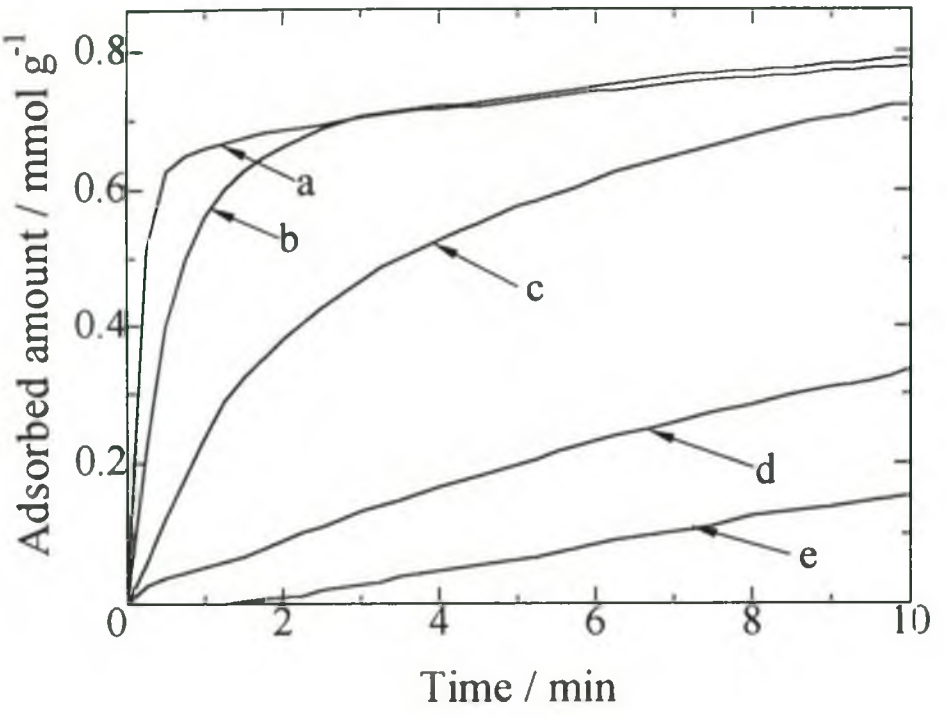

Fig. 2.14. Adsorption of 2-methylpentane on silicalite and CVD-silicalites.

(a) Silicalite, (b) 0.75 wt %, (c) 1.3 wt %, (d) 1.9 wt % and (e) 2.7 wt % CVD-silicalite.

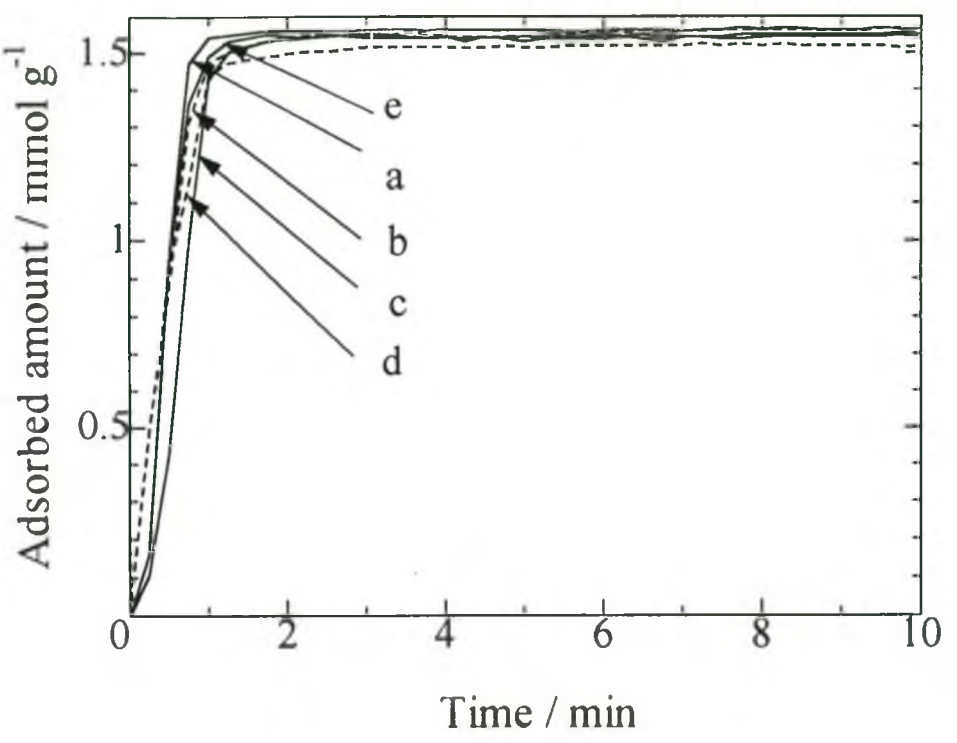

Fig. 2.15. Adsorption of butane on silicalite and CVD-silicalites.

(a) Silicalite, (b) 0.75 wt %, (c) 1.3 wt %, (d) 1.9 wt % and (e) 2.7 wt % CVD-silicalite.

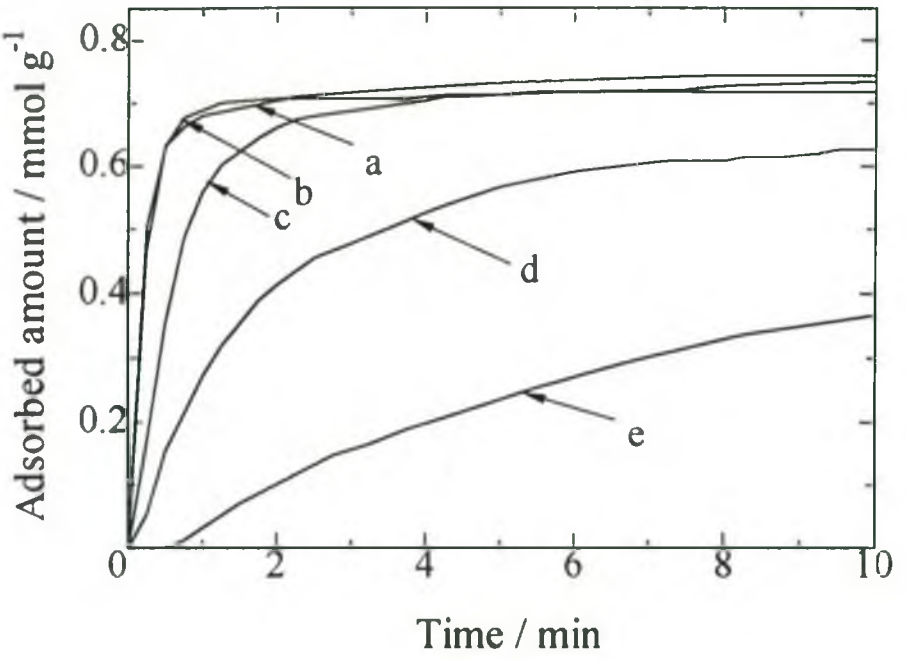

Fig. 2.16. Adsorption of 2-methylpropane on silicalite and CVD-silicalites.

(a) Silicalite, (b) 0.75 wt %, (c) 1.3 wt %, (d) 1.9 wt %, and (e) 2.7 wt % CVD-silicalite.

Table 2.4. Initial rate constant (k) of linear and branched paraffins on silicalite and CVD-silicalites.

Adsorbent	Initial rate constant[a], k ($min^{-1/2}$)			
	Butane[b]	Hexane[b]	2-Methylpropane[c]	2-Methylpentane[c]
silicalite	1.03	1.20	1.25	1.20
0.75 wt % CVD-silicalite	0.96	0.98	1.29	0.68
1.3 wt % CVD-silicalite	0.80	1.09	0.74	0.30
1.9 wt % CVD-silicalite	0.88	0.85	0.35	0.07
2.7 wt % CVD-silicalite	0.93	0.81	0.20	0.013

[a]Adsorption temperature = 298 K.
[b]Kinetic diameter σ = 0.43 nm.
[c]Kinetic diameter σ = 0.50 nm.

2.3.4.2. Adsorption study by chromatographic method

In all cases, the elution chromatograms are completed within a very short time. The elution chromatograms are presented in Fig. 2.17 and Fig. 2.18. The chromatograms show that hexane and 2-methylpentane are completely adsorbed by the silicalite and there is no tailing in the chromatograms (Fig. 2.17). A weak elution peak of 2-methylpentane is observed for 0.75 wt % CVD-silicalite and the peaks are gradually intensified with the increase of deposited silica on silicalite. 2-methylpentane is eluted without adsorption on 2.7 wt % CVD-silicalite (Fig. 2.17).

Hexane and butane are almost completely adsorbed on the CVD-silicalites (Fig. 2.17 and Fig. 2.18). 2-Methylpropane starts elution from 1.3 wt % CVD-silicalite and the intensity of the elution peak increases gradually as the deposited silica on silicalite increases (Fig. 2.18). Thus the trends of adsorption of adsorbates as found by gravimetric method are corroborated by the elution chromatograms.

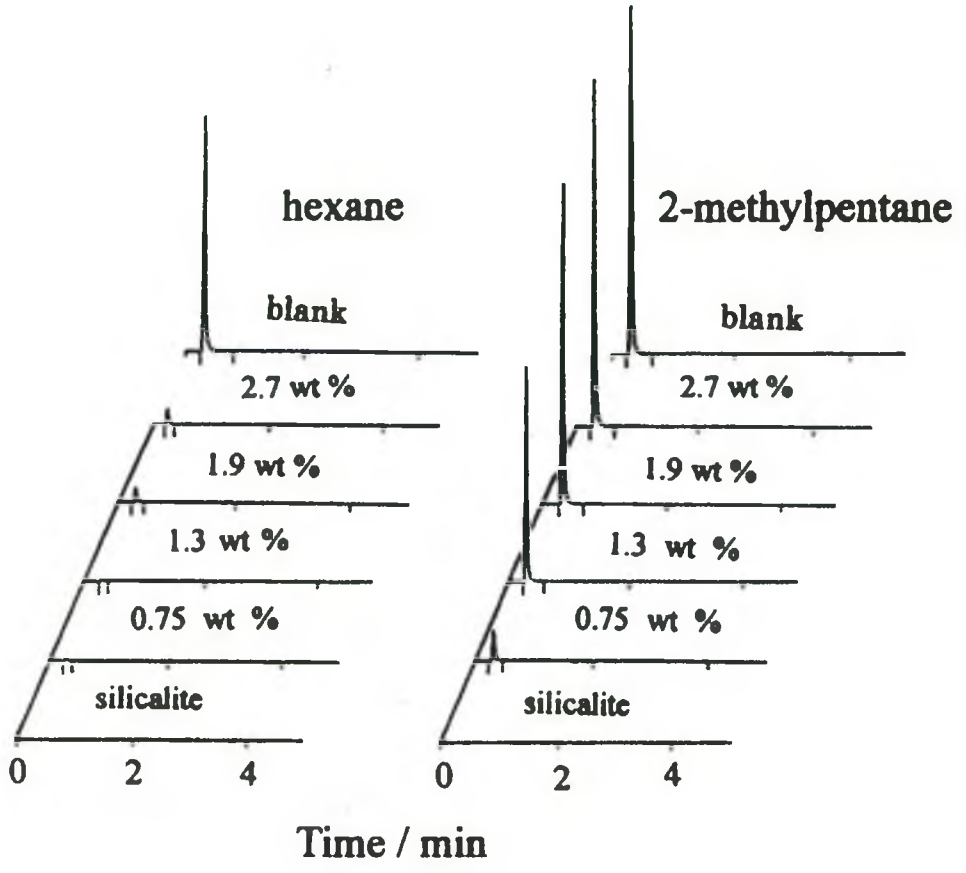

Fig. 2.17. Elution chromatograms of hexane and 2-methylpentane on silicalite and CVD-silicalites (chromatograms are magnified 8 times for hexane).

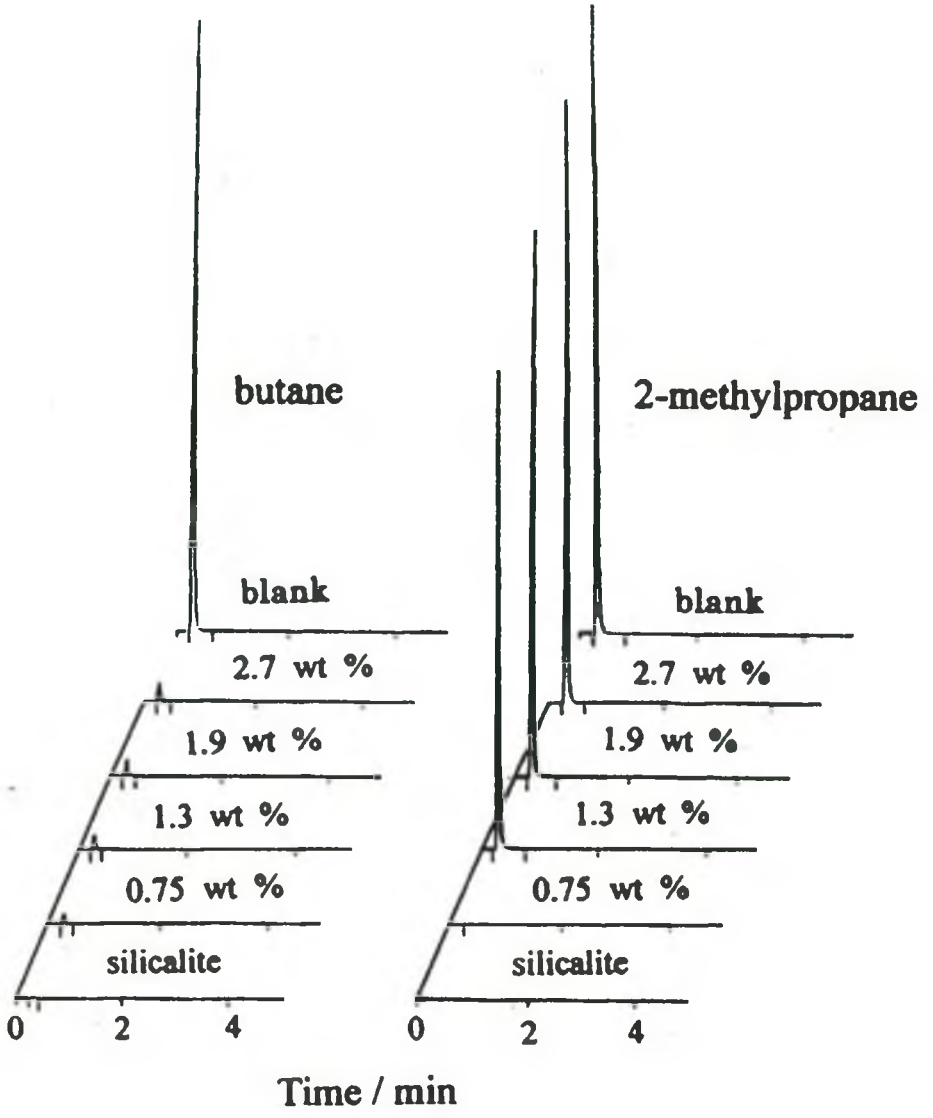

Fig. 2.18. Elution chromatograms of butane and 2-methylpropane on silicalite and CVD-silicalites.

2.4. Discussion

2.4.1. *Chemical vapour deposition*

Fig. 2.9 shows that about 0.2 wt % weight increase occurs quickly at the initial stage of deposition. At this stage, the weight of the deposited silica is about 40 % of the deposited material. This is because after oxidation of 0.5 wt % deposited material, about 0.2 wt % silica is obtained at 513 K (Table 2.2). The weight of silica at the initial stage is estimated to be *ca.* 0.1 wt %, corresponding to 8 Si-atom nm^{-2} on the external surface of silicalite. Since the surface concentration 8.91 Si atom nm^{-2} is required to form a monolayer [14], the monolayer of silica is supposed to be formed quickly at the early stage of deposition. This behaviour seems to be independent of temperature as indicated by the convergence of the plots at 0.2 wt % (Fig. 2.9). After that, multilayer formation starts with time. Higher temperature favours higher deposition of silica on the silicalite crystals.

The numbers of the layers formed upon deposition of silica on the external surface of the silicalite has been estimated. It is found that about twenty-three layers of silica are formed on the silicalite in the case of 2.7 wt % CVD-silicalite (Table 2.3). The deposited silica effectively controls the pore-opening size of silicalite, and suppresses the adsorption of one-branched alkanes (σ = 0.50 nm) more than that of linear alkanes (σ = 0.43 nm) (Table 2.4). It has been reported [28] that fifteen silica layers are required to control the pore-opening size of HZSM-5, (SiO_2/Al_2O_3 ratio 76.4 and external surface area = 10.8 $m^2\ g^{-1}$), and the modified zeolite (14.4 wt % Si-HZSM-5) can suppress the adsorption of one-branched alkane, effectively.

Nitrogen adsorption isotherms also show that adsorption rates remain unaffected by deposition of silica on the silicalite crystals (Fig. 1.12).

2.4.2. *Control of pore-opening size*

Chemical vapour deposition of $Si(OCH_3)_4$ on silicalite controls the pore-opening size only, because the molecular size of $Si(OCH_3)_4$ is larger than the pore size of silicalites, and the alkoxide cannot enter into the silicalite pores. The deposited silica thus controls the diffusion of molecules in the pore opening. From the adsorption results of 2-methylpentane (σ = 0.50 nm), the effective control of the pore-opening size of silicalite has been observed. The rate of adsorption of 2-methylpentane decreases significantly with the increase of deposited silica on silicalite (Fig. 2.14 and Table 2.4). It is to be noted that the rate of adsorption of hexane (σ = 0.43 nm) has not been influenced significantly by the deposited silica on silicalite (Fig. 2.13 and Table 2.4). Similar adsorption behaviour is observed in the cases of butane and 2-methylpropane (Fig. 2.15 and Fig. 2.16). It appears that the adsorption rate for 2-methylpropane (σ = 0.50 nm) decreases significantly with the increase of deposited silica on silicalite while very small difference in the rate is observed in case of butane (σ = 0.43 nm) (Table 2.4).

Although the deposited silica on the silicalite is the same the rate of adsorption of 2-methylpentane is suppressed more than that of 2-methylpropane (Fig. 2.14 and Fig. 2.16). This observation reflects that not only the width, but also the length of hydrocarbon chain show considerable influence on the adsorption behaviour. This is consistent with the results found in the case of olefins [19]. Generally, the adsorption rate decreases with the increase of the chain length of hydrocarbons for CVD-silicalites [29].

2.4.3. *Morphology of CVD-silicalites*

The TEM images of 1.9 wt % and 2.7 wt % CVD-silicalite crystals (Fig. 2.11) show that the CVD silica forms a homogeneous layer on the external surface of the silicalite crystals. The thickness of CVD silica layer on all faces of the crystal is identical but the thickness varies from crystal to crystal, as there is a variation of the surface morphology. These suggest that the silica layer covers the silicalite crystals uniformly.

Both the TEM results and the adsorption results suggest that there are channels existing in the CVD layer. These channels are not three-dimensional channels as are present in the silicalite crystals. Rather, they are one-dimensional straight features that are formed in the CVD silica layer on every face of the silicalite crystal. The channels in the layer on the (010) and (100) faces are orthogonal to the surfaces of the crystals. The channels in the layer interlink with the channels in the crystal so that the adsorbate molecules can go into the silicalite crystal through the CVD silica layer [30]. The pore-opening size of the one-dimensional channels decreases gradually, as the deposited silica layer becomes thicker. Fig. 2.19 qualitatively describes a model of channel structure in the CVD silica layer on the (010) surface of the silicalite crystal.

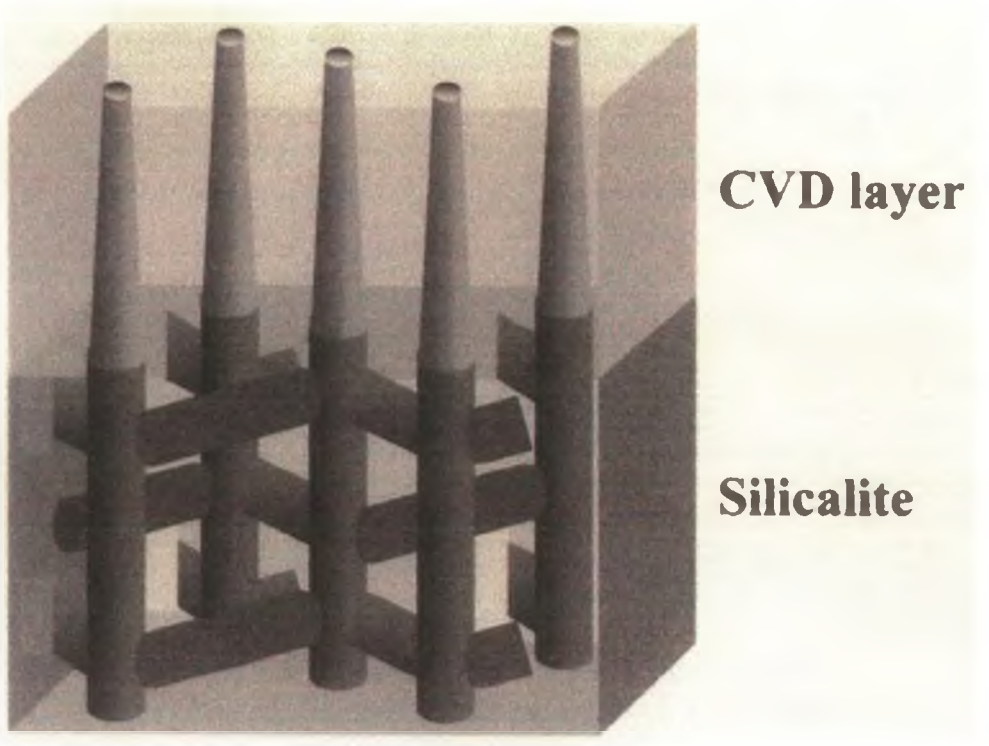

Fig. 2.19. A model of the one-dimensional channel structure in a CVD silica layer on the (010) surface of a silicalite crystal.

2.5. Conclusion

In the case of chemical vapour deposition (CVD) of tetramethoxysilane on silicalite crystals, its non-acidic nature requires relatively high temperature (773 K) to have thicker silica layers that are sufficient for making them selective adsorbents. Adsorption of linear and branched alkanes on silicalite and CVD-silicalites, have been measured gravimetrically and chromatographically, at about 298 K. Both methods have given identical results. It has been found that the adsorption behaviour is almost unchanged for hexane and butane. On the other hand, the adsorption of 2-methylpentane and 2-methylpropane is suppressed with the increase of the deposited silica on silicalite. The extent of suppression depends on the kinetic diameter, chain length of paraffins and on the amount of deposited silica on silicalite. Thus, the linear and the branched paraffins can be separated by choosing the extent of silica deposition on silicalite.

2.6. References

[1] Flanigen, E. M., Bennett, J. M., Grose, R. W., Cohen, J. P., Patton, R. L., Kirchner, R. M. and Smith, J. V., *Nature*, **271,** 512 (1978).

[2] Sun, M. S., Shah, D. B., Xu, H. H. and Talu, O., *J. Phys. Chem. B.*, **102**, 1466 (1998).

[3] Talu, O., Guo, C. J. and Hayhurst, D. T., *J. Phys. Chem.*, **93,** 7294 (1989).

[4] Sun, M. S., Talu, O. and Shah, D. B., *J. Phys. Chem.*, **100,** 17276 (1996).

[5] Abdul-Rehman, H. B., Hasanain, M. A. and Loughlin, K. F., *Ind. Eng. Chem. Res.*, **29,** 1525 (1990).

[6] Hufton, J. R. and Danner, R. P., *AIChE J.*, **39,** 954 (1993).

[7] Cavalcante, C. L., Jr. and Ruthven, D. M., *Ind. Eng. Chem. Res.*, **34,** 177 (1995).

[8] Cavalcante, C. L., Jr. and Ruthven, D. M., *Ind. Eng. Chem. Res.*, **34,** 185 (1995).

[9] Funke, H. H., Kovalchick, M. G., Falconer, J. L. and Noble, R. D., *Ind. Eng. Chem. Res.*, **36,** 137 (1997).

[10] Golden, T. C. and Sircar, S., *J. Colloid Interface Sci.*, **162,** 182 (1994).

[11] Miyamoto, T., Katada, N., Kim, J. -H., Niwa, M. and Tsutsumi, K., *J. Phys. Chem. B,* **102,** 6738 (1998).

[12] Katada, N., Miyamoto, T., Begum, H. A., Naito, N., Niwa, M., Matsumoto, A. and Tsutsumi, K., *J. Phys. Chem. B,* **104,** 5511 (2000).

[13] Niwa, M., Kato, S., Hattori, T. and Murakami, Y., *J. Chem. Soc., Faraday Trans. 1.*, **80**, 3135 (1984).

[14] Niwa, M., Morimoto, S., Kato, M., Hattori, T. and Murakami, Y., in "Proceedings of 8th International Congress on Catalysis", Verlag Chemie, Weinheim, p. IV-701, (1984).

[15] Niwa, M., Kato, M., Hattori, T. and Murakami, Y., *J. Phys. Chem.*, **90**, 6233 (1986).

[16] Hibino, T., Niwa, M. and Murakami, Y., *J. Catal.*, **128,** 551 (1991).

[17] Kim, J. -H., Ishida, A., Okajima, M. and Niwa, M., *J. Catal.*, **161,** 387 (1996).

[18] Niwa, M., Yamazaki, K. and Murakami, Y., *Ind. Eng. Chem. Res.*, **30,** 38 (1991).

[19] Niwa, M., Yamazaki, K. and Murakami, Y., *Ind. Eng. Chem. Res.*, **33,** 371 (1994).

[20] Argauer, R. J. and Landolt, G. R., U.S. Patent 3,702,886 (1972).

[21] Treacy, M. M. J. and Newsam, J. M., *Ultramicroscopy*, **23**, 411 (1987).

[22] Csencsits, R. and Gronsky, R., *Ultramicroscopy*, **23**, 421 (1987).

[23] Niwa, M. and Murakami, Y., *J. Phys. Chem. Solids*, **50,** 487 (1989).

[24] Furusawa, T., Suzuki, M. and Smith, J. M., *Catal. Rev. Sci. Eng.*, **13,** 43 (1976).

[25] Lechert, H. and Schweitzer, W., *Stud. Surf. Sci. Catal.*, **24,** 427 (1985).

[26] Zecchina, A., Bordiga, S., Spoto, G., Marchese, L., Petrini, G., Leofanti, G. and Padovan, M., *J. Phys. Chem.*, **96,** 4985 (1992).

[27] Barrer, R.M. and Brook, D. W., *Trans. Faraday Soc.*, **49,** 1049 (1953).

[28] Niwa, M., Senoh, N., Hibino, T., Nakatsuka, Y. and Murakami, Y., *Stud. Surf. Sci. Catal.*, **83,** 155 (1985).

[29] Begum, H. A., Katada, N. and Niwa, M., *Micropor. Mesopor. Mater.*, **46,** 13 (2001).

[30] Lu, D., Kondo, J. N., Domen, K., Begum, H. A., and Niwa, M., submitted for publication in *Angew. Chem. Int. Ed. Engl*, (2002).

Chapter Three

Modification of USY Zeolite by Chemical Vapour Deposition of Tetramethoxysilane

3.1. Previous studies

Zeolite Y has the faujasite (FAU) structure with typical Si/Al ratio between 1.50 and 3. The faujasite topology can be described as a linking of sodalite cage (14-hedron, also called β-cage) through hexagonal prisms containing a center of symmetry (Section 1.2.4.3) [1].

Zeolite Y is used mainly as catalyst in the fluid catalytic cracking (FCC) process and hydrocracking process. It is generally accepted that the cracking activity can be attributed to the Brønsted acidity of the zeolite [2]. Catalytic cracking of *iso*-propylbenzene in the presence of zeolites takes place as follows:

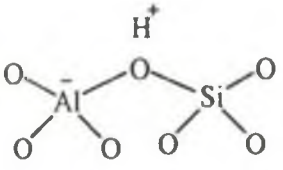

Brønsted acid site

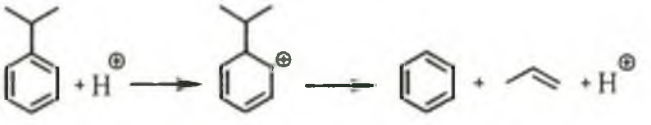

Cracking of *iso*-propylbenzene

The zeolite is modified in order to adapt its properties to the catalytic application. Dealumination is a method to prepare the ultrastable Y (USY) zeolite. The dealumination consists generally of a hydrothermal treatment in order to dealuminate the zeolite framework, followed acid leaching, which solubilizes the extra-framework species created during steaming process. Prepared samples possess high thermal stability and structural stability in atmosphere [3-5]. The degree of dealumination depends on the partial pressure of steam. It is observed that the greater the hydrothermal environment, the more aluminium is removed from the framework [6, 7].

The acidic form of ultrastable Y (H-USY) zeolite, prepared by steam dealumination of Y zeolite, is a highly active hydrocarbon cracking

catalyst. Brønsted acid sites are generated in USY zeolite by thermal decomposition of ammonium ions, which are exchanged for H^+ ions in the zeolite, after the Y zeolite has undergone steam dealumination. Steam dealumination of NH_4-Y and Na-Y zeolite at temperatures of 600-1100 K causes partial removal of Al^{3+} ions, from the zeolite framework. Aluminium oxide or hydroxide in the zeolite framework hosts these aluminium cations [8-12]. These Al species are referred to as extraframework or nonframework Al (Al_{NF}).

H-Y zeolite can also be prepared without nonframework Al by repeated exchange of NH_4^+ ions for Na^+ ions of Na-Y zeolite, followed by slow (dry) calcination at moderate temperatures to decompose the NH_4^+ ions. Because of its high Al content, H-Y zeolite displays poor thermal and hydrothermal stability, making it unsuitable for many commercial applications. Despite more acid sites in H-Y zeolite than in H-USY zeolite the catalytic activity of H-Y zeolite is much lower compared to H-USY zeolite [13].

A number of explanations have been proposed for the higher activity of H-USY zeolite than of H-Y zeolite. The most prevalent proposal is that it is a result of increased Brønsted acid strength in H-USY zeolite. Temperature programmed desorption (TPD) shows an increase in the ammonia desorption temperature due to the increase of this acid strength [14]. This is supported by a shift of the hydroxyl band frequency in IR [15], and by microcalorimetric adsorption of bases [16-18].

Two reasons have been advanced to explain the higher activity and stronger acidity of H-USY zeolite [13]. First, isolated framework Al (Al_F), *i.e.*, those with no second nearest Al neighbours, is believed to be more acidic [19-22]. Steam dealumination of the zeolite removes Al_F and presumably creates more isolated Al_F. Second, it has been proposed [8, 9]

that nonframework Al species (Al_{NF}) next to Al_F withdraw electron of the oxygen ions from the zeolite lattice. The Al_{NF} cations are likely to be located in the sodalite cages [13] or in the Lewis acid sites near the Brønsted site [8, 9, 22]. The latter proposal is consistent with the observations that a small concentration of sodium [11, 23, 24], potassium [24], or ammonium [25] ions can destroy the activity of H-USY zeolite as formed during cracking of C_4-C_7 hydrocarbons [26].

3.2. Experimental

3.2.1. *Materials and reagents*

Two types of USY zeolite were used in this study. The high siliceous USY zeolite was denoted as HS-USY zeolite (SiO_2/Al_2O_3 = 29.0, Tosoh Co. Ltd., Japan) and low siliceous USY zeolite was denoted as LS-USY zeolite (SiO_2/Al_2O_3 = 7.51, Catalysis and Chemical Industries, Japan). 1,3,5-Trimethylbenzene or 1,3,5-TMB (Nacalai tesque, Japan) and 1,3,5-triisopropylbenzene or 1,3,5-TIPB (Tokyo Chemical Industries, Ltd., Japan) were used in this study. All other reagents and chemicals were of analytical grade. When necessary chemicals were also purified.

3.2.2. *Chemical vapour deposition of tetramethoxysilane on USY zeolites*

Chemical vapour deposition (CVD) of tetramethoxysilane on HS-USY and LS-USY zeolites was performed by using the usual static vacuum system (Fig. 2.3) at 593 K (Section 2.2.4.1). The deposition and evacuation cycle was repeated to obtain the desired weight increase of the deposit. This was followed calcination and oxidation by oxygen (200 Torr) at 673 K to remove the carbonaceous residues associated with the deposition. Then the system was evacuated to measure the weight gain, which showed the extent of modification by deposition of silica on USY zeolite.

3.2.3. *Characterization of the silica deposited USY zeolites*

3.2.3.1. X-ray diffraction (XRD)

All of the prepared silica deposited USY zeolites were characterized by the powder X-ray diffraction (XRD) method, using a Rigaku, Miniflex Plus

Diffractometer with 0.45 kW CuKα (30 kV, 15 mA). The parameters used for the X-ray diffractometer were described in Section 2.2.3.1.

3.2.3.2. Temperature programmed desorption (TPD) of ammonia

The TPD experiments were carried out using an all-glass apparatus with thermal conductivity detector and/ or a mass spectrophotometer, as shown in Fig. 3.1.

To measure the acid amount in the zeolite by temperature programmed desorption of ammonia, zeolite sample (0.1 g) was packed into the quartz cell installed in a TPD equipment [Bel Japan Inc., TPD-1-AT (NH3)]. Then it was evacuated (~10^{-3} Torr) at 773 K for 1 h. Then ammonia (100 Torr) was introduced into the cell, the pressure was kept stable for 30 min at 373 K and then the system was evacuated for 30 min. Water vapour was introduced into the sample cell; *i.e.*, the sample was exposed to water vapour (~ 22 Torr, at room temperature) at 373 K for 30 min, followed by evacuation for 30 min. The water vapour treatment was repeated. To completely remove *l*-peak without affecting *h*-peak on H- and Na-mordenite and Y zeolite this procedure has been found very effective [27-29]. Subsequently, the adsorbed ammonia (*h*-peak) was desorbed by helium flow (0.044 mol s^{-1}) under *ca.* 100 Torr total pressure by heating at the rate of 10 K min^{-1} starting from 373 K. The desorbed ammonia was detected by mass spectrometer (ANELVA M-QA 100F). Although the molecular weight of ammonia is 17, the fragment with m/e = 16 was used to quantify ammonia, because the parent peak with m/e = 17 was affected by the desorbed water. Afterwards, a known amount of ammonia was fed to the system to calibrate the mass spectrum intensity.

The amount of desorbed ammonia C_g was calculated using the equation described in Section 1.6.3.3.

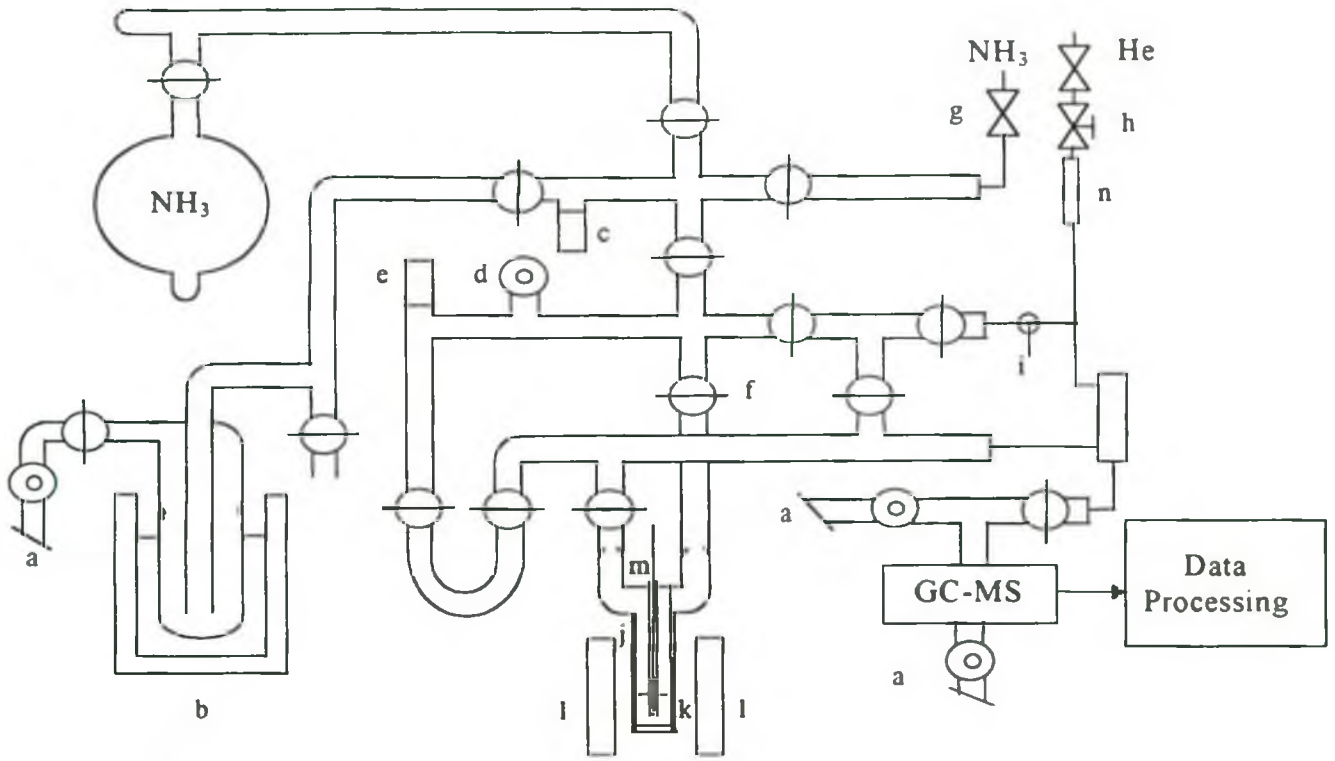

Fig. 3.1. Experimental set up for TPD of ammonia.

(a) Rotary pump, (b) liquid nitrogen trap, (c) pressure-voltage transducer (for high pressure), (d) pirani gauge, (e) pressure-voltage transducer (for low pressure), (f) stop valve, (g) flow controller, (h) needle valve, (i) 3-way valve, (j) thermocouple, (k) zeolite sample, (l) electric furnace, (m) quartz cell (n) moisture trap.

3.2.3.3. Infrared (IR) studies

Infrared measurements were performed with a Fourier transform infrared (FTIR) spectrometer (JASCO FTIR-5300) using a quartz cell. A schematic diagram is shown in Fig. 3.2. About 10 mg sample was pressed into a thin self-supporting wafer. The sample was evacuated at 773 K (10^{-3} Torr) for 1 h and IR spectra were measured at room temperature (about 298 K). In each case background peak was subtracted.

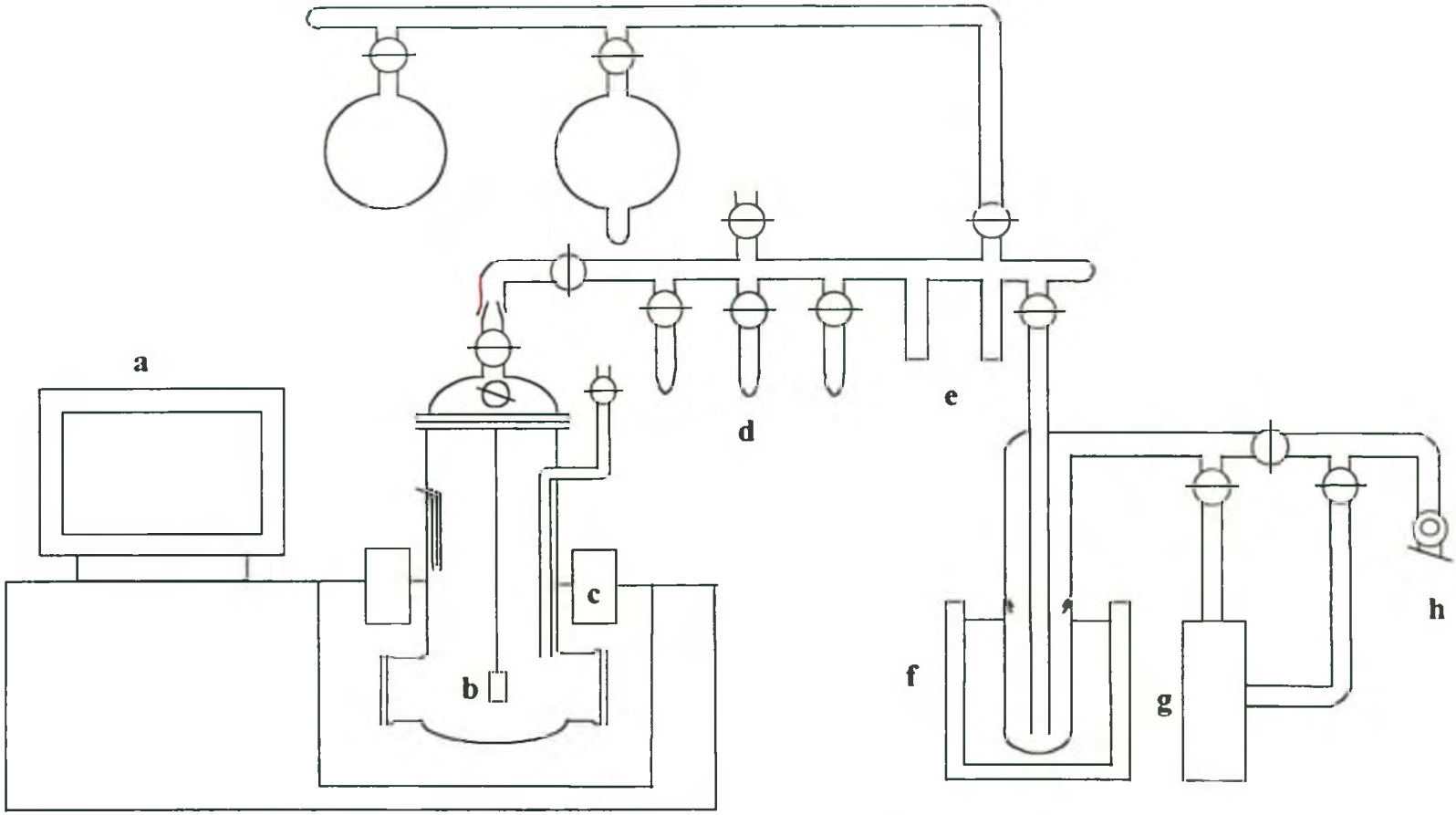

Fig. 3.2. Apparatus for IR experiment.

(a) FTIR instrument, (b) sample disc, (c) electric furnace, (d) liquid reservoir,
(e) pressure-voltage transducer, (f) liquid nitrogen trap, (g) diffusion pump (h) rotary pump.

3.2.3.4. Determination of aluminium and sodium by inductively coupled plasma (ICP) emission spectroscopy

Inductively coupled plasma (ICP) emission spectrophotometer (Shimadzu ICPS-5000) was used for this purpose. About 25 mg accurately weighed zeolite sample was digested with a mixture of conc. H_2SO_4 and HF in a teflon coated beaker. The solution was evaporated to dryness. The dried mass was dissolved in conc. H_2SO_4. The residual sulphur containing compounds (H_2S and SO_2) were removed by heating. Then solution was taken in a standard volumetric flask and deionised water was added to make up the volume.

Standard aluminium ion solutions of 0.2, 2.0, 5.0 and 10 ppm were prepared by diluting standard 1000 ppm aluminium ion solution (Nacalai tesque, Japan). The intensity of emissions of these solutions at different concentrations was measured at 396.153 nm. A standard calibration curve was obtained by plotting intensity of standard solutions vs. concentrations. The unknown concentrations of aluminium ions in zeolite solutions were determined by using this calibration curve. Aluminium content of a zeolite was expressed in mol kg^{-1}.

Using similar procedure, the concentration of sodium ion content in zeolite was determined. The intensity of emissions for sodium ion of different standard concentrations and the sample solutions were measured at 588.995 nm. A standard calibration curve was prepared by plotting intensity of the standard solutions vs. concentrations. The unknown concentrations of sodium ions in zeolite solutions were determined by using this calibration curve. Sodium content of a zeolite was expressed in mol kg^{-1}.

3.2.4. *Gravimetric measurements of rate of adsorption of 1,3,5-triisopropylbenzene*

1,3,5-TIPB and the USY zeolite sample (0.1 g) were taken in the system (Fig. 2.3) and according to previously described procedure [Section 2.2.4.1]. The liquid reservoir was closed. The USY zeolite samples were evacuated at about 10^{-3} Torr and heated at 673 K for 2 h until constant weight. As mentioned earlier [Section 2.2.4.1], a transducer monitored the change of weights of samples and the data were transferred to a personal computer. Temperature of the sample was fixed at 393 K. Adsorption was started by opening the stop-cock of the liquid reservoir maintained at 298 K. This allowed the vapour of 1,3,5-TIPB to be adsorbed on the sample. The extent of adsorption was recorded by noting the weight change.

3.2.5. *Catalytic cracking of 1,3,5-trimethylbenzene and 1,3,5-triisopropylbenzene*

Catalytic cracking of 1,3,5-TMB and 1,3,5-TIPB was performed by the pulse technique using the system shown in Fig. 3.3. 2.0 to 5.0 mg catalysts were taken in a glass column in between two quartz-wool plugs. The catalyst was pretreated at 773 K for 1 h with a flow of 50 mL min^{-1} of dry nitrogen. 1 μl of reactant was injected into the column containing catalyst with a carrier (N_2) flow rate 50 mL min^{-1}, at 523 K for 1,3,5-TIPB and 623 K for 1,3,5-TMB. Products were analyzed by Shimadzu GC-14A gas chromatograph. An FID detector and a capillary column ULBON HR-17 (25 m long and 0.25 mm ID), operating from 313 K to 523 K or 623 K at 5 K min^{-1} heating, were used. The chromatogram was recorded by Shimadzu C-R4A Chromatopac as integrator.

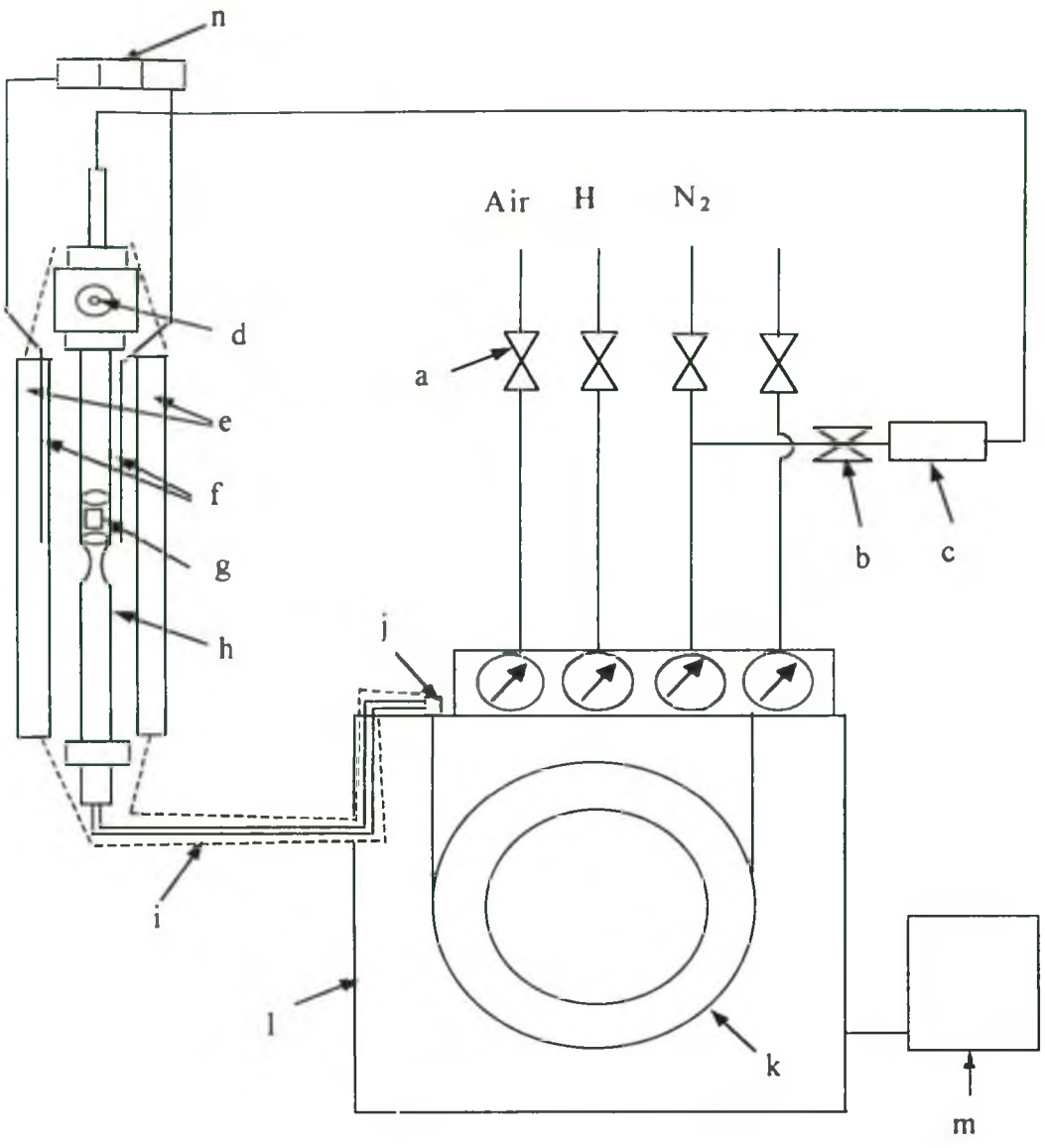

Fig. 3.3. Schematic representation of the catalytic cracking experiment.

(a) Stop valve, (b) flow controller valve, (c) drier,
(d) injection port, (e) furnace, (f) thermocouple,
(g) catalyst bed, (h) glass column, (i) ribbon heater,
(j) GC injection port, (k) capillary column, (l) GC oven,
(m) integrator (n) temperature controller.

3.3. Results

3.3.1. *Modification of USY zeolites by chemical vapour deposition of tetramithoxysilane*

Modification of high and low siliceous USY zeolites was carried out at 593 K using tetramethoxysilane. In the present study, modified zeolites were prepared with silica deposition of 2.6 wt %, 5.0 wt %, 10.2 wt %, 13.2 wt %, 21.6 wt % on HS-USY and 6.8 wt %, 10.7 wt % on LS-USY.

3.3.2. *Characterization of modified zeolites*

The unmodified USY zeolites and silica-deposited modified USY zeolites were characterized by XRD, NH_3-TPD and IR.

X-ray diffraction

The results of X-ray diffraction patterns of modified and unmodified HS-USY and LS-USY zeolites are shown in Fig. 3.4 and Fig. 3.5, respectively. To observe the effect of deposited silica on peak intensity, percent peak intensity of crystallinity (at 331 plane) is plotted against the amount of deposited silica of HS-USY and LS-USY zeolites in Fig. 3.6.

The crystallinities and unit cell constants (a_0) of the zeolites have been obtained from XRD data using 2θ of (533) planes. The number of framework Al atoms per unit cell (Al_F/u.c.) for USY zeolites has been calculated using the following equation [30],

$$Al_F/u.c. = 112.4(a_0 - 24.233) \quad \ldots\ldots\ldots\ldots\ldots\ldots 3.1$$

The XRD patterns are given in Appendix A.1 and A.2.

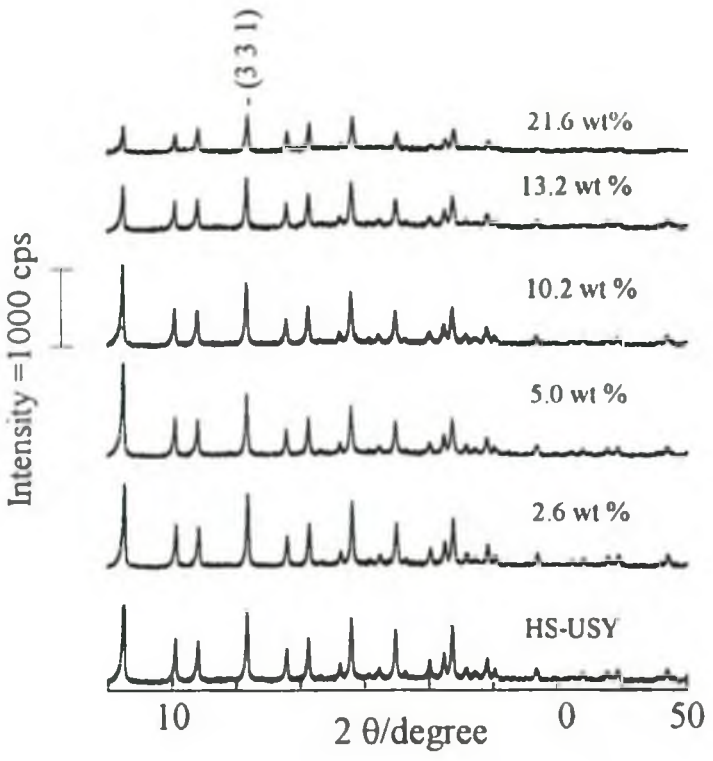

Fig. 3.4. XRD pattern of HS-USY and CVD-HS-USY zeolites.

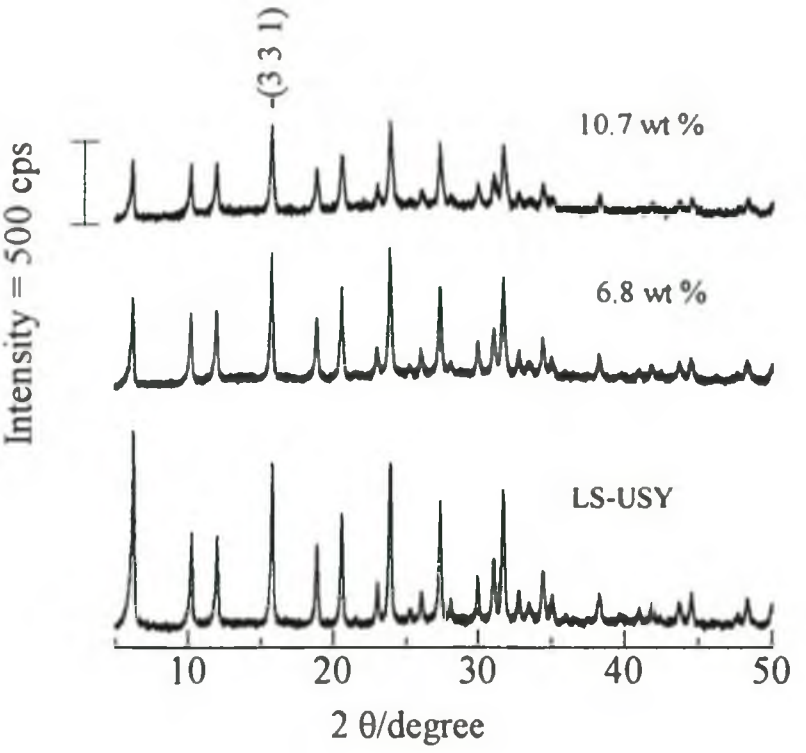

Fig. 3.5. XRD pattern of LS-USY and CVD-LS-USY zeolites.

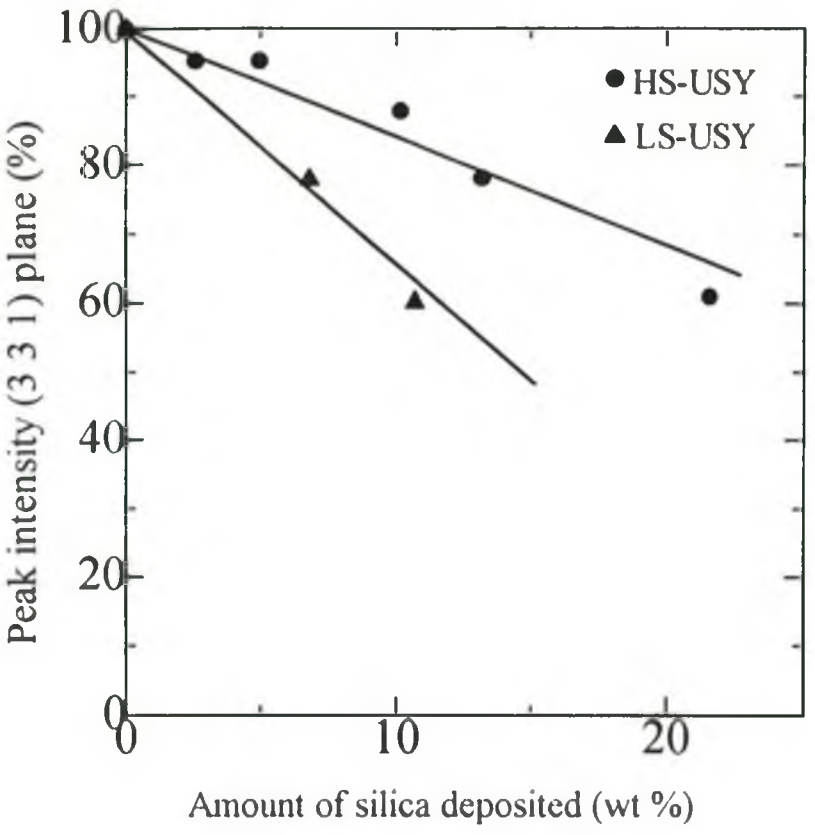

Fig. 3.6. The effect of deposited silica on the crystallinity peak intensity of HS-USY and LS-USY zeolites.

NH_3-TPD

The acid amount of HS-USY, LS-USY zeolites and their silica-deposited samples were measured by NH_3-TPD, are shown in Fig. 3.7 and Fig. 3.8, respectively.

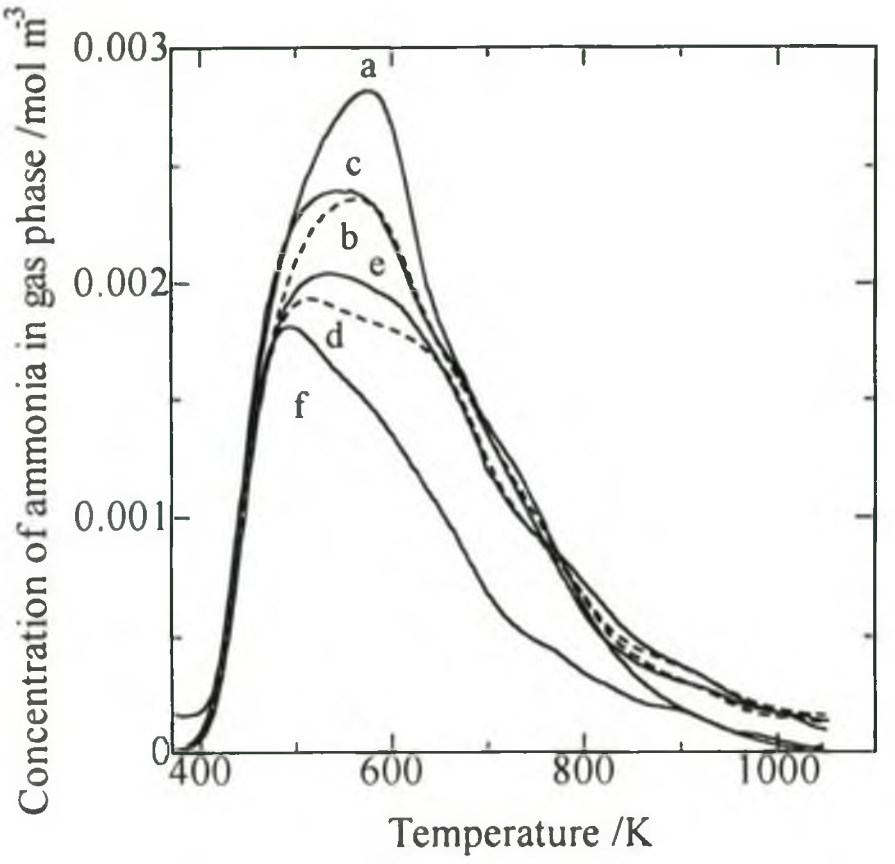

Fig. 3.7. TPD spectra of HS-USY and CVD-HS-USY zeolites.

(a) HS-USY, (b) 2.6 wt %, (c) 5.0 wt %, (d) 10.2 wt %, (e) 13.2 wt % and (f) 21.6 wt % CVD-HS-USY.

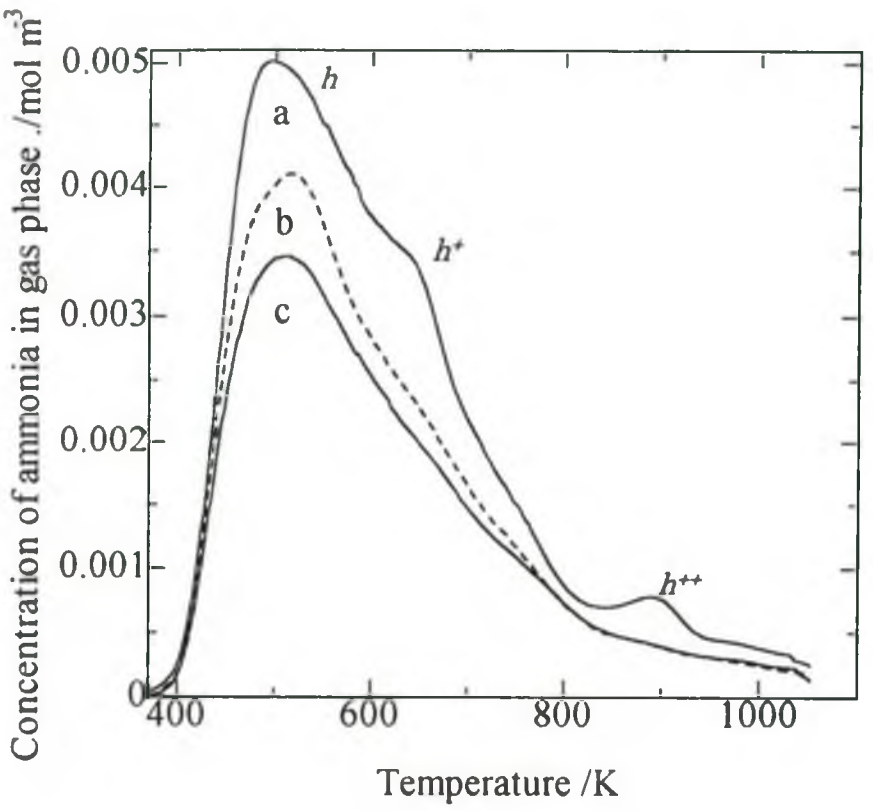

Fig. 3.8. TPD spectra of LS-USY and CVD-LS-USY zeolites.

(a) LS-USY, (b) 6.8 wt % and (c) 10.7 wt % CVD-LS-USY.

IR-studies

IR-spectral measurements of unmodified and modified USY zeolites were done (Fig. 3.9 and Fig. 3.10) in order to measure any change in the -OH groups on the zeolites.

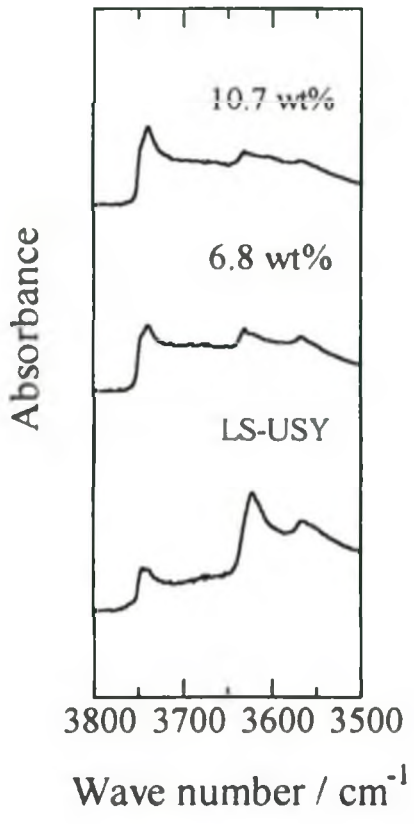

Fig. 3.9. IR spectra of LS-USY and CVD-LS-USY zeolites.

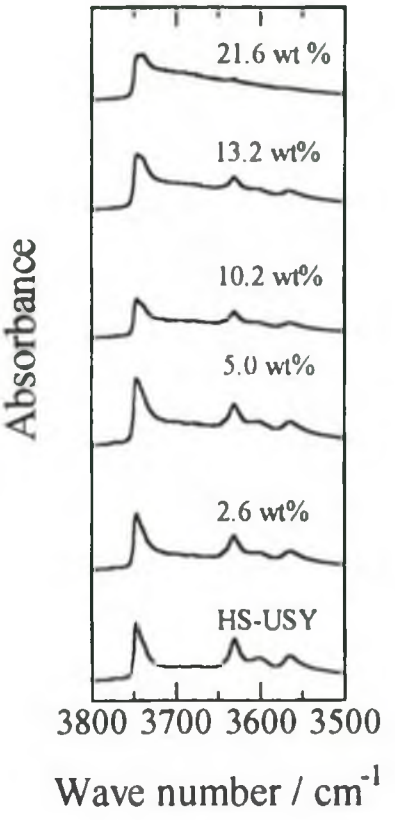

Fig. 3.10. IR spectra of HS-USY and CVD-HS-USY zeolites.

3.3.3. *Adsorption of 1,3,5-triisopropylbenzene on modified and unmodified USY zeolites*

In order to carry out the gravimetric adsorption experiment, adsorption temperature was selected carefully (393 K), so that, 1,3,5-TIPB was adsorbed without reaction on the zeolite surface. It was found that no reaction could take place below 423 K. Fig. 3.11 shows the adsorption profile with time for 1,3,5-TIPB on modified and unmodified HS-USY zeolite. Fig. 3.12 shows the adsorption profile with time for 1,3,5-TIPB on modified and unmodified LS-USY zeolite.

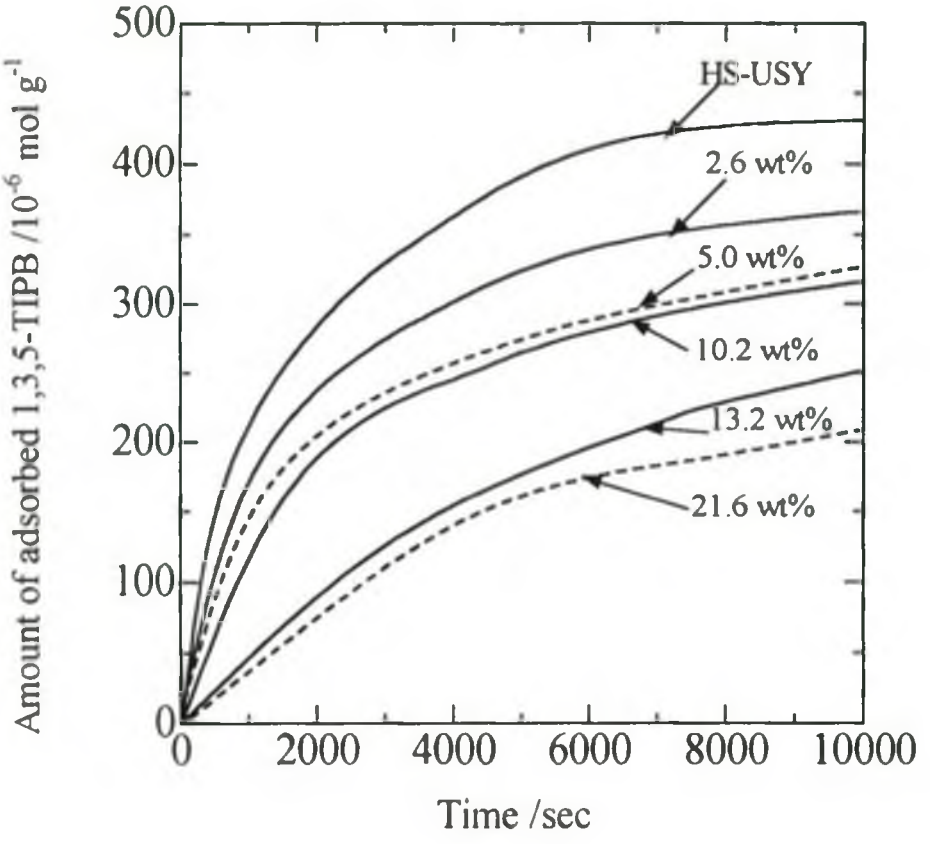

Fig. 3.11. Adsorption of 1,3,5-TIPB over HS-USY and CVD-HS-USY zeolites.

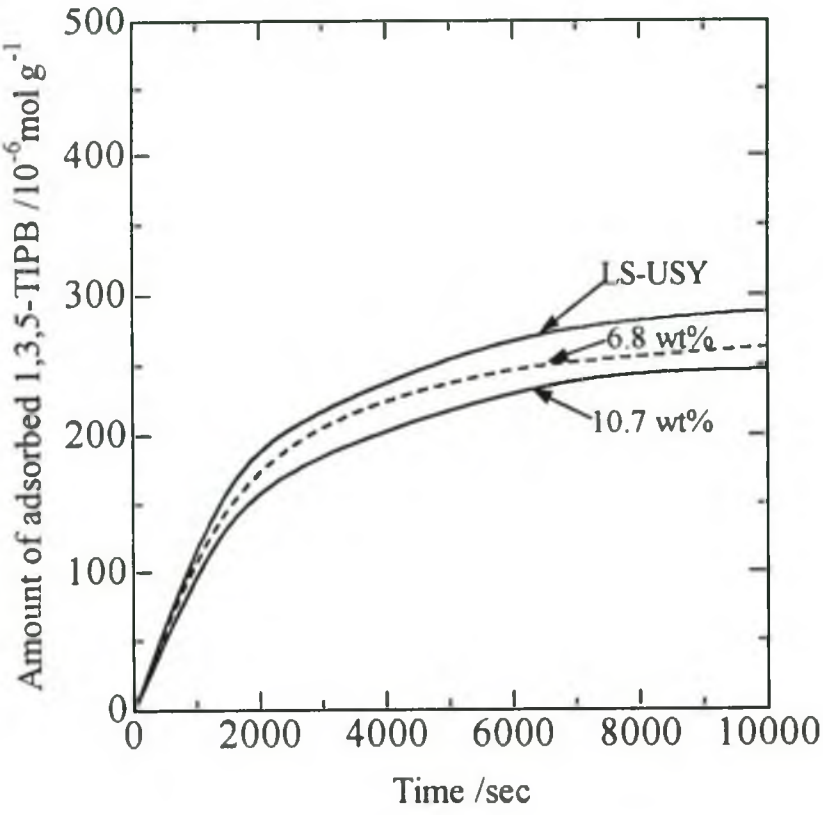

Fig. 3.12. Adsorption of 1,3,5-TIPB over LS-USY and CVD-LS-USY zeolites.

3.3.4. *Catalytic cracking of 1,3,5-trimethylbenzene and 1,3,5-triisopropylbenzene on modified and unmodified USY zeolites*

Catalytic cracking of 1,3,5-TMB and 1,3,5-TIPB by unmodified and modified USY zeolites was studied to measure the shape selective catalytic cracking property. The extent of catalytic cracking of a reactant is expressed as percent conversion of the reactant. Percent conversion by catalytic cracking of 1,3,5-TMB on HS-USY and silica-deposited HS-USY zeolites is shown in Table 3.1 and Fig. 3.13. For LS-USY and silica-deposited LS-USY zeolites, the percent conversion of 1,3,5-TMB by catalytic cracking is also shown in Table 3.1 and Fig. 3.13.

Catalytic cracking of 1,3,5-TIPB, on modified/unmodified HS-USY and LS-USY zeolites was also studied (Table 3.1 and Fig. 3.14).

Table 3.1. Percent conversion of catalytic cracking of 1,3,5-TMB and 1,3,5-TIPB on USY and silica-deposited (CVD) USY zeolites

Zeolite	1,3,5-TMB[a]	1,3,5-TIPB[b]
HS-USY	56.3	20.8
2.6 wt % CVD-HS-USY	54.7	16.4
5.0 wt % CVD -HS-USY	54.8	10.8
10.2 wt % CVD -HS-USY	48.7	10.2
13.2 wt % CVD -HS-USY	39.9	7.3
21.6 wt % CVD -HS-USY	33.1	3.1
LS-USY	72.2	26.0
6.8 wt % CVD -LS-USY	64.3	17.5
10.7 wt % CVD-LS-USY	48.9	9.2

[a] 5.00 ± 0.01 mg zeolite was taken in each catalytic cracking experiment and reaction temperature was 623 K.

[b] 2.00 ± 0.01 mg zeolite was taken in each catalytic cracking experiment and reaction temperature was 523 K.

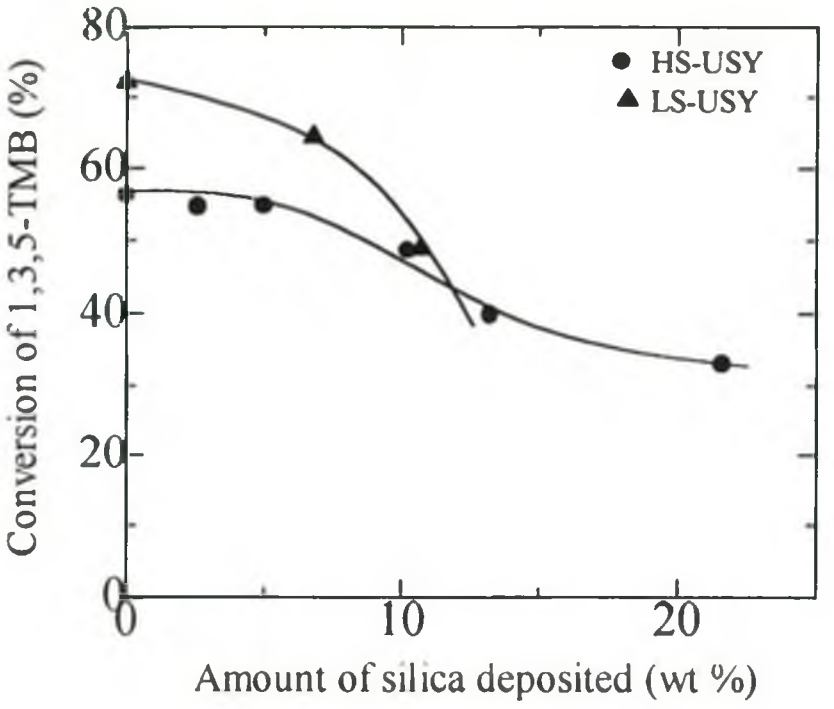

Fig. 3.13. Percent conversion of 1,3,5-TMB on USY and silica-deposited USY zeolites.

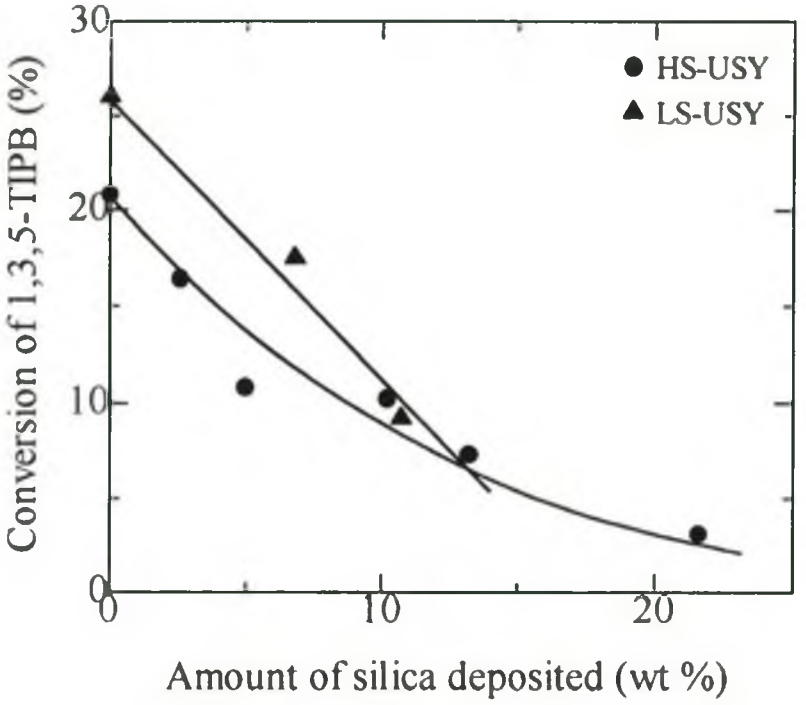

Fig. 3.14. Percent conversion of 1,3,5-TIPB on USY and silica-deposited USY zeolites.

3.4. Discussion

3.4.1. *Effect on crystallinity upon deposition*

Depositions of amorphous silica on HS-USY zeolite, causes slight decrease in crystallinity (at 331 plane). This decrease in the crystallinity is much more prominent for the silica deposited LS-USY zeolite samples (Fig. 3.6).

3.4.2. *Effect of CVD on acidity of USY zeolite*

The NH_3-desorption profile on LS-USY zeolite (Fig. 3.8) shows one major *h*-peak (high temperature peak ascribed to the ammonia or ammonium cation adsorbed on the acid site showing an acidic property) with two minor peaks (h^+ and h^{++} peaks). We have, followed previous reports [31, 32] in designating the peaks. These two minor peaks originate from extra-framework Al species. The NH_3-desorption profile for silica-deposited LS-USY zeolite does not show any one of these two peaks (Fig. 3.8b and 3.8c). In the case of HS-USY zeolite, desorption peak is flattened to some extent for almost all of the CVD-samples (Fig. 3.7b-3.7f), but the nature of the peak spectra are not changed upon deposition of silica on HS-USY zeolite. This flattening of the shape occurs due to deposition of amorphous silica on the zeolite surface. It means that the alkoxide reacts with the silanol groups on the external surface of HS-USY zeolite [33].

The acid amount of modified and unmodified USY zeolites is calculated and the results are presented in Table 3.2. The acid amount is plotted against the amount of deposited silica (Fig. 3.15). The acid amount decreases with the increase of deposited silica on LS-USY zeolite, but in the case of HS-USY zeolite, the total amount of acid is not affected much by the deposition of silica (Fig. 3.15 and Table 3.2). For the low siliceous

USY zeolites, the silane compound reacts with the external hydroxyl group as well as with the acidic hydroxyl group inside the pores of the zeolite. As a result, a continuous decrease of acid amount is observed.

The total Al content and the framework Al content, determined by ICP and XRD (using equation 3.1), respectively, are shown in Table 3.3 and 3.4. The amount of non-framework Al is obtained by subtracting the framework Al content from total Al content (Table 3.4). The results show that LS-USY zeolite has higher amount of extra-framework (non-framework) Al species than that of HS-USY zeolite (Table 3.4). The aluminium concentration of USY zeolite may be considered as a prime factor for the reactivity of silane compounds with acid sites of zeolites. When the aluminium concentration is high the silane compound is likely to react preferentially with acid sites, originated from aluminium, inside the pore than with the silanol groups on the external surface. As a result, a decrease of acid amount is observed for the silica deposited LS-USY zeolite samples (Fig. 3.15 and Table 3.2). However, these internal acid sites in HS-USY zeolites seem to be mostly unavailable for reaction and there is hardly any change in the acid amount with deposited silica.

Table 3.2. Determination of the total acid amount from NH_3-TPD for USY and silica-deposited (CVD) USY zeolites

Zeolite	Acid amount excluding deposited SiO_2 mol/kg
HS-USY	0.41
2.6 wt % CVD-HS-USY	0.41
5.0 wt % CVD-HS-USY	0.42
10.2 wt % CVD-HS-USY	0.40
13.2 wt % CVD-HS-USY	0.45
21.6 wt % CVD-HS-USY	0.32
LS-USY	0.85
6.8 wt % CVD-LS-USY	0.69
10.7 wt % CVD-LS-USY	0.62

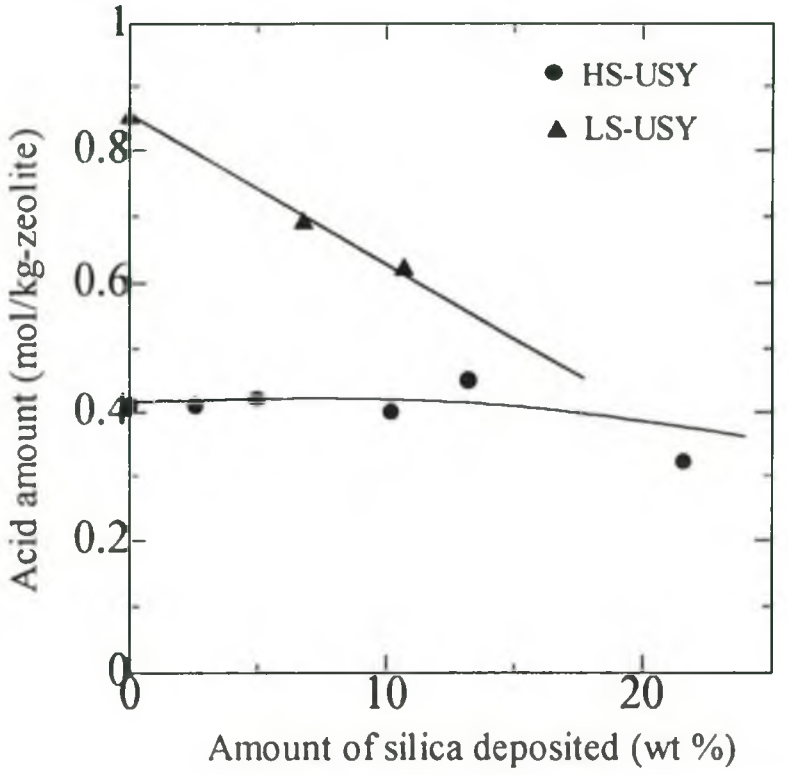

Fig. 3.15. Relationship between acid amounts with the amount of deposited silica on HS-USY and LS-USY zeolites.

Table 3.3. Determination of SiO_2/Al_2O_3 ratio (by ICP)

Sample	Water content (%) (from TG)	[Al] (mol/kg)	[Na] (mol/kg)	[Al] –[Na] (mol/kg)	SiO_2/Al_2O_3
HS-USY	22.90	1.07	0.24	0.83	29.15
LS-USY	29.06	3.46	0.09	3.37	7.89

Table 3.4. Data for Al_F and Al_{NF} from XRD (Fig. 3.4 and Fig. 3.5) and ICP (Table 3.3)

Sample	2θ at 533 plane (°)	d-value (Å)	a_0 (Å)	[Al] (mol/kg) (from ICP)	[Al_F] (atom/ u.c.) (from XRD)	[Al_F] (mol/kg)	[Al_{NF}] (mol/kg)
HS-USY	23.96	3.71	24.33	0.83	10.90	0.72	0.11
LS-USY	23.90	3.72	24.39	3.37	17.65	0.98	2.39

3.4.3. *Interaction of tetramethoxisilane on USY zeolite*

In the case of LS-USY zeolite, the -OH bands at 3630 and 3560 cm^{-1} disappear for any deposition (Fig. 3.9). In the case of HS-USY zeolite, only the intensities of the -OH band at 3633 and 3560 cm^{-1} are slightly decreased, but there is no change of any peak position (Fig. 3.10).

The disappearance of -OH bands of LS-USY zeolite at 3630 and 3560 cm^{-1} are due to the interaction of silicon alkoxide with the internal acidic hydroxyl group. Thus the results from IR spectra also support that deposition occurs inside the pore, and reaction with the acidic -OH group takes place inside the pore. In the case of HS-USY, the intensities of the -OH band at 3633 and 3560 cm^{-1} are slightly decreased because of the deposition of silica on the external surface of USY zeolite (Fig. 3.10). In this case, the peak intensity decreases with the increase of deposited amorphous silica. In the case of high deposition, such as 21.6 wt %, on HS-USY, considerable weakening and broadening of peak intensity are observed (Fig. 3.10).

3.4.4. *Extent of the control of pore-opening size on the silica-deposited USY zeolites with high and low silica concentration*

The pore-opening sizes of HS-USY and LS-USY zeolites were investigated by the adsorption of large molecule, namely 1,3,5-TIPB. Fig. 3.11 shows adsorption of 1,3,5-TIPB on HS-USY zeolite having different amounts of deposited silica. Adsorption of 1,3,5-TIPB decreases gradually with the increase of deposited silica on the zeolite surface. In the case of LS-USY zeolite, the adsorption of 1,3,5-TIPB is not changed much with the amount of deposited silica (Fig. 3.12).

The initial adsorption rate constant (k) of 1,3,5-TIPB for different samples has been calculated and the values are shown in Table 3.5. The basis of calculation is the same as previously reported [34]. For different silica-deposited HS-USY zeolite samples, the rate constant decreases from 13.2 $\times$ 10^{-3} $sec^{-1/2}$ to 3.5 $\times$ 10^{-3} $sec^{-1/2}$ with the increase of deposited silica amount. This suggests that the pore-opening size is narrowing by deposition. Only a small difference in the decrease of adsorption rate constant is observed for different silica deposited LS-USY zeolites (Table 3.5). It seems that only a small number of the alkoxide molecules react with the hydroxyl group inside the pore of LS-USY zeolite. However, in the case of low silicious HY zeolite hydroxyl groups at the pore-mouth have been suggested to react with the alkoxide [35].

Table 3.5. Initial adsorption rate constant (k) of 1,3,5-TIPB on USY and silica-deposited (CVD) USY zeolites.

Zeolite	Initial rate constant[a] (k) ($sec^{-1/2}$) × 10^3
HS-USY	13.2
2.6 wt % CVD-HS-USY	10.6
5.0 wt % CVD-HS-USY	9.6
10.2 wt % CVD-HS-USY	8.7
13.2 wt % CVD-HS-USY	3.9
21.6 wt % CVD-HS-USY	3.5
LS-USY	10.7
6.8 wt % CVD-LS-USY	10.3
10.7 wt % CVD-LS-USY	9.2

[a]Adsorption temperature = 393 K.

3.4.5. *Inertisation of external surface of USY zeolites*

A small decrease in the extent of cracking of 1,3,5-TMB is observed for HS-USY zeolite having up to 5.0 wt % silica deposition (Table 3.1 and Fig. 3.13). The small deposition to this extent may inertise some of the active acid sites on the surface but the pore opening sizes remain largely unaffected. On the other hand when the deposition exceeds 10 wt %, considerable decrease in the extent of cracking is observed. This is because pore size narrowing caused by high deposition, prevents the molecules from entering into the pores. It can only react with the residual acid sites on the surface. However, the number of these acid sites decreases with their progressive inertisation due to higher deposits on the surface (Table 3.1 and Fig. 3.13).

In the case of LS-USY and silica deposited LS-USY zeolites, decrease in the extent of cracking of 1,3,5-TMB with the increase of deposited silica amount is also observed (Table 3.1 and Fig. 3.13). Comparing with HS-USY zeolite, the decrease in the extent of cracking is much sharper on LS-USY zeolite. Since, LS-USY zeolite has high concentration of acid sites and of extra-framework aluminium, the deposition of silica on LS-USY zeolite occurs not only on the external surface but also inside the pore. As a result, the deposited silica inertise both the external surface acid sites and internal pore acid sites.

For large molecule like 1,3,5-TIPB, the extent of cracking is gradually decreased from low silica deposited (2.6 wt %) HS-USY zeolite to high silica deposited (21.6 wt %) HS-USY zeolite (Table 3.1 and Fig. 3.14). The deposited silica narrows the pore-opening size and inertise the external surface of HS-USY zeolites. Similar results are also found for silica deposited LS-USY zeolite samples, but the decrease in the extent of cracking of 1,3,5-TIPB is much sharper than that of HS-USY zeolite (Fig.

3.14). This is because, the inertisation of acid sites occurs in the pore as well as on the external surface of LS-USY zeolite.

3.5. Conclusion

The pore-opening size of high siliceous USY zeolite can be controlled by chemical vapour deposition using tetramethoxisilane. The pore-opening size of the low siliceous USY zeolite is hardly controlled by the chemical vapour deposition because of its higher amount of extra-framework aluminium. The silane compound reacts preferentially with acid sites, originated from aluminium, inside the pore than with the silanol groups on the external surface. Thus, the aluminium concentration, particularly the concentration of the extra-framework aluminium, plays an important role in determining the efficiency of CVD on the USY zeolite.

3.6 References

[1] Martens, J. A., Xiong, Y. L., Feijen, E. J. P., Grobet, P. J. and Jacobs, P. A., *J. Phys. Chem.*, **97**, 5132 (1993).

[2] Gates, B. C., in "Catalytic Chemistry", Wiley, New York (1992).

[3] McDaniel, C. V. and Maher, P. K., in "Molecular Sieves", Society of Chemical Industry, London, p. 186 (1968).

[4] Lynch, J., Raatz, F. and Dufresne, P., *Zeolites*, **7**, 333 (1987).

[5] Choi-Feng, C., Hall, J. B., Higgins, B. J. and Beyerlein, R. A., *J. Catal.* **140**, 395 (1993).

[6] Engelhardt, G., Lohse, U., Patzelová, V., Magi, M. and Lippmaa, E., *Zeolites*, **3**, 239 (1983).

[7] Beaumont, R. and Barthomeuf, D., *J. Catal.*, **26**, 218 (1972).

[8] Miradatos, C. and Barthomeuf, D., *J. Chem. Soc. Chem. Comm.*, 39, (1981).

[9] Miradatos, C., Ha, B. H., Otsuka, K. and Barthomeuf, D., in "Proceedings of 5th International Conference on Zeolites", edited by Rees, Heyden, London, p. 382 (1980).

[10] Shannon, R. D., Gardner, K. H., Staley, R. H., Bergeret, G., Gallezot, P. and Aroux, A., *J. Phys. Chem.*, **89**, 4778 (1986).

[11] Fritz, P. O. and Lunsford, J. H., *J. Catal.*, **118**, 85 (1989).

[12] Shertukde, P. V., Hall, W. K., Dereppe, J., and Marcelin, G., *J. Catal.*, **139**, 468 (1993).

[13] Lunsford, J. H., in "Fluid Catalytic Cracking II", edited by M. L. Occelli, American Chemical Society, Washington, D.C., p. 1 (1991).

[14] Makarova, M. A. and Dwyer, J., *J. Phys. Chem.*, **97**, 6337 (1993).

[15] Makarova, M. A. Al-Ghefaili, K. M. and Dwyer, J., *J. Chem. Soc. Faraday Trans.*, **90**, 383 (1994).

[16] Aroux, A. and Ben Taarit, Y., *Thermochim. Acta*, **122**, 63 (1987).

[17] Křivánek, M., Dung, N. T. and Jíru, P., *Thermochim. Acta,* **115**, 91 (1987).

[18] Lohse, U., Parlitz, B. and Patzelová, V., *J. Phys. Chem.*, **93**, 3677 (1989).

[19] Dempsey, E., *J. Catal.* **33**, 497 (1974).

[20] Dempsey, E., *J. Catal.* **39**, 155 (1975).

[21] Mikovsky, R. J. and Marshall, J. F., *J. Catal.*, **44**, 170 (1976).

[22] Zhidomirov, G. M. and Kazanasky, V. B., *Adv. Catal.*, **34**, 131 (1986).

[23] Beyerlein, R. A., McVicker, G. B., Yacullo, L. N. and Ziemiak, J. J., in "Preprints," Division of Petroleum Chemistry, American Chemical Society, Washington, D.C., Vol. **31**, p. 190 (1986).

[24] Kumar, R., Chenh, W. C., Rajagopalan, K., Peters, A. W. and Basu, P., *J. Catal.*, **143**, 594 (1993).

[25] Lombardo, E. A., Sill, G. A. and Hall, W. K., *J. Catal.*, **119**, 426 (1989).

[26] Aboul-Gheit, A. K., *Thermochim. Acta,* **191,** 233 (1991).

[27] Katada, N., Igi, H., Miyamoto, T., Kim, J. -H. and Niwa, M., *Shokubai (Catalysts & Catalysis),* **39**, 444 (1997).

[28] Igi, H., Katada, N. and Niwa, M., in "Preprints of ZMPC '97", Japan Association of Zeolites, Tokyo, p. 88 (1997).

[29] Igi, H., Katada, N. and Niwa, M., in "Proceeding of 12th International Zeolites Conference", edited by M. M. J. Treacy, B. K. Marcus, M. E. Bisher and J. B. Higgins, Materials Research Society, Warrendale, p. 2643 (1999).

[30] Kuehne, M. A., Kung H. H. and Miller J. T., *J. Catal.*, **171**, 293 (1997).

[31] Miyamoto, T., Katada, N., Kim, J. -H., Niwa, M. and Tsutsumi, K., *J. Phys. Chem. B,* **102**, 6738 (1998).

[32] Katada, N., Miyamoto, T., Begum, H. A., Naito, N., Niwa, M., Matsumoto, A. and Tsutsumi, K., *J. Phys. Chem. B*, **104**, 5511 (2000).

[33] Niwa, M., Kato, S., Hattori, T. and Murakami, Y., *J. Chem. Soc., Faraday Trans. 1*, **80**, 3135 (1984).

[34] Begum, H. A., Katada, N. and Niwa, M., *Micropor. Mesopor. Mater.*, **46**, 13 (2001).

[35] Kim, J. -H., Ikoma, Y. and Niwa, M., *Micropor. Mesopor. Mater.*, **32**, 37 (1999).

Appendix

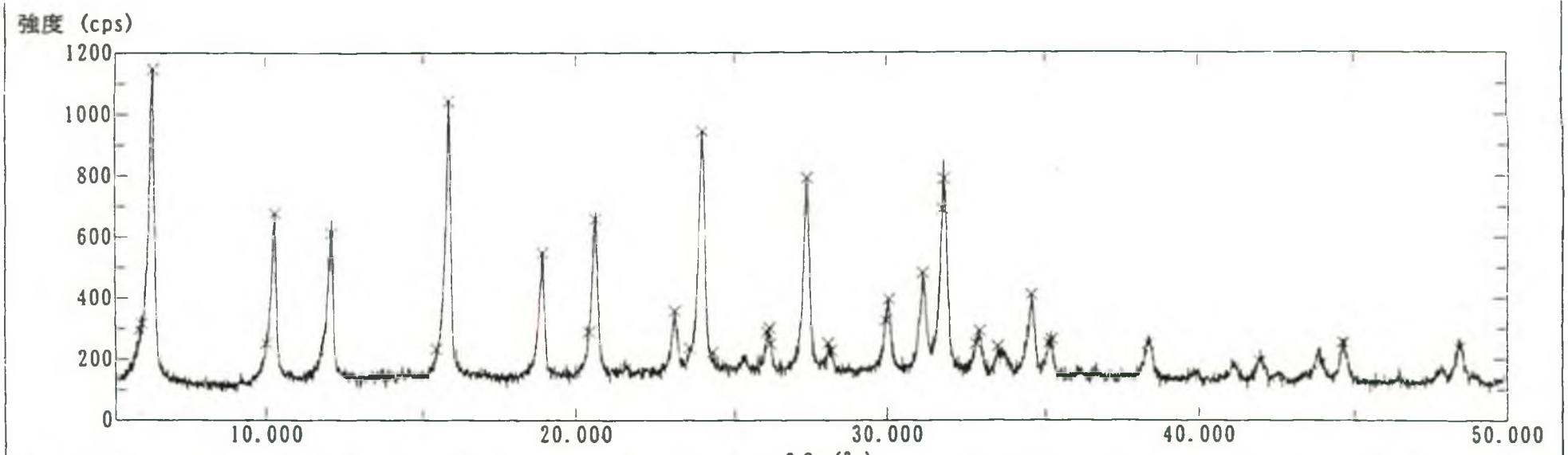

Peak	2θ	Area	d-value	Intensity	Ratio	ピーク番号	2 θ	半価幅	d 値	強 度	相対強度
1	5.790	0.059	15.2508	297	26	16	26.070	0.059	3.4151	289	26
2	5.870	0.059	15.0432	316	28	17	26.140	0.059	3.4061	303	27
3	6.260	0.153	14.1068	1148	100	18	26.180	0.059	3.4010	250	22
4	10.010	0.059	8.8289	253	22	19	27.400	0.212	3.2522	794	70
5	10.270	0.153	8.6059	678	60	20	28.080	0.071	3.1750	252	22
6	12.030	0.094	7.3505	613	54	21	28.180	0.059	3.1640	228	20
7	15.440	0.059	5.7340	233	21	22	29.960	0.059	2.9799	328	29
8	15.840	0.165	5.5901	1044	91	23	30.060	0.094	2.9702	398	35
9	18.930	0.071	4.6840	549	48	24	31.140	0.082	2.8696	484	43
10	20.420	0.059	4.3454	290	26	25	31.750	0.059	2.8159	694	61
11	20.620	0.153	4.3037	659	58	26	31.810	0.153	2.8107	792	69
12	23.080	0.118	3.8503	358	32	27	32.800	0.059	2.7281	251	22
13	23.540	0.059	3.7761	238	21	28	32.920	0.118	2.7184	293	26
14	23.960	0.176	3.7108	947	83	29	33.480	0.071	2.6742	243	22
15	24.300	0.071	3.6597	223	20	30	34.550	0.106	2.5938	413	36

Page-1

A.1. XRD pattern of HS-USY zeolite

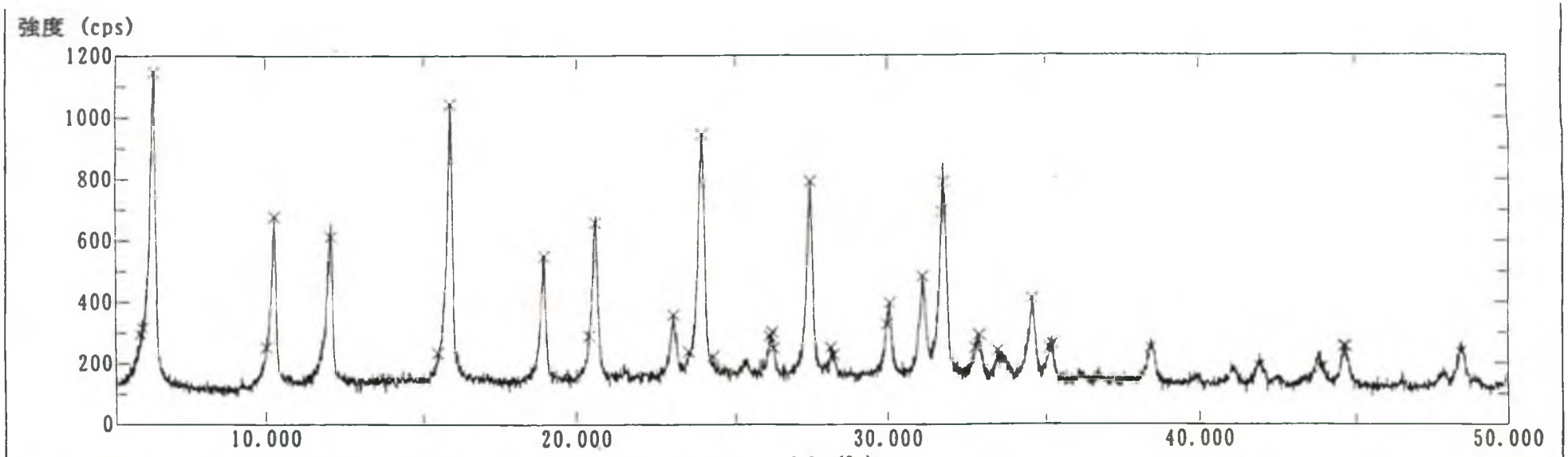

Peak	2θ	Area	d-value	Intensity	Ratio
31	35.110	0.059	2.5537	251	22
32	35.190	0.059	2.5481	265	24
33	38.360	0.071	2.3445	251	22
34	41.930	0.071	2.1528	192	17
35	43.900	0.059	2.0606	185	17
36	44.610	0.071	2.0295	257	23
37	44.690	0.059	2.0260	256	23
38	48.440	0.071	1.8776	236	21

ﾋﾟｰｸ番号	2 θ	半価幅	d 値	強 度	相対強度

Page-2

A.1. XRD pattern of HS-USY zeolite

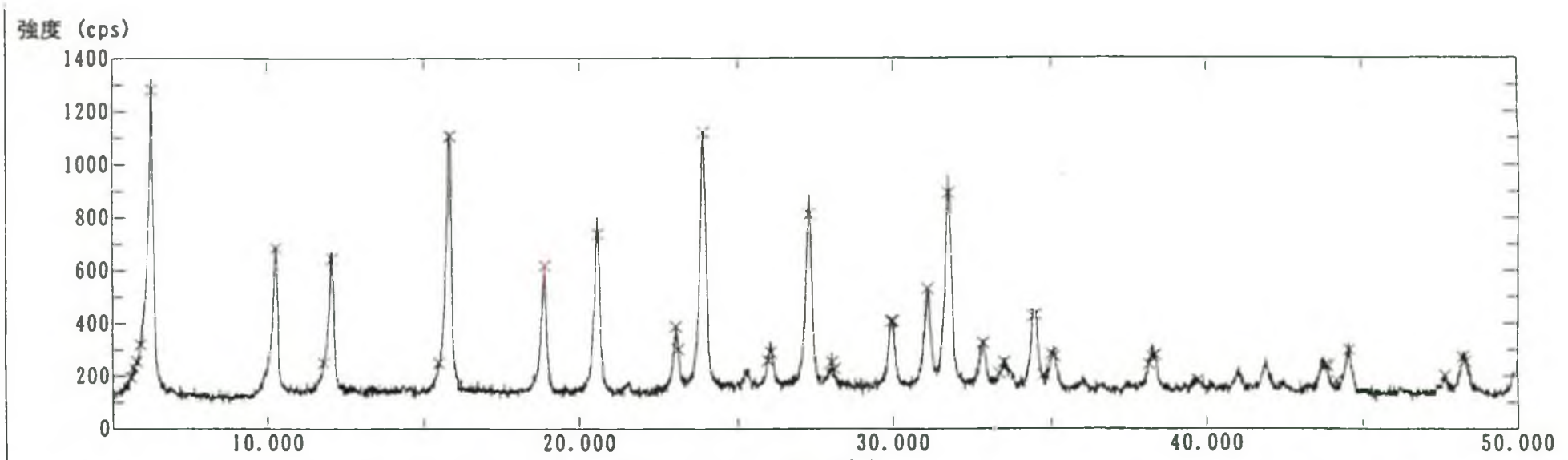

Peak	2θ	Area	d-value	Intensity	Ratio
1	5.570	0.059	15.8527	195	16
2	5.650	0.059	15.6284	233	19
3	5.770	0.071	15.3036	255	20
4	5.890	0.059	14.9921	320	25
5	6.270	0.129	14.0843	1282	100
6	10.260	0.129	8.6143	684	54
7	11.770	0.059	7.5123	249	20
8	12.010	0.129	7.3627	645	51
9	15.480	0.059	5.7192	251	20
10	15.830	0.153	5.5936	1108	87
11	18.900	0.165	4.6913	619	49
12	20.580	0.176	4.3120	739	58
13	23.020	0.082	3.8602	388	31
14	23.090	0.059	3.8486	303	24
15	23.900	0.176	3.7200	1122	88

ピーク番号	2 θ	半価幅	d 値	強 度	相対強度
16	25.960	0.059	3.4293	259	21
17	26.050	0.118	3.4176	290	23
18	27.320	0.141	3.2616	814	64
19	28.000	0.059	3.1839	212	17
20	28.070	0.071	3.1761	253	20
21	28.150	0.059	3.1673	228	18
22	29.930	0.082	2.9828	408	32
23	29.990	0.071	2.9770	409	32
24	31.070	0.153	2.8759	531	42
25	31.730	0.188	2.8176	894	70
26	32.810	0.106	2.7273	326	26
27	33.320	0.082	2.6867	211	17
28	33.470	0.059	2.6750	253	20
29	34.410	0.082	2.6040	428	34
30	34.500	0.094	2.5975	433	34

Page-1

A.2. XRD pattern of LS-USY zeolite

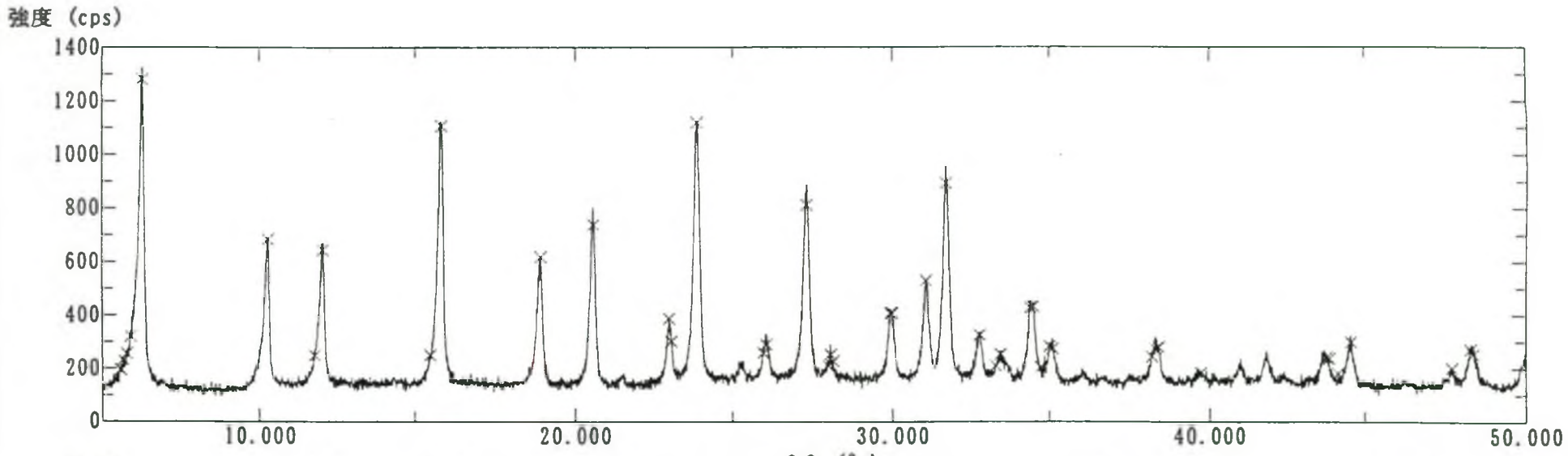

Peak	2θ	Area	d-value	Intensity	Ratio
31	34.740	0.059	2.5801	205	16
32	35.010	0.071	2.5608	283	23
33	35.090	0.059	2.5551	274	22
34	38.180	0.059	2.3551	244	20
35	38.290	0.082	2.3486	273	22
36	38.380	0.094	2.3433	280	22
37	39.710	0.059	2.2679	184	15
38	43.780	0.059	2.0660	243	19
39	43.860	0.059	2.0624	238	19
40	44.140	0.059	2.0500	183	15
41	44.560	0.059	2.0316	300	24
42	47.690	0.059	1.9053	202	16
43	48.270	0.094	1.8838	273	22
44	48.360	0.059	1.8805	255	20

ピーク番号	2 θ	半価幅	d 値	強 度	相対強度

Page-2

A.2. XRD pattern of LS-USY zeolite.

A.3. Published paper

ELSEVIER

Microporous and Mesoporous Materials 46 (2001) 13–21

MICROPOROUS AND MESOPOROUS MATERIALS

www.elsevier.nl/locate/micromeso

Chemical vapor deposition of silica on silicalite crystals and shape-selective adsorption of paraffins

Hosne Ara Begum, Naonobu Katada, Miki Niwa *

Department of Materials Science, Faculty of Engineering, Tottori University, Koyama-cho, Tottori 680-8552, Japan

Received 6 June 2000; received in revised form 2 November 2000; accepted 24 December 2000

Abstract

Chemical vapor deposition (CVD) of $Si(OCH_3)_4$ was carried out on silicalite crystals in order to control the pore-opening size. Due to the non-acidity, relatively high temperature such as 773 K was required to deposit thicker silica layers sufficient for obtaining selective adsorbents. Adsorption of linear and branched alkanes on silicalite and CVD-silicalites was performed gravimetrically and chromatographically at about 298 K. Both methods showed that adsorption behavior was almost unchanged for hexane and butane on CVD-silicalites but the adsorption for 2-methylpentane and 2-methylpropane was suppressed with the increase of the silica amount on silicalite. The extent of suppression depended upon the length of paraffins and the amount of deposited silica on silicalite. Thus, linear and branched paraffins can be separated by choosing the extent of silica deposition on silicalite.

Keywords: Silicalite; CVD; Pore-opening size; Shape-selective adsorption; Paraffins

1. Introduction

Silicalite is the aluminum free form of ZSM-5, having an MFI structure. It has elliptical pore opening of 0.51×0.57 nm^2 interconnected by zigzag channels with a nearly circular cross-section of about 0.54 nm in diameter [1]. It has hydrophobic and organophilic nature compared to other zeolites. Owing to this characteristics, silicalite can be used to selectively adsorb non-polar hydrocarbon molecules in water for environmental applications [2]. Another important character of silicalite/ZSM-5 is that its 10-member oxygen ring opening is similar to the size of aromatic molecules such as benzene and xylene [3]. The structure and the size of the micropore of silicalite make it suitable for application in shape-selective adsorption of hydrocarbons and aromatic compounds.

Adsorption equilibria of hydrocarbons on silicalite and ZSM-5 zeolites have been studied by many researchers. Flanigen et al. [1] reported synthesis, crystal structure and properties of silicalite. They studied the adsorption of different hydrophobic and hydrophilic adsorbates on silicalite. The adsorption isotherms of C_1 to C_4 alkanes and isobutane, CO_2, SF_6 and C_5–C_{10} normal alkanes on silicalite were reported by Sun and coworkers [2,4]. Gravimetric equilibrium isotherms for the adsorption of branched and cyclic C_6 paraffins on

* Corresponding author. Tel./fax: +81-857-315256.
E-mail address: mikiniwa@chem.tottori-u.ac.jp (M. Niwa).

1387-1811/01/$ - see front matter
PII: S1387-1811(01)00270-0

silicalite were studied by Cavalcante and Ruthven [5,6].

Chemical vapor deposition (CVD) of silica on zeolite is an established method to control the pore-opening size of zeolites to improve the shape-selective adsorption of mixtures of gases and liquids. Our previous papers reported both the fine control of the pore-opening size of zeolites by CVD of silicon alkoxide and the shape-selective reaction and adsorption of different hydrocarbons [7–13]. The pore-opening size of H-mordenite was effectively reduced by ≈0.1 and 0.2 nm upon formation of one to two and three molecular layers of silicon oxide [7], and thus modified mordenite was used for selective cracking of octane isomers [8]. Selective formation of *para*-xylene in not only methanol conversion [9] but also toluene alkylation [10] was observed for modified HZSM-5, and this study was extended to the deposition using various silicon compounds [11]. The CVD technique was also applied to the development of selective adsorbents. The separation of oxygen and nitrogen was studied using CVD zeolite A [12]. Deposited silica control the pore-opening size so precisely that it effectively suppresses the rate of adsorption of nitrogen of which molecular sizes is larger than oxygen only by 0.02 nm [12]. Separation of C_2–C_4 olefins was also studied by using Si-deposited zeolite A. The chromatographic response and gravimetric measurements showed that the rate of adsorption of olefins was suppressed by the deposition of silica on zeolite A. The suppression of the diffusion rate of olefins depended on the length of olefins and the amount of deposited silica [13].

Presently, we are interested in the separation of branched-chain and straight-chain hydrocarbons by the use of silicalite. Since silicalite is suitable for hydrocarbon adsorption due to its non-acidic property, the control of pore-opening size by CVD of silica might make it an interesting new material for shape-selective separation of hydrocarbons. However, only one report has been published on the CVD of silica on silicalite by Nomura et al. [14]. In this report, silicalite membranes were modified by the ozone and alkoxide counter-diffusion CVD technique and the deposition conditions were optimized to deposit the silica on the non-acidic material without decomposing the membrane structure. Deposition of silicon alkoxide on such a non-acidic material proceeds fast only on the top of the zeolite, and the further deposition is usually slow, as observed in this study (vide infra) as well as on Na-mordenite [15]. Therefore, an investigation on the simple thermal CVD on silicalite is needed in order to prove the possibility for the development of selective adsorbents of hydrocarbons. Herein, we report the CVD of silica on silicalite crystals and its application to shape-selective adsorption of linear and branched alkanes. Observation of morphology and precise determination of thickness of deposited silica layer on the silicalite crystal, not encountered so far, is an important and additional merit in this investigation.

2. Experimental

2.1. Synthesis of silicalite

Silicalite was synthesized according to Argauer and Landolt [16]. An aqueous solution of Ludox HS40 colloidal silica and an aqueous solution of tetra-*n*-propylammonium bromide in H_2SO_4 were added dropwise into an aqueous solution of sodium chloride. The pH of the solution was adjusted to 10.3. Thus the mixed solution was stirred, and heated at 443 K for 24 h in an autoclave. The product was filtered, washed with deionized water, and dried overnight in an oven at 373 K. Finally, the solid product was calcined in air at 803 K for 3 h in a furnace. To remove the impurities, prepared silicalite was washed thoroughly with a 0.1 M NH_4NO_3 solution for 3 h at 353 K. This process was repeated for several times, and then the sample was calcined again for 3 h at 803 K in air. Throughout the experiments, any stress for the silicalite was avoided, since the crystallites collapsed under high pressure.

2.2. Characterization

Powder X-ray diffraction (XRD) was performed by a Rigaku, Miniflex Plus diffractometer with 0.45 kW CuKα (30 kV, 15 mA). Scanning electron microscopy (SEM) photographs were taken using

a JEOL JSM-5800 scanning microscope to find the morphology and the crystal size of silicalite with the magnification of 6000–10 000. Before taking SEM photographs, the samples were loaded on mounted plastic tapes, and Au vapor was deposited in vacuo using a Giko IB-3 Ion-coater for 40 s with 5–6 mA current. Infrared (IR) spectra were collected on self-supporting disks with 10 mm of the diameter molded from 8 to 10 mg of the silicalite powders in an in situ cell by a JASCO FTIR-5300 spectrometer. Nitrogen adsorption isotherm was measured at 77 K for the silicalite sample.

2.3. Preparation of CVD-silicalites at different temperatures

A conventional vacuum system equipped with a quartz microbalance is used as the laboratory apparatus in the CVD method described elsewhere [13]. The silicalite crystal (about 0.3 g) was set in a quartz basket hung on the quartz spring, and $Si(OCH_3)_4$ was kept in a liquid reservoir. Before deposition of the $Si(OCH_3)_4$, the silicalite was evacuated at 673 K for 2 h until no weight change was observed for a considerable time. The vapor of $Si(OCH_3)_4$ was then admitted onto the sample at a desired temperature. The vapor pressure was kept at ≈2.5 Torr (1 Torr = 133.3 Pa) by chilling the reservoir with an ice bath and the degree of evacuation was $\approx 10^{-3}$ Torr. The gas phase was then evacuated for removing reaction products e.g., methanol. This process was repeated several times. The resultant increase in weight was measured in situ by the quartz microbalance. The materials thus deposited were calcined and oxidized by oxygen (200 Torr) at 673 K to remove carbonaceous residues through the deposition. Then the system was again evacuated to measure the constant weight gain, which showed the extent of modification upon deposition on silicalite. This experiment was carried out at 513, 593, 673 and 773 K through which the same process was undertaken.

2.4. Adsorption of linear and branched paraffins on silicalite and CVD-silicalites

Gravimetric measurements of rate of sorption: Adsorption experiments of different adsorbates, hexane (Tokyo Chemical Industry Co. Ltd., Japan), 2-methylpentane (Wako Pure Chemical Industries Ltd., Japan), butane (Sumitomo-Seika, Japan) and 2-methylpropane (Fluka, Switzerland), were carried out gravimetrically by the McBain method in the static system [13]. All the adsorbates were purified before use. 0.1 g of silicalite or CVD-silicalite sample was taken for each experiment. The sample was evacuated at 673 K for 2 h and the adsorption measurement was carried out at about 298 K. During the adsorption, the partial pressures of hexane and 2-methylpentane were kept constant at its vapor pressure at 273 K, and the pressures of butane and 2-methylpropane were kept at 40 Torr at about 298 K.

Chromatographic response: Chromatographic adsorption experiments were performed to show the adsorption behavior of silicalite and CVD-silicalites at about 298 K. 0.82 μmol of hexane or 1.1 μmol of 2-methylpentane was injected with a syringe into 0.05 g of the silicalite or CVD-silicalites [17,18] with a carrier (He) flow rate 30 ml min^{-1}. The elution chromatograms were detected by an FID detector. Before the experiment, silicalite or CVD-silicalite was pretreated at 673 K for 1 h with a flow of 30 ml min^{-1} of helium. The same method was followed in the adsorption experiments of butane and 2-methylpropane on silicalite and CVD-silicalites. In each case, 4.1 μmol of gas was injected with a syringe into 0.05 g of the adsorbent.

3. Results

3.1. Characterization of silicalite

From the XRD measurements, the prepared silicalite was identified as the MFI type structure. The shape and the size of the silicalite sample were measured by SEM. The shape of silicalite was hexagonal flat plate with an average crystal size of $5.3 \times 3.1 \times 1.5$ μm^3, as shown in Fig. 1. Based on this SEM photograph, the geometrical external surface area of silicalite was found as 1.3 $m^2 g^{-1}$, the density being 1.76 g cm^{-1} as usual. The band for Si–OH at 3740 cm^{-1} with a weak intensity was observed in the IR spectrum of silicalite (not shown). The nitrogen adsorption isotherm showed

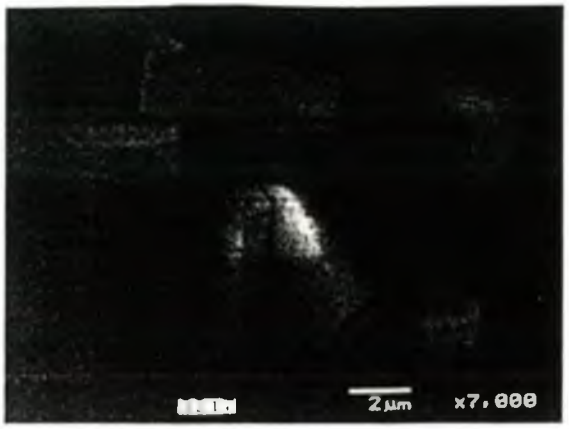

Fig. 1. SEM image of silicalite crystal sample.

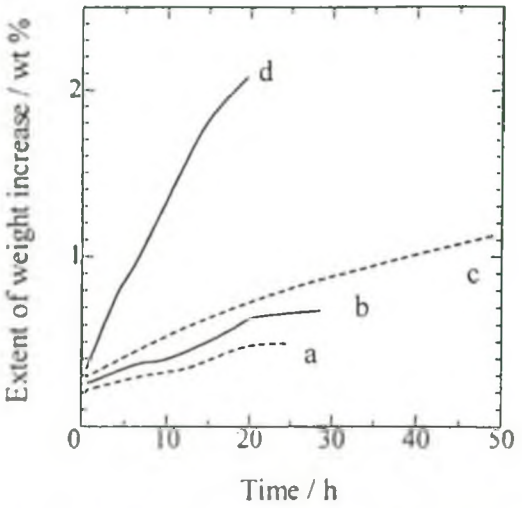

Fig. 2. CVD of $Si(OCH_3)_4$ on silicalite at different temperatures (a) 513 K, (b) 593 K, (c) 673 K and (d) 773 K.

a type IV (stepped) isotherm for silicalite (not shown). The stepped adsorption isotherm on silicalite has been reported already [19].

3.2. Chemical vapor deposition

The increase of the weight by CVD of silica on silicalite at different temperatures is shown in Fig. 2 and Table 1. From this figure, it was observed that the rate of deposition of silica on silicalite was low at lower temperature (513 and 593 K) due to the lack of acid site on silicalite, and it was very difficult to get high deposition at this rate. Even at 673 K, the deposition rate was slow, and not so practical for preparing highly silica deposited silicalite. At 773 K, the deposition rate was high enough to prepare various types of silica deposited silicalite within a reasonable time. For this reason, in our present study, 773 K was chosen as the deposition temperature for preparing various CVD-silicalites having different amounts of deposited silica by varying the contact time. Four different CVD-silicalites (0.75, 1.3, 1.9, and 2.7 wt.%) were prepared having different amounts of deposited silica at 773 K, as described in Table 2.

No significant change was observed in the SEM image due to CVD of silica on silicalite crystals at such a high temperature as 773 K for about 20 h (Figs. 1 and 3). Silicalite and CVD-silicalites also showed no difference in the nitrogen adsorption isotherms (figure not shown).

3.3. Adsorption experiment

The adsorption of hexane and 2-methylpentane was measured gravimetrically on silicalite and CVD-silicalites with different degrees of silica deposition, as shown in Figs. 4 and 5, respectively. The equilibrium adsorption amount of hexane

Table 1
CVD of $Si(OCH_3)_4$ on silicalite at different temperatures

Deposition temperature (K)	Deposition time (h)	Weight increase upon deposition (wt.%)	Extent of weight increase after oxidation (wt.%)	Surface concentration[a] of Si atom (nm^{-2})
513	25	0.50	0.2	15
593	29	0.73	0.5	39
673	49	1.15	0.8	62
773	19	2.1	1.9	147

[a] Surface concentration on the external surface of silicalite.

Table 2
Preparation of silica deposited silicalite at different contact times at 773 K

Run no.	Contact time for deposition (h)	Extent of weight increase after oxidation (wt.%)	Surface concentration[a] of Si atom (nm^{-2})
1	9	0.75	58
2	14	1.3	100
3	19	1.9	147
4	44	2.7	208

[a] Surface concentration, on the external surface of silicalite.

Fig. 3. SEM image of 1.9 wt.% CVD-silicalite sample.

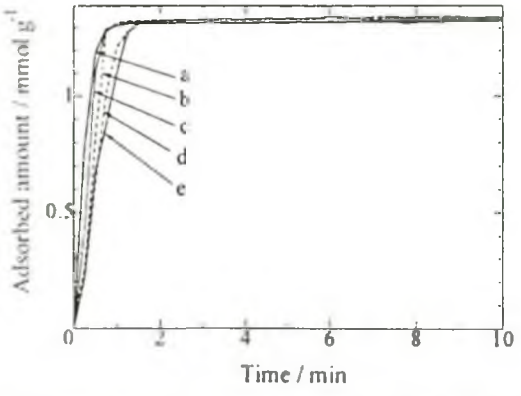

Fig. 4. Adsorption of hexane on silicalite (a), 0.75 wt.% (b), 1.3 wt.% (c), 1.9 wt.% (d), and 2.7 wt.% (e) CVD-silicalite.

seems higher than that of 2-methylpentane on unmodified silicalite (Figs. 4a and 5a). The adsorption of hexane was slightly suppressed on the

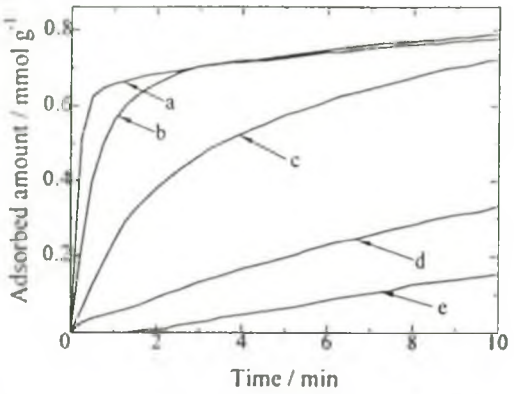

Fig. 5. Adsorption of 2-methylpentane on silicalite (a), 0.75 wt.% (b), 1.3 wt.% (c), 1.9 wt.% (d), and 2.7 wt.% (e) CVD-silicalite.

CVD-silicalites (Fig. 4b–e). The adsorption of 2-methylpentane was suppressed distinctly on 0.75 wt.% of CVD-silicalite (Fig. 5b) and this suppression became significant with increasing the silica amount on silicalite from 1.3 to 2.7 wt.% (Fig. 5c–e). The adsorption of butane and 2-methylpropane was also studied gravimetrically. The adsorption of butane (Fig. 6) showed similar adsorption behavior of hexane (Fig. 4). The adsorption of 2-methylpropane was significantly suppressed on 1.3 wt.% CVD-silicalite (Fig. 7c), and this suppression of adsorption was markedly increased with the increase of deposited silica amount on silicalite (Fig. 7d and e).

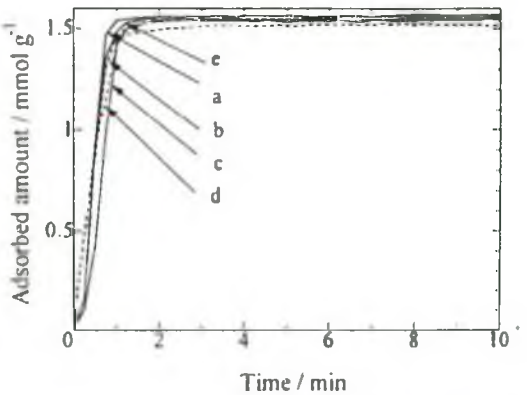

Fig. 6. Adsorption of butane on silicalite (a), 0.75 wt.% (b), 1.3 wt.% (c), 1.9 wt.% (d), and 2.7 wt.% (e) CVD-silicalite.

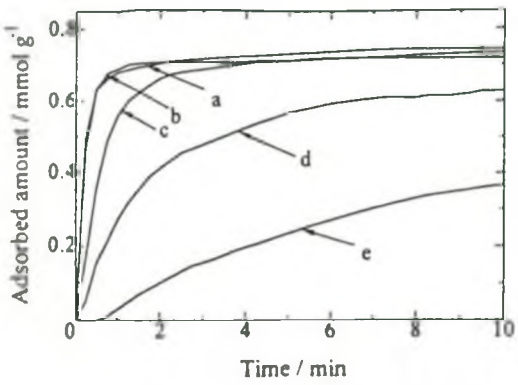

Fig. 7. Adsorption of 2-methylpropane on silicalite (a), 0.75 wt.% (b), 1.3 wt.% (c), 1.9 wt.% (d), and 2.7 wt.% (e) CVD-silicalite.

In order to understand quantitatively these adsorption profiles, the kinetics of adsorption was analyzed from the root-t plot: the rate constant was calculated from the curvature of the adsorbed amount against $t^{1/2}$ at the initial stage of adsorption. The rate of adsorption can be analyzed based on the following equation [20]:

$$\frac{Q_t}{Q_e} = \frac{6}{r}\left(\frac{D}{\pi}\right)^{1/2} t^{1/2} = kt^{1/2} \quad \text{taking } \frac{6}{r}\left(\frac{D}{\pi}\right)^{1/2} \text{ as } k$$

where Q_t and Q_e are the amount adsorbed at time t and at the equilibrium, respectively, r is the radius of the zeolite crystal, D is the diffusion constant, and k is the adsorption rate constant. On the basis of this equation the adsorption rate constants (k) of the adsorbates were calculated from the slope of the adsorption curve and the results are presented in Table 3. The adsorption equilibrium for hexane or butane on silicalite/CVD-silicalites was established very quickly. But in case of 2-methylpentane or 2-methylpropane, on the other hand, it was very difficult to reach adsorption equilibrium on silicalite/CVD-silicalites. To simplify our calculation, we assumed the Q_e value for each adsorbate as the adsorbed amount on silicalite in 1 h. The exact estimation of the kinetic parameter was difficult because only a few points were observed before the saturation of the adsorption of n-paraffins on silicalite/CVD-silicalites. However, significant changes were observed by the CVD on the branched paraffins. It was observed that the adsorption rate constant of 2-methylpentane was greatly suppressed with increasing the silica deposition on silicalite, while the adsorption rate constant of hexane on CVD-silicalites was slightly varied with the deposited silica amount. The adsorption rate constant of 2-methylpropane also showed a suppression similar to 2-methylpentane, while the adsorption of butane showed very low suppression for CVD-silicalites (Table 3).

The elution chromatographic method was applied to investigate the adsorption behavior of hexane and 2-methylpentane on silicalite and CVD-silicalites. In all cases, the elution chromatograms were observed within a very short elapsed time. The chromatograms are presented in Fig. 8. Hexane and 2-methylpentane were completely adsorbed by the inherent silicalite and did not show any responses in the chromatograms (Fig. 8a and a'). A weak elution peak of 2-methylpentane was observed for 0.75 wt.% CVD-silicalite (Fig. 8b') and the elution peaks were gradually intensi-

Table 3
Adsorption rate constant (k) of linear and branched paraffins derived from the adsorption at the initial stage

Adsorbent	Adsorption rate constant ($min^{-1/2}$)			
	Butane[a]	Hexane[a]	2-Methylpropane[b]	2-Methylpentane[b]
Silicalite	1.03	1.20	1.25	1.20
0.75 wt.% CVD-silicalite	0.96	0.98	1.29	0.68
1.3 wt.% CVD-silicalite	0.80	1.09	0.74	0.30
1.9 wt.% CVD-silicalite	0.88	0.85	0.35	0.07
2.7 wt.% CVD-silicalite	0.93	0.81	0.20	0.013

[a] $\sigma = 0.43$ nm.
[b] $\sigma = 0.50$ nm.

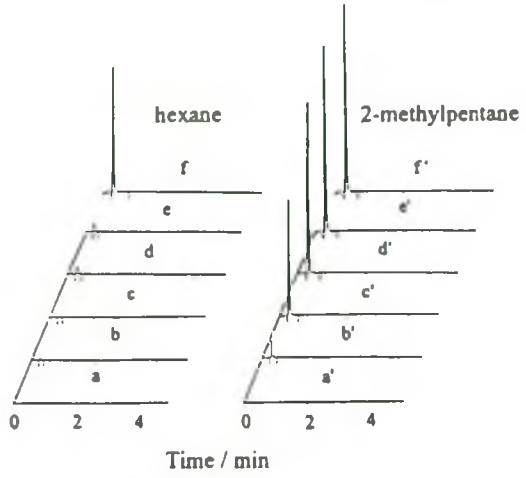

Fig. 8. Elution chromatograms of hexane and 2-methylpentane on silicalite (a,a'), 0.75 wt.% (b,b'), 1.3 wt.% (c,c'), 1.9 wt.% (d,d'), and 2.7 wt.% (e,e') CVD-silicalite, respectively (elution chromatograms are magnified eight times for the adsorption of hexane on silicalite and CVD-silicalites). The intensities of the elutions in the blank experiments are shown in (f,f').

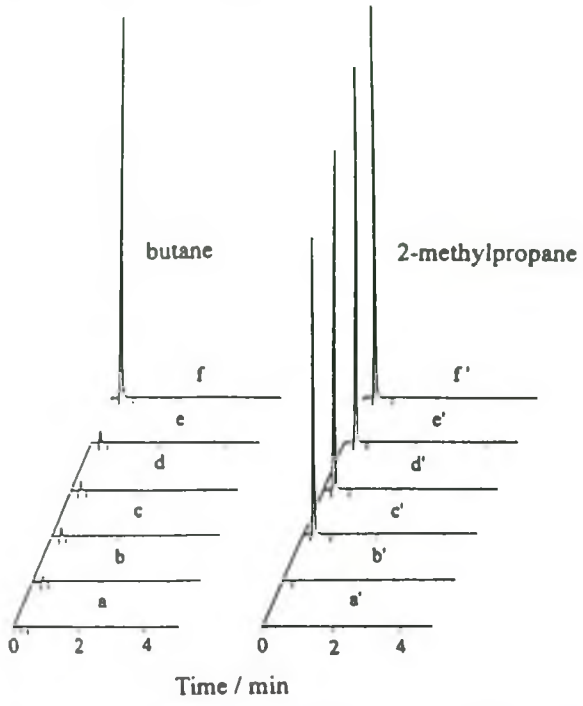

Fig. 9. Elution chromatograms of butane and 2-methylpropane on silicalite (a,a'), 0.75 wt.% (b,b'), 1.3 wt.% (c,c'), 1.9 wt.% (d,d'), and 2.7 wt.% (e,e') CVD-silicalite, respectively. The intensities of the elutions in the blank experiments are shown in (f,f').

fied with the increase of deposited silica amount on silicalite (Fig. 8c' and d'). 2-methylpentane was eluted without adsorption on 2.7 wt.% CVD-silicalite (Fig. 8e'). However, hexane was almost completely adsorbed on the CVD-silicalites (Fig. 8b–e). Butane followed a similar adsorption behavior of hexane (Fig. 9a–e). 2-Methylpropane was eluted from 1.3 wt.% CVD-silicalite with an intense peak (Fig. 9b'). The intensity of the elution peak was increased gradually with the deposited amount of silica on silicalite (Fig. 9c'–e'). The findings on the elution chromatograms are thus in good agreement with those of the gravimetric measurements.

4. Discussion

4.1. Chemical vapor deposition

At the initial stage of deposition, about 0.2 wt.% of weight increase occurred quickly (Fig. 2). At this stage, the weight of the silica should be about 40% of the deposited material because after oxidation about 0.2 wt.% silica was obtained from 0.5 wt.% deposited material that was formed in the deposition at 513 K (Table 1). Therefore the weight of silica at the initial stage is estimated to be ≈0.1 wt.%, corresponding to eight Si atom nm^{-2} of the concentration of Si on the external surface of silicalite. Since the surface concentration 8.91 Si atom nm^{-2} is required to form a monolayer [8], the monolayer of silica was supposed to be formed quickly at the early stage of deposition. This behavior was independent of the temperature, as shown in Fig. 2. After that, multilayer formation seems to be continued with time. Higher temperature was favored for higher deposition of silica on the silicalite.

We estimated the number of the layer formed upon deposition of silica on the external surface of the silicalite and found that about 23 layers of

silica were formed on the silicalite in case of 2.7 wt.% CVD-silicalite (Table 2). The deposited silica effectively controlled the pore-opening size of silicalite, and could suppress the adsorption of one-branched alkanes (kinetic diameter $\sigma = 0.50$ nm) over linear alkanes ($\sigma = 0.43$ nm), shown in Table 3. From our previous report [21], it was observed that 15 silica layers were required to control the pore-opening size of HZSM-5 with a Si/Al_2 ratio 76.4 (external surface area = 10.8 $m^2 g^{-1}$, 14.4 wt.% Si-HZSM-5), and the modified zeolite could suppress the adsorption of one-branched alkane, effectively.

4.2. Control of pore-opening size

CVD of $Si(OCH_3)_4$ on silicalite controlled the pore-opening size only, because the molecular size of $Si(OCH_3)_4$ is larger than the pore size of silicalite, and the alkoxide cannot enter into the silicalite pore. The deposited silica thus controlled the diffusion of molecules in the pore opening. For 2-methylpentane ($\sigma = 0.50$ nm), the effective control of the pore-opening size was observed. The rate of adsorption of 2-methylpentane decreased significantly with the increase of deposited silica amount on silicalite (Fig. 5 and Table 3). But, the rate of adsorption of hexane ($\sigma = 0.43$ nm) was not influenced significantly by the deposited silica amount on silicalite (Fig. 4). Similar adsorption behavior was observed in cases of butane and 2-methylpropane showed in Figs. 6 and 7. From these results, it was observed that the adsorption rate constant for 2-methylpropane ($\sigma = 0.50$ nm) was decreased with the increase of deposited silica on silicalite while very small difference was observed in case of butane ($\sigma = 0.43$ nm) (Table 3).

From the comparison between Figs. 5 and 7, the higher suppression for 2-methylpentane than 2-methylpropane was observed at the same silica amount on silicalite. This observation reflects that not only the width of hydrocarbon, but also the length of hydrocarbon considerably influenced the adsorption behavior, which is consistent with the results of olefins [13]. The adsorption rate was decreased with the increase of the length of hydrocarbons for CVD-silicalites.

5. Conclusion

The present study described the CVD of silica on silicalite crystals. Due to the non-acidity of silicalite, high temperature deposition was favored to prepare the silica overlayer deposited on silicalite. The deposited silica layer successfully controlled the pore-opening size and showed the shape-selective separation of branched and linear paraffins. The selectivity of the separation depends on the kinetic diameter and the length of paraffins along with the amount of deposited silica on silicalite.

References

[1] E.M. Flanigen, J.M. Bennett, R.W. Grose, J.P. Cohen, R.L. Patton, R.M. Kirchner, J.V. Smith, Nature 271 (1978) 512.
[2] M.S. Sun, D.B. Shah, H.H. Xu, O. Talu, J. Phys. Chem. B 102 (1998) 1466.
[3] O. Talu, C.J. Guo, D.T. Hayhurst, J. Phys. Chem. 93 (1989) 7294.
[4] M.S. Sun, O. Talu, D.B. Shah, J. Phys. Chem. 100 (1996) 17276.
[5] C.L. Cavalcante Jr., D.M. Ruthven, Ind. Eng. Chem. Res. 34 (1995) 177.
[6] C.L. Cavalcante Jr., D.M. Ruthven, Ind. Eng. Chem. Res. 34 (1995) 185.
[7] M. Niwa, S. Kato, T. Hattori, Y. Murakami, J. Chem. Soc., Faraday Trans. 1 80 (1984) 3135.
[8] M. Niwa, S. Morimoto, M. Kato, T. Hattori, Y. Murakami, Proceedings of 8th International Congress on Catalysis, Verlag Chemie, Weinheim, 1984, p. IV-701.
[9] M. Niwa, M. Kato, T. Hattori, Y. Murakami, J. Phys. Chem. 90 (1986) 6233.
[10] T. Hibino, M. Niwa, Y. Murakami, J. Catal. 128 (1991) 551.
[11] J.H. Kim, A. Ishida, M. Okajima, M. Niwa, J. Catal. 161 (1996) 387.
[12] M. Niwa, K. Yamazaki, Y. Murakami, Ind. Eng. Chem. Res. 30 (1991) 38.
[13] M. Niwa, K. Yamazaki, Y. Murakami, Ind. Eng. Chem. Res. 33 (1994) 371.
[14] M. Nomura, T. Yamaguchi, S. Nakao, Ind. Eng. Chem. Res. 36 (1997) 4217.
[15] T. Hibino, M. Niwa, Y. Kawashima, Y. Murakami, in: T. Inui, S. Namba, T. Tatsumi (Eds.), Chemistry of Microporous Crystals, Kodansha/Elsevier, Tokyo, 1991, p. 151.
[16] R.J. Argauer, G.R. Landolt, US Patent 3 702 886, 1972.
[17] T. Furusawa, M. Suzuki, J.M. Smith, Catal. Rev. Sci. Eng. 13 (1976) 43.

[18] H. Lechert, W. Schweitzer, Stud. Surf. Sci. Catal. 24 (1985) 427.
[19] A. Zecchina, S. Bordiga, G. Spoto, L. Marchese, G. Petrini, G. Leofanti, M. Padovan, J. Phys. Chem. 96 (1992) 4985.
[20] R.M. Barrer, D.W. Brook, Trans. Faraday Soc. 49 (1953) 1049.
[21] M. Niwa, N. Senoh, T. Hibino, Y. Nakatsuka, Y. Murakami, Stud. Surf. Sci. Catal. 83 (1985) 155.

A.4. Submitted paper

Ordered Microporous Straight Channels in the CVD Silica Layer on Silicalite Crystals

Daling Lu,[1] Junko Nomura Kondo,[2] Kazunari Domen,[1,2]* Hosne Ara Begum[3,4] and Miki Niwa[3]*

Controlling pore-size of zeolite material is quite important on shape-selectivity. Chemical vapor deposition (CVD) is an effective method for the fine control of zeolite pore-size. However, until nowadays there has been no any direct evidence to show what is present in the CVD layer formed on the surface of zeolite. In this paper the evidence that there exists a microporous straight channel structure in the CVD silica layer formed on silicalite crystals is presented by TEM. The straight channels in the CVD layer directly connect to the micropores in silicalite.

[1]Core Research for Evolutional Science and Technology, Japan Science and Technology, 2-1-13, Higashiueno, Taito-ku, Tokyo, 110-0015 Japan. [2]Chemical Resources Laboratory, Tokyo Institute of Technology, 4259 Nagatsuta, Midori-ku, Yokohama, 226-8503 Japan. [3]Department of Materials Science, Faculty of Engineering, Tottori University, Koyama-cho, Tottori, 680-8552 Japan. [4]Present address: Department of Chemistry, University of Dhaka, Dhaka-1000, Bangladesh.

* To whom correspondence should be addressed.

E-mail: kdomen@res.titech.ac.jp